

Alma Mater Studiorum – Università di Bologna

DOTTORATO DI RICERCA IN

Ingegneria Chimica dell’Ambiente e della
Sicurezza

Ciclo _27_

Settore Concorsuale di afferenza: 09D2

Settore Scientifico disciplinare: ING/IND-24

SOLUBILITY, DIFFUSIVITY AND PERMEABILITY OF GASES IN GLASSY
POLYMERS

Presentata da: AWEKE ELIAS GEMEDA

Coordinatore Dottorato

Prof. SERENA BANDINI

Relatore

Prof. GIULIO CESARE SARTI



Co Relatore

Dr. Ing. MARIA GRAZIA DE ANGELIS

Esame finale anno 2015

ABSTRACT

Gas separation membranes of high CO₂ permeability and selectivity have great potential in both natural gas sweetening and carbon dioxide capture. Polymer of intrinsic microporosity (PIM) has got many promising results in this regard. Many modified PIM membranes results permselectivity above Robinson upper bound. The big problem that should be solved for these polymers to be commercialized is their aging through time.

In high glassy polymeric membrane such as PIM-1 and its modifications, solubility selectivity has more contribution towards permselectivity than diffusivity selectivity. So in this thesis work pure and mixed gas sorption behavior of carbon dioxide and methane in three PIM-based membranes (PIM-1, TZPIM-1 and AO-PIM-1) and Polynonene membrane is rigorously studied. Sorption experiment is performed at three different temperatures (25°C, 35°C and 50°C) and three different molar fraction of carbon dioxide up to a pressure range of 35 atm.

Sorption isotherms found from the experiment shows that there is a decrease of solubility as the temperature of the experiment increases for both gases in all polymers. There is also a decrease of solubility due to the presence of the other gas in the system in the mixed gas experiments due to competitive sorption effect. Variation of solubility is more visible in methane sorption than carbon dioxide, which will make the mixed gas solubility selectivity higher than that of pure gas solubility selectivity.

Modeling of pure and mixed gas sorption of carbon dioxide and methane in the polymers above is also performed using dual mode sorption model and Non-equilibrium lattice fluid model. The results estimate the experimental data's correctly. This reveals that the models can be used to estimate pure and mixed gas sorption data's in the absence of experimental results.

To see the effect of physical aging on sorption results of carbon dioxide and methane in glassy polymeric membrane, experiment is carried out on heat treated and untreated samples. The result shows that the sorption isotherms don't vary due to the application of heat treatment for both carbon dioxide and methane in PIM-1 and TZPIM-1. But there is a decrease in the diffusivity coefficient and permeability of pure gases due to heat treatment. Both diffusivity coefficient and permeability decreases with increasing of heat treatment temperature.

Diffusivity coefficient calculated from transient sorption experiment and steady state permeability experiment is also compared in this thesis work. The results reveal that transient diffusivity coefficient is higher than steady state diffusivity selectivity.

ACKNOWLEDGEMENTS

It has been a privilege to be a student of The University of Bologna for more than four years, undertaking both Master's and PhD studies. The research work for this PhD thesis would not have been possible without the support and understanding of a number of people whom I would like to acknowledge.

Firstly, to my primary supervisor Prof. Guilio Cesare Sarti, thank you for being so supportive and helpful in every aspect of this project. Thank you for your open-door approach to my postgraduate study despite your numerous commitments to the departments and other students. Thank you for responding my midnight and weekend emails so promptly to de-bottleneck my experiments. Thank you for your guidance not only to the research work, but also my future career planning.

To my secondary supervisor, Dr. Ing Maria Grazia De Angelis, thank you for leading me to the research world. Your technical input and valuable comments to this PhD project and my research work are greatly appreciated. Thank you for leading me through the difficult times.

To Prof Ferruccio Doghieri, thank you for unofficially supervising me for the past few years. Thank you for guiding me into the world of membrane science and chemical engineering. Your input and comments to my laboratory work and my course work are sincerely appreciated.

I would like to acknowledge the University of Bologna, the Department of Chemical, civil, environmental and materials engineering for providing access to both chemicals and equipment during the project.

To the friends I have made in Diffusion in Polymer Group and DICAM, thank you for your support, friendship, and encouragement over the last few years.

I would like to express my gratitude to my wife, Elsedon Yeshitila. Elsi, your endless support, understanding and encouragement have made my PhD journey so much easier. Thank you for your love and the happy demeanor after my long hours of laboratory work. Thanks to my son, Yoni, who was born during my PhD study, I want to say that you are my happiness.

Finally, I would like to thank my parents, Mrs. Shewaye Bekele and Mr. Elias Gameda, my sisters Wubitu Elias and Lemlem Elias, and my brother Nebiyu Elias. I could have achieved nothing today without your commitment and dedication to help me succeed in my studies. Thank you all for my upbringing and your unconditional support to my life choices

TABLE OF CONTENTS

ABSTRACTS.....	i
ACKNOWLEDGEMENTS.....	iii
TABLE OF CONTENTS.....	v
LIST OF FIGURES.....	viii
LIST OF TABLES.....	xii
NOMENCLATURE.....	xiii
Chapter 1 General Introduction.....	1
Chapter 2 Literature Review.....	5
2.1 INTRODUCTION.....	5
2.2 DIFFERENT TECHNOLOGIES FOR GAS SEPARATION.....	6
2.2.1 Adsorption based technologies.....	6
2.2.2 Cryogenic separation.....	7
2.2.3 Absorption process.....	8
2.2.4 Membrane technology.....	10
2.3 POLYMERIC MEMBRANE FOR GAS SEPARATION.....	13
2.3.1 Advantages of Polymeric membrane gas separation over other technologies.....	16
2.3.2 Disadvantage Polymeric membrane gas separation compared other technologies...	17
2.4 PENETRANT TRANSPORT MECHANISMS.....	18
2.5 PENETRANT SORPTION AND TRANSPORT IN GLASSY POLYMERS.....	22
2.5.1 Solubility.....	24
2.5.1.1 Gas sorption in glassy polymer.....	24
2.5.1.2 Free volume in glassy polymer.....	26
2.5.1.3 Competitive sorption in multi component system.....	28
2.5.2 Diffusivity.....	28
2.5.3 Permeability.....	29
2.5.4 Selectivity.....	31
2.6 PHYSICAL AGING.....	32
2.7 TEMPERATURE DEPENDENCE OF TRANSPORT PARAMETERS.....	34
2.8 OBJECTIVE OF THE RESEARCH.....	36
Chapter 3 Experimental Methods.....	38
3.1 INTRODUCTION.....	38
3.2 MATERIALS AND MEMBRANE PREPARATION.....	39

3.2.1 Polymers and polymer synthesis.....	39
3.2.2 Gas supply and analysis.....	42
3.2.3 Solvent analysis.....	42
3.2.4 Preparation of dense polymeric films.....	43
3.3 MEASUREMENT OF PHYSICAL PROPERTIES.....	44
3.3.1 Membrane thickness.....	44
3.3.2 Membrane density.....	45
3.4 HEAT TREATMENT OF POLYMERS.....	45
3.5 MEASUREMENT OF PENETRANT TRANSPORT PROPERTIES.....	46
3.5.1 Experimental set-up.....	46
3.5.2 Pure gas sorption measurement.....	48
3.5.3 Mixed gas sorption measurement.....	48
3.5.4 Pure gas permeability measurement.....	49
Chapter 4 Mixed Gas Sorption in PIM-Based Polymers.....	51
4.1 INTRODUCTION.....	51
4.2 PURE GAS SORPTION IN PIM-BASED POLYMERS.....	51
4.3 MIXED GAS SORPTION IN PIM-BASED POLYMERS.....	53
4.4 PURE AND MIXED GAS SOLUBILITY COEFFICIENT.....	59
4.5 SOLUBILITY SELECTIVITY OF PIM-BASED POLYMERS.....	65
4.6 COMPARISON OF PURE AND MIXED GAS SOLUBILITY IN PIM-BASED POLYMER.....	69
4.7 TEMPERATURE DEPENDENCE OF SORPTION IN PIM-BASED POLYMERS.....	73
4.8 CONCLUSIONS.....	75
Chapter 5 Mixed Gas Sorption in Polynonene Polymer.....	77
5.1 INTRODUCTION.....	77
5.2 PURE GAS SORPTION IN POLYNONENE POLYMERS.....	78
5.3 MIXED GAS SORPTION IN POLYNONENE POLYMERS.....	79
5.4 SOLUBILITY SELECTIVITY OF POLYNONENE POLYMERS.....	83
5.5 COMPARISON OF SOLUBILITY OF POLYNONENE AND OF PIM-BASED POLYMERS.....	84
5.6 CONCLUSIONS.....	88
Chapter 6 Modeling of Mixed Gas Sorption in Glassy Polymers.....	89
6.1 INTRODUCTION.....	89
6.2 DUAL MODE SORPTION MODEL.....	90

6.2.1 Basic concept.....	90
6.2.2 Dual mode sorption model for pure gas sorption.....	91
6.2.3 Dual mode sorption model for mixed gas sorption.....	94
6.3 NON-EQUILIBRIUM LATTICE FLUID MODEL.....	96
6.3.1 Basic concept.....	96
6.3.2 Non-equilibrium lattice fluid model for pure gas sorption.....	97
6.3.3 Non-equilibrium lattice fluid model for mixed gas sorption.....	99
6.4 CONCLUSION.....	102
Chapter 7 Effect of Heat Treatment on Solubility, Diffusivity and Permeability of Gases in Glassy Polymers.....	103
7.1 INTRODUCTION.....	103
7.2 EFFECT OF HEAT TREATMENT ON SOLUBILITY OF PURE GASES IN GLASSY POLYMER.....	104
7.3 EFFECT OF HEAT TREATMENT ON DIFFUSIVITY OF PURE GASES IN GLASSY POLYMER.....	108
7.4 EFFECT OF HEAT TREATMENT ON PERMEABILITY OF PURE GASES IN GLASSY POLYMER.....	110
7.5 CONCLUSION.....	112
Chapter 8 Transient and Steady State Diffusivity of CO₂ and CH₄ in PIM-1.....	114
8.1 INTRODUCTION.....	114
8.2 TRANSIENT DIFFUSIVITY OF CO₂ IN PIM-1.....	115
8.3 STEADY STATE DIFFUSIVITY OF CO₂ IN PIM-1.....	116
8.4 COMPARISON OF TRANSIENT AND STEADY STATE DIFFUSIVITY.....	119
8.5 CONCLUSION.....	120
Chapter 9 Conclusions and Future Perspectives.....	121
9.1 CONCLUSIONS.....	121
9.2 FUTURE PERSPECTIVES.....	123
Chapter 10 References.....	124

LIST OF FIGURES

Figure 1.1: Milestones in the development of membrane gas separation [10].....	3
Figure 2.1: Robeson “upper bound” correlation for CO ₂ /CH ₄ separation (TR, thermally rearranged) [79].....	12
Figure 2.2: Schematic of membrane separation process with different driving forces that are Present.....	19
Figure 2.3: Three different mechanisms for membrane separation [110].....	20
Figure 2.4: Typical gas sorption isotherm in a glassy polymer represented by DMS model.....	26
Figure 2.5: The relationship between the polymer specific volume and temperature in amorphous Polymers [119].....	27
Figure 2.6: Transport of gas A and B across a membrane [135].....	31
Figure 3.1: Structure of PIM-1 polymer.....	40
Figure 3.2: Conversion of PIM-1 to TZPIM via the T ₂ C ₃ U cycloaddition reaction between aromatic nitrile groups and sodium azide, producing a tetrazole functional group [180].....	40
Figure 3.3: Synthetic scheme for amidoxime-functionalized PIM-1(AO-PIM-1) [21].....	41
Figure 3.4: Structure of poly (3, 4-TCNSi ₂).....	41
Figure 3.5: Solution casting/solvent casting procedure.....	44
Figure 3.6: The location pattern of thickness measurement, where the circular shaded edge is 5 mm wide.....	45
Figure 3.7: Schematic drawing of pressure decay for pure and mixed gas sorption experiment.....	46
Figure 3.8: Layout of permeation apparatus.....	47
Figure 4.1: (a). Pure CO ₂ gas sorption (b), Pure CH ₄ sorption in PIM-1 at 25°C.....	52
Figure 4.2: Pure and Mixed gas CO ₂ Sorption a) in PIM-1 at 50°C b) TZPIM at 35°C and c) in AO-PIM-1 at 35°C.....	54
Figure 4.3: Pure and mixed gas CH ₄ Sorption a) in PIM-1 at 50°C b) TZPIM at 35°C and c) in AO-PIM-1 at 35°C.....	56
Figure 4.4: Pure and mixed gas CO ₂ Sorption versus fugacity of CO ₂ a) in PIM-1 at 50°C b) TZPIM at 35°C and c) in AO-PIM-1 at 35°C.....	58
Figure 4.5: Pure and mixed gas CH ₄ Sorption versus fugacity of CH ₄ a) in PIM-1 at 50°C b) TZPIM at 35°C and c) in AO-PIM-1 at 35°C.....	59
Figure 4.6: Solubility coefficient of CO ₂ versus total pressures for a) PIM-1 at 50°C, b) TZPIM at 50°C and c) AO-PIM-1 at 35°C.....	61
Figure 4.7: Solubility coefficient of CH ₄ versus total pressures for a) PIM-1 at 50°C, b) TZPIM at	

50°C and c) AO-PIM-1 at 35°C.....	62
Figure 4.8: Solubility coefficient of CO ₂ versus CO ₂ fugacity of the gases for a) PIM-1 at 50°C, b) TZPIM at 50°C and c) AO-PIM-1 at 35°C.....	64
Figure 4.9: Solubility coefficient of CH ₄ versus CH ₄ fugacity for a) PIM-1 at 50°C, b) TZPIM at 50°C and c) AO-PIM-1 at 35°C.....	65
Figure 4.10: Real and Ideal CO ₂ /CH ₄ solubility selectivity versus CO ₂ fugacity for a) PIM-1 at 50°C, b) TZPIM at 50°C and c) AO-PIM-1 at 35°C.....	67
Figure 4.11: The Ratio of Real and Ideal CO ₂ /CH ₄ solubility selectivity versus CO ₂ concentration for a) PIM-1 at 50°C, b) TZPIM at 50°C and c) AO-PIM-1 at 35°C.....	69
Figure 4.12: Pure gas sorbed concentration comparison of PIM-1, TZPIM-1 and AO-PIM-1 at 35°C; a) CO ₂ , b) CH ₄	70
Figure 4.13: Mixed gas sorbed concentration comparison of PIM-1, TZPIM-1 and AO-PIM-1 at 35°C; a) CO ₂ , b) CH ₄	71
Figure 4.14: Real and Ideal Solubility selectivity of PIM-1, TZPIM-1 and AO-PIM-1 at 25°C; a) Ideal, b) Real.....	72
Figure 4.15: Pure gas sorption of CO ₂ and CH ₄ at 25°C, 35°C [223], 50°C.....	73
Figure 4.16: Logarithm of solubility of pure CO ₂ and pure CH ₄ versus inverse temperatures (results at 35°C are taken from [223]).....	74
Figure 4.17: Ratio between mixed and pure gas selectivity coefficient, versus CO ₂ molar concentration at 25°C, 35°C [223] and 50°C.....	75
Figure 5.1: (a) Pure CO ₂ gas sorption, (b) Pure CH ₄ sorption in Polynonene at 35°C.....	78
Figure 5.2: Pure and mixed gas in Polynonene membrane at 35°C a) CO ₂ , b) CH ₄	79
Figure 5.3: Pure and mixed gas sorption versus fugacity of gases at 35°C; a) CO ₂ , b) CH ₄	80
Figure 5.4: Ratio between mixed and pure gas solubility coefficient of a). CO ₂ , b) CH ₄ , versus total gas pressure at 35.0°C for different molar fractions of CO ₂ in the gas mixture.....	82
Figure 5.5: Ratio between mixed and pure gas Solubility coefficient S of (a) CH ₄ , (b) CO ₂ , versus 2nd component molar concentration at 35°C.....	83
Figure 5.6: (a) Pure-gas (ideal) and (b) mixed-gas (real) solubility-selectivity for the CO ₂ -CH ₄ mixture in Polynonene at 35°C, for different molar fractions of CO ₂ in the gas mixture, versus total pressure.....	84
Figure 5.7: Pure gas sorption comparison between polynonene and PIM-based membranes at 35°C; a). CO ₂ and b).CH ₄	85
Figure 5.8: Mixed gas sorption comparison between polynonene and PIM-based membranes at	

35°C and 50.9% CO ₂ ; a). CO ₂ and b).CH ₄	86
Figure 5.9: a) Pure gas solubility selectivity, b) mixed gas solubility selectivity of glassy polymers versus fugacity of CO ₂ at 35°C.....	88
Figure 6.1: Dual mode model results of pure gas sorption in different membranes at 35°C; a) CO ₂ , b) CH ₄	92
Figure 6.2: Pure gas sorption of PIM-1 at different temperature with dual mode model results; a) CO ₂ , b) CH ₄	93
Figure 6.3: Pure and mixed gas sorption of carbon dioxide with dual mode model versus total pressure; a) PIM-1 at 50°C, b). TZPIM-1 at 25°C and c). Polynonene at 35°C.....	95
Figure 6.4: Pure and mixed gas sorption of methane with dual mode model versus total pressure; a) PIM-1 at 50°C, b). TZPIM-1 at 25°C and c). Polynonene at 35°C.....	96
Figure 6.5: NELF model results of pure gas sorption in different membranes at 35°C; a) CO ₂ , b) CH ₄	98
Figure 6.6: Pure gas sorption of PIM-1 at different temperature with NELF model results; a) CO ₂ , b) CH ₄	99
Figure 6.7: Pure and mixed gas sorption of carbon dioxide with NELF model versus total pressure; a) PIM-1 at 50°C, b). TZPIM-1 at 25°C and c). Polynonene at 35°C.....	101
Figure 6.8: Pure and mixed gas sorption of methane with NELF model versus total pressure; a) PIM-1 at 50°C, b). TZPIM-1 at 25°C and c). Polynonene at 35°C.....	102
Figure 7.1: Sorption isotherms of pure gases in thermally untreated and treated PIM-1 at 35°C; a) CO ₂ , b).CH ₄	105
Figure 7.2: Solubility coefficient of pure gases in thermally untreated and treated PIM-1 at 35°C; a) CO ₂ , b).CH ₄	106
Figure 7.3: Sorption isotherms of pure gases in thermally untreated and treated TZPIM-1 at 35°C; a) CO ₂ , b).CH ₄	107
Figure 7.4: Solubility coefficient of pure gases in thermally untreated and treated TZPIM-1 at 35°C; a) CO ₂ , b).CH ₄	108
Figure 7.5: Diffusivity coefficient of pure gases in thermally untreated and treated PIM-1 at 35°C; a) CO ₂ , b).CH ₄	109
Figure 7.6: Diffusivity coefficient of pure gases in thermally untreated and treated TZPIM-1 at 35°C; a) CO ₂ , b).CH ₄	110
Figure 7.7: Permeability of pure gases in thermally untreated and treated PIM-1 at 35°C; a) CO ₂ , b).CH ₄	111

Figure 7.8: Permeability of pure gases in thermally untreated and treated TZPIM-1 at 35°C; a) CO ₂ , b).CH ₄	112
Figure 8.1: Sorption kinetics of pure gas experiment in polymeric membrane.....	115
Figure 8.2: Transient results of a) Diffusivity versus sorbed concentration of CO ₂ , b) Sorption isotherm at different temperatures.....	116
Figure 8.3: Permeation kinetics of pure gas experiment in polymeric membrane.....	117
Figure 8.4: Steady state results of a) Diffusivity versus sorbed concentration of CO ₂ , b) Sorption isotherm and c) Permeability at different temperatures.....	119
Figure 8.5: Comparison of Transient and steady state diffusivity at different temperatures.....	120

LIST OF TABLES

Table 2.1: Molecular weight and kinetic diameter of gases encountered in membrane gas separation [111].....	20
Table 3.1: Properties of PIM-1 and TZPIM films modified under different conditions.....	40
Table 3.2: Gas suppliers and purities used in this thesis work.....	42
Table 3.3: List of solvent suppliers and purity.....	43
Table 6.1: Dual mode parameters for pure CO ₂ and pure CH ₄ at 35°C.....	92
Table 6.2: Dual mode parameters for pure CO ₂ and pure CH ₄ in PIM-1 at different temperature..	93

NOMENCLATURE

A_D	Interaction of the vapor molecule and the microvoid
b	Langmuir affinity constant
B_D	Constant for diffusivity-FFV correlation
C	Penetrant concentration in the polymer (cm^3 (STP)/ cm^3 (pol))
C'_H	Maximum Langmuir sorption capacity
D	Fickian diffusivity (cm^2s^{-1})
D_O	Infinitely diluted Fickian diffusion coefficient
D_T	Thermodynamic diffusion coefficient (cm^2s^{-1})
f	Fugacity
FFV	Fractional free volume
F_R	Thermodynamic resistance
J	Flux (cm^3 (STP) cm^2s^{-1})
K_D	Henry's law constant
l	Half of membrane thickness
M	Mass of penetrant absorbed by the polymer
p	Pressure
P	Permeability (Barrer)
R	Universal gas constant ($\text{Jmol}^{-1}\text{K}^{-1}$)
S	Solubility (cm^3 (STP) cm^{-3} (pol) atm^{-1})
t	Time (s)
T	Temperature (K)
T_G	Glass transition temperature (K)
u	Velocity (cms^{-1})
V	Specific volume of the polymer (cm^3g^{-1})
V_o	Occupied volume of the polymer chains (cm^3g^{-1})
V_w	van der Waals volume (cm^3g^{-1})
W	Mass of membrane sample
x	Mole fractions in the feed
y	Mole fractions in the permeate
z	Distance from the membrane surface
α	Selectivity

θ	Permeation time lag (s)
μ	Chemical potential
ρ	Density (gcm^{-3})

1. General Introduction

Jean Antoine Nollet reported, in 1748, a pig bladder which is a natural membrane was more permeable to water than ethanol. This is considered as the first recorded description of semi-permeable membranes [1-3]. After this many experiments were carried out that indicate various gases passed through the same material at different rates, this concept plays important role in development of polymeric gas separation membrane [4].

Polymer-based gas separation membranes have many contributions towards a number of important energy and environmental technologies. Air separation, hydrogen recovery, natural gas sweetening [5, 6] and carbon dioxide capture [7, 8] are among the hot application areas of gas separation membranes which became widely applicable in the past two decades [9]. They have simple concept and operation which gives them an advantage of low cost and better energy efficiency.

There was a significant increase in gas separation membrane market since its beginning in the late 1970's and it is expected to continue growing in the future [10]. This is expected since there are different researches going on to develop new membrane materials for gas separation, with higher permeability and selectivity. According to Baker et al. [10] the market potential for membrane gas separation will double from \$350 million in 2010 to \$760 million in 2020. A milestone chart summarizing the development of membrane gas separation technology is displayed in Figure 1.1 [10].

Amine absorption technology was more abundantly used in separation of carbon dioxide from natural gas before introduction of membrane technology. Early membrane technologies show difficulties in achieving lower loss of methane during processing compared to amine absorption technique. Better membranes and improved process design have since improved the competitiveness of membranes in this area [12].

Membrane-based removal of natural gas contaminants is the most rapidly growing segment of the membrane gas separation industry, especially in applications for the separation of carbon dioxide, nitrogen, and heavy hydrocarbons. Improvements in polymer performance, membrane structure, module fabrication, and process design have all contributed to increasing the potential range of applications for membranes in natural gas treatment. Membranes now give natural gas producers an additional tool for upgrading the quality of the gas streams that they can deliver to the natural gas market [11].

Current carbon dioxide/Natural gas separating units use cellulose acetate membranes with carbon dioxide/methane selectivity of 15. Replacement of these membranes by polyimides or polyaramide with selectivities of 20-25 will certainly increase the membrane market share. If membranes with selectivities of 40 can be made commercially, membrane technology will replace most amine plants. Membrane materials with these selectivities have been reported in laboratory studies, so the issue is one of scale-up and commercialization [10].

Different materials are being used in membrane gas separation, either polymeric or inorganic. Polymeric membranes used for gas separation are generally asymmetric or composite and their transport mechanism is based on solution-diffusion model. These membranes, made as flat sheet or hollow fibres, have thin, dense skin layer on a micro-porous support that provides mechanical strength [13]. With respect to porous inorganic materials polymeric membranes show high but finite selectivity due to their low free-volume [14]. There are limited numbers of polymeric materials used for preparing at least 90% of the membranes in use [10] such as polysulfone, polyimide and silicone rubber to list some.

Polymeric membranes can be fabricated from either rubbery or glassy polymers. Rubbery and glassy polymers are categorized by the temperature at which the amorphous polymeric material is used.

Glassy membranes, which operate below the polymers glass transition temperature, have drawn more attention in recent research, because the more restricted segmental motions in glassy polymers enhance the “mobility selectivity” compared to rubbery polymers [15, 16]. For instance, glassy polyimide-based membranes have been proved to exhibit good separation performance and have already been used in many natural gas applications [10]. However, the implementation of CO₂ separation systems using glassy polymeric membranes poses significant challenges, including membrane plasticization, physical aging, thermal/chemical attack, and the influence of impurities such as water vapour, hydrocarbons, SO_x and NO_x [7].

Even though they cannot withstand high temperature and aggressive chemical environment, polymeric membranes represent a good solution for application in small to medium scale separation and non-stringent product purity requirement due to the low cost, ease of processing and low footprint requirements [11]. Many polymers can be swollen or plasticized when exposed to hydrocarbons or CO₂ at high partial pressure, which may reduce selectivity dramatically.

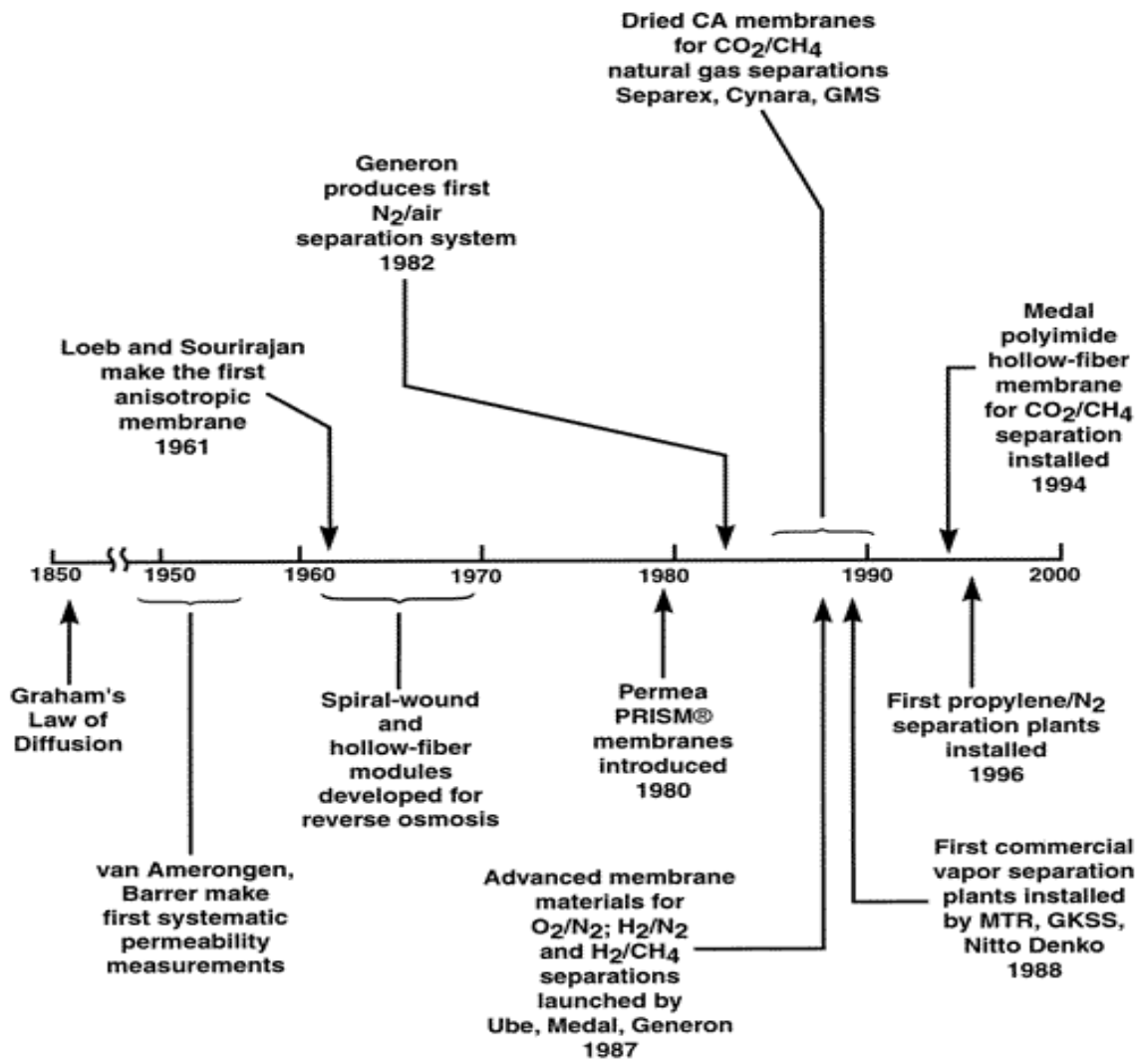


Fig 1.1. Milestones in the development of membrane gas separation [10].

Recently, new class of polymers of intrinsic microporosity (PIM) was reported by Budd et al [17] for different gas separation application. These materials have contorted ladder-like backbones which consist of spiro-centers and rigid fused dioxane rings that prohibit the relaxation of the porous structure. The rigidity of their structure gives rise to remarkable microporosity which gives high permeability and selectivity of gases, and allows locating PIM1 in the high performance region of Robinson's plot [18].

Du N et al reported a modified polymer of intrinsic microporosity using "click chemistry" [2+3] cycloaddition reaction to yield a novel PIM containing tetrazole group [19]. CO₂-philic tetrazole group added to the PIM structure via post-polymerization increases the solubility of carbon dioxide more than other gases. TZPIMs are of interest for their potential to yield both high CO₂ permeability

and high CO₂/light gas selectivity because of the presence of strongly CO₂-sorbing tetrazole heterocyclic rings bound to a highly porous polymer matrix.

Yavuz et al [20] reported amidoxime-functionalized PIM membranes using noninvasive functionalization to improve carbon dioxide capacity without adversely affecting physicochemical properties. Mixed gas permeability of CO₂/CH₄ mixture using this membrane is reported by Ingo et al [21] which shows there is an improvement in permselectivity of the membrane.

Our present aim is to study the mixed gas solubility and solubility selectivity of CO₂/CH₄ mixtures, in view of analysing their relevance in the removal of carbon dioxide from methane stream in natural gas processing or biogas purification using different glassy polymers. Carbon dioxide is the common contaminant of natural gas and must be removed to the level of <8% (usually <2%) to meet the quality requirements for CH₄ distribution pipelines, to minimize corrosion of the pipe line and improve the heating performance of methane [11].

Modelling of mixed gas solubility and solubility selectivity of CO₂/CH₄ mixture at different molar fraction of CO₂ and pressure is carried out using Dual mode sorption model and Non-equilibrium lattice fluid model. Studying the effect of physical aging through high temperature treatment to the glassy polymers is also a part of this research work. Transient and steady state diffusivity is also examined to show the difference in the results of diffusivity coefficient from pressure decay (sorption) and permeability experiment.

2. Literature Review

2.1. Introduction

This chapter comprises the relevant background and review of peer-reviewed research literature in the areas of membrane gas separation and its transport mechanisms in glassy polymers. Different technologies used for gas separation are studied in comparison with that of polymeric membrane gas separation. Advantages and disadvantages of polymeric membrane gas separation technology are presented briefly.

The transport mechanism of gases in different type of materials is introduced. The governing laws of transport mechanisms of gases in polymeric membrane are presented thoroughly. Solubility, diffusivity and permeability of gases in membranes are explained with literature review. Permselectivity which is the ratio between the permeability of the highly permeable gas to that of permeability of less permeable gas is explained. Permselectivity is due to diffusivity selectivity and solubility selectivity of gases in the polymer.

The solution diffusion model which is the governing principles in the transport of gases in dense materials is discussed. It says that the polymer is sorped at one side of the polymer (membrane), diffuse through the membrane and finally dissorpes at the other side of the membrane.

Permeability in high free volume glassy polymer is mostly due to solubility selectivity so this work mostly discusses about the solubility selectivity of CO₂/CH₄ mixture in different high free volume glassy polymers. The effect of one gas presence on the other gas solubility selectivity is also presented to show how it affects the solubility selectivity.

The effect of physical aging and temperature on solubility of gases in polymeric membrane is discussed in detail. The major problem of polymeric membranes is their aging through time which reduces the selectivity. In this work we tried to see the effect of physical aging on solubility coefficient of both CO₂ and CH₄ in different polymers.

The effect of temperature on solubility is described by Vant' Hoff equation in which the solubility coefficient decreases as the temperature increases. Enthalpy of sorption is calculated for all pure and mixed gas solubility coefficients and its value is negative which shows sorption experiment is exothermic process. Finally the objective of this research work (PhD Thesis) is presented in detail.

2.2 Different technologies for gas separation

2.2.1 Adsorption-based technologies

Since the invention of synthetic-zeolites in the 1940s, with the emergence of various adsorbents and the development of adsorption-based separation processes, adsorption has become a key gas separation tool in industry [22-24].

With the synthesis of more and more new sorbent materials with tailor-made porosity and surface properties and the urgent demand for green separation procedures, adsorptive separation will become increasingly more important. Thus, adsorptive separation will likely play a key role in future energy and environmental technologies [23, 26].

A general process of adsorptive gas separation or purification includes passing a gas mixture through a column packed with adsorbents or fixed-bed adsorbers to yield a product enriched in the more weakly adsorbed component. This is then followed by desorption of the strongly adsorbed component so that adsorbent can be reused [26]. The high separating power is the result of the continuous contact and equilibration between the gas and adsorbent. A number of such cyclic processes are available depending on the method of the adsorbent regeneration, including thermal swing adsorption (TSA) cycles, pressure swing adsorption (PSA) cycles, inert purge cycles, displacement cycles, and so on.

In adsorptive separation processes, gas separation is achieved based on the differences of adsorption capability of different components in the adsorbent. The performance of any such process is directly determined by the characteristics of the adsorbent in both adsorption equilibrium and kinetics [27, 28]. The related basic principles of adsorption are described in detail elsewhere [28- 30]. In addition to acceptable mechanical properties, a promising adsorbent should possess not only good adsorption capacity and selectivity, but also favorable adsorption kinetics and regenerability. To satisfy these requirements, the adsorbent should first have a reasonably high surface area as well as relatively large pore sizes for porous materials to allow adsorbate molecules to approach the interior surface. For instance, zeolites, with their uniform and somewhat tunable pores, have played a major role in the development of adsorption technology and are widely used in industrial separation [31, 32]. Notably, in practical separation processes, adsorbents often require binder materials to provide mechanical strength and to reduce the pressure drop in adsorbent columns. These inert diluents also

provide a suitable mesoporous or macroporous structure to facilitate transport of the adsorbate molecules from the external gas phase to the adsorbent pores.

Experimentally, at a given temperature, the adsorption quantity of a gas can be measured by an adsorption isotherm which is generally carried out by one of two methods: volumetric or gravimetric. The adsorption isotherm (namely equilibrium isotherm) characterizes the adsorption equilibrium, which is the foundation for the evaluation of adsorptive separation. The equilibrium isotherm is also the predominant scientific basis for adsorbent selection.

Commonly used materials for gas separation and purification in industry are mainly limited to four types: activated carbon, zeolites, silica gel, and activated alumina. Future applications of adsorptive separation depend on the availability of new and better adsorbents. “Ideally, the adsorbent should be tailored with specific attributes to meet the needs of each specific application” [26]. Exploitation of better adsorbents, especially those easily tailored, can thus improve the performance of the current industrial processes

2.2.2 Cryogenic separation

Cryogenic separation involves compression and cooling of gas mixtures at various levels to facilitate phase change of one gas along with constituents which can then be separated using distillation [33]. The advantages of this process are that no chemical absorbent is needed, can be operated at atmospheric pressure and its compatibility with both pre-and oxy-combustion carbon capture with easy transport of liquid CO₂ formed. Its draw backs are its feasibility at high CO₂ concentrations (450%), formation of ice or solid CO₂ clathrates in the presence of water vapor leading to serious plugging, pressure build-up issues and reduction of heat transfer rates due to thick CO₂ layers formed on heat exchange surfaces [34- 36].

Cryogenic separation of air is known from the early 19th century onwards. Cryogenic separations suitable for high CO₂/H₂S gases in natural gas were mostly employed for off-shore applications. Some of the noted processes patented are the Ryan Holmes method (1982) [37], the controlled freeze zone (CFZ) method (1985 at Exxon Mobil Upstream Research Company) [38, 39], the Cryocell method (developed by Cool Energy Ltd and tested in collaboration with Shell in Australia, Perth) [40], Twister technology (2004) [41] and the Sprex method (developed jointly by IFP, Total,

and Prosernat, 2007) [42]. It has been noted by Yongliang Li [43] that separation by the cryogen occurs due to decrease in its internal energy with increase in exergy and also it can be an efficient medium to recover heat due to their low critical temperature. Oxygen is produced commercially either by cryogenic distillation processor by adsorption based processes such as VPSA. The detail process for air separation using cryogenic separation is presented elsewhere [44].

2.2.3 Absorption process

Absorption with simultaneous chemical reaction is used widely to remove acid gases such as CO₂ and H₂S from hydrocarbon and inert mixtures. The chemical reaction can significantly increase the solubility of a gas, reducing the required solvent flow rate for a given removal specifications. Furthermore if the chemical reaction is fast enough, it increases the rate of absorption, thus increasing the over-all liquid-phase mass transfer coefficient and subsequently reducing the size of the required absorption column. If the solvent is reactive preferably toward one particular gas in a mixture, it can be used for selective removal [45].

At present, absorption is one of the most widely applied technologies for upgrading biogas [46]. Water and amine are the two representative absorbents for CO₂ capture [47]. For the water scrubbing process, the microbial growth on the surface of packing material and the low flexibility toward variation of input gas are the main drawbacks. In addition, water consumption is huge and the CO₂ cannot be recycled [48]. Amines are the widely used chemical solvents which can enhance CO₂ absorption rate and capacity. However, the degradation of amine, the high energy consumption during regeneration and the loss of the amine are the common problems [49].

Absorption based carbon capture employs physical or chemical inter-actions between the CO₂ and the absorbent [50, 51]. Solvents like rectisol, selexol, etc. are employed for physical absorption [34]. For chemical absorption, solvents like amines, alcohols and their compatible blends, liquid ammonia and alkalies like NaOH, K₂CO₃, and Na₂CO₃ are employed. Chemical absorption is widely employed due to higher capture efficiencies even at low concentrations of CO₂ and higher selectivity's [52- 58].

Physical absorption of gas or gas mixture components in a liquid solvent comprises mass transfer at the gas– liquid interface and mass transport within the phases. It depends on the gas solubility and

the operating conditions (e.g. pressure and temperature). A classic example of physical absorption of a gas into a liquid is the absorption of carbon dioxide (CO₂) into water (H₂O) – usual in the beverage industry. Chemical absorption, also known as reactive absorption (RA), is based on a chemical reaction between the absorbed substances and the liquid phase. It largely depends on the stoichiometry of the reaction, concentrations of the reactants and mass transfer rates.

Among them, chemical absorption (e.g., amine and hot aqueous K₂CO₃ solution) is effective for dilute CO₂ streams, such as coal combustion flue gases, which typically contain only about 10% - 15% CO₂ by volume [59- 61]. From the perspective of energy consumption, physical absorption (e.g., Selexol solvent) is typically used for CO₂ removal from syngas before combustion because it exhibits good absorption property at high pressure [62, 63].

Both these absorption methods have drawn considerable attention and have been applied in some demonstration projects because of their relatively high maturity and feasibility for large-scale utilization; however, these methods continue to present certain difficulties such as the stability of the solvents and the huge energy requirements for stripping CO₂ from the loaded solvent [63- 65].

A number of materials have the ability to absorb oxygen at one set of pressure and temperature condition, and desorbs it at a different set of condition. These materials used to separate air into its main component nitrogen and oxygen through absorption. MOLTOXTM is one of such materials investigated by Air products and Chemicals (Allentown, PA). The process is based on absorption of oxygen by a circulating molten salt stream, followed by desorption through combination of heat and pressure reduction of the salt stream [66].

Current research activities concerning reactive absorption for the removal of CO₂ and/or H₂S containing gases are mostly addressed to carbon capture and storage. When integrating amine scrubbers into a power plant, the energy requirements will increase enormously [67]. However, Rochelle [68] claims that amine scrubbing will probably be the dominant technology for CO₂ capture from coal-fired power plants in 2030. Hence, there is a huge potential for optimization which will require significant research work.

2.2.4 Membrane technology

Application of membrane technology in gas separation was introduced by Thomas Graham [69] in a study on permeation rate of different gases across a semi-permeable membrane. In the early 1980s, an industrial unit using amine columns for CO₂ and H₂S removal from a gas stream was installed incorporating polyimide (PI) membranes [70]. Some researchers have proposed combination of membrane and amine processes to make the process more effective and less expensive [11]. In 1981, the industrial membrane gas separation was initiated by Henis and Tripodi [71]. They coated a thin permeable polymer layer on the asymmetric membrane and fabricated a composite membrane suitable for gas separation.

There are three important operational variables affecting gas separation membrane process performance, including stage cut, transmembrane pressure and membrane selectivity [69]. In addition, many other factors have a crucial impact on membrane performance such as membrane material and structure, configuration (e.g., flat, spiral-wound, hollow fiber), membrane thickness and module and system design. Among others, membrane materials and structures have the strongest effect on membrane performance [72]. A wide range of materials are employed for fabrication of membranes. Metals, molecular sieves, polymers and glasses are the most widely used materials. The diversity of materials makes membranes applicable in a wide range of industrial separation processes, including air separation, hydrogen recovery, natural gas processing and light gas separations [73].

Molecular sieve membranes provide considerable discrimination based on size or shape of gas molecules by letting some of component gases to preferentially pass through. Structures of molecular sieves with their pores in the range of angstrom make them good candidates for use in gas separation. Their internal voids are made in different sizes and shapes of cavities and channels [74]. The properties of molecular sieve membranes such as high thermal and chemical stability, high mechanical strength as well as their high separation performances, make them exceptionally good candidates for harsh operational conditions. However, fabricating molecular sieve membranes of large surface areas for commercial exploitation is laborious and costly, thus hindering its large-scale industrial applications [75]. Difficulties in preparing a defect-free membrane as well as high manufacturing cost are major drawbacks for the large-scale implementation of inorganic membranes [76].

On the other hand, academic investigators and industrial suppliers have employed organic polymers as asymmetric nonporous membranes that offer many desired properties including low operating cost and ease of construction and excellent processability. Polymeric membranes, due to the trade-off relationship between selectivities and permeabilities, generally undergo an upper bound limitation. This upper bound for various binary gas pairs was first suggested by Robeson in 1991 [77]. The transition state theory also expressed the presence of a superior limit (an upper bound) [78]. For binary gas pairs, the slope of the upper bound limit remains constant because it is dependent only on the gas kinetic diameters. Typically, over the last two decades, many efforts have been made to elevate the upper bound limits for separation of various gas pairs using different materials [79]. Recently, Robeson again has collected empirical data for a number of gas pairs including O_2/N_2 , CO_2/CH_4 , H_2/N_2 , He/N_2 , H_2/CH_4 , He/CH_4 , He/H_2 , H_2/CO_2 and He/CO_2 to renew the upper bound limit. As a result, the upper bound line for various binary gas pairs exhibited only minor shifts [31]. The intercept of the upper bound is a strong function of the properties of the gases that permeate through the polymeric membranes. Robeson's trade-off curve for CO_2/CH_4 separation is shown in Fig. 2.1. [79]. This figure indicates that polymeric intrinsic microporosity fall close to or above the trade-off line. As well, it is indicated that polymers close to the upper bound are inherently rigid [80].

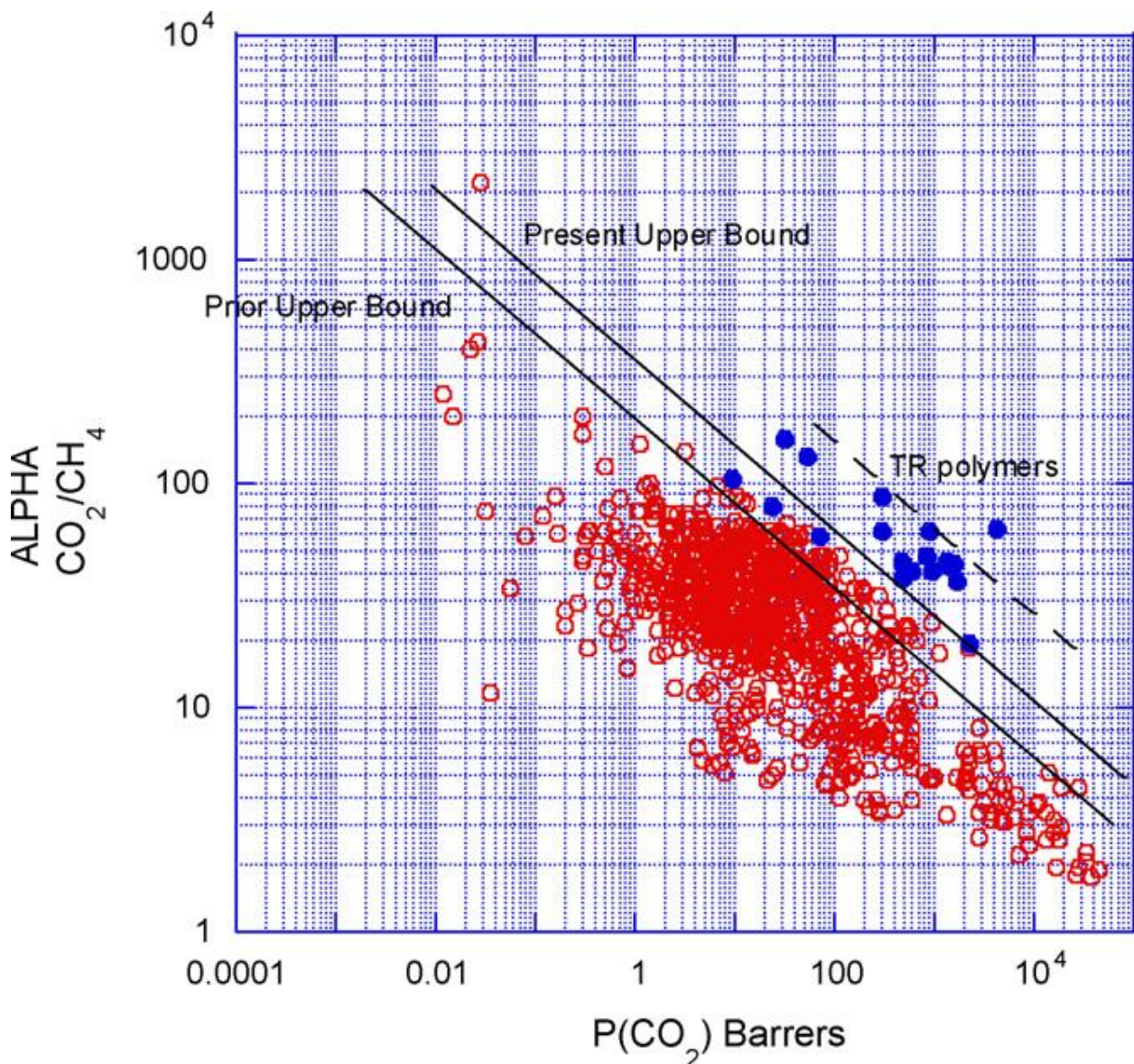


Fig. 2.1. Robeson “upper bound” correlation for CO_2/CH_4 separation (TR, thermally rearranged) [79]. Copyright 2008, Reproduced with permission from Elsevier Science Ltd.

Although there are many opportunities for membrane-based gas separation applications, as mentioned, current membrane materials cannot economically exploit these opportunities. Therefore, even today, many researchers are working on new emerging materials in order to develop novel membranes with higher separation performances [70, 81- 84]. The physical and chemical properties of materials should be considered in order to prepare suitable membranes. To improve current levels of membrane performance, different approaches have been employed such as polymer blending, grafting, crosslinking and mixing with proper molecular sieve fillers [85]. Although, the membrane technology is potentially more cost effective due to its lower energy requirement and simple operation, the urgent need to reduce the material costs propels researchers to expand the idea

of embedding nanostructured porous materials into the polymer matrix, which leads to an economic compromise.

2.3 Polymeric membrane for gas separation

Now days, polymeric membranes have many application in different significant scientific and technological areas such as tissue repair [86], protective garments [87], pharmaceuticals production [88], food and beverage packaging [89], microelectronics [90], sensors [91], fuel cells [92], water purifications [93], and gas and vapor separations [4, 94, 95]. The vital property for which membranes are utilized is their ability to adjust the permeation rate of a chemical component through the membrane with driving forces such as pressure, concentration, and electrical potential. Among these driving forces, pressure difference across the membrane is mostly used in ultrafiltration (UF), microfiltration (MF), reverse osmosis (RO), pervaporation (PV), and gas separation (GS) [96, 97].

Polymer based membrane gas separation is actually developing industrial membrane separation technologies, and the market size and number of applications served are expanding because it offers a number of advantages in terms of energy and capital cost. In principle, all films made of polymers can selectively separate gases from gaseous mixtures by the differential permeation of the components.

Current polymer-based membrane gas processes and potential applications include hydrogen separation and recovery from ammonia purge gas, refinery, and syngas stream in the petrochemical industry. Other applications include carbon-dioxide-enhanced oil recovery, natural gas processing, landfill gas upgrading, air separation (oxygen enrichment or nitrogen production), air dehydration, and helium recovery [98]. The market for polymer membranes for gas separation has expanded annually and sales of membrane gas separation systems have become an approximately \$500 million per year business. The primary reasons for the fast growth of membrane markets and sales include consumer demand for higher quality products, increased regulatory pressures, deteriorating natural resources, and the need for environmental and economic sustainability. The worldwide sales of all synthetic membranes are estimated at over \$2 billion. Since membranes account for only 40% of the total investment of a membrane separation system, the total annual turnover for the membrane-based industry can be estimated around \$5 billion. The annual growth rate in sales of all

membrane products has been estimated as approximately 12–15%. The gas separation market is a \$455 million per year business, totaling 24% of the whole membrane market. The future market will expand and further growth of this technology is expected for the next 10 years or so [99].

To select a suitable polymer membrane and design for each gas separation application, the nature of the polymer membrane (glassy or rubbery) must be considered as well as the target separating mixtures (permanent gas/permanent gas or condensable vapor/permanent gas). The main factors contributing to selectivity (solubility-selective or diffusivity-selective materials) can then be determined and used to improve separation efficiency with minimal loss of productivity. The most ideal membrane material design is to improve both diffusivity-selectivity and solubility-selectivity, but it is difficult to achieve both simultaneously. Moreover, for a given polymer membrane, both diffusivity and solubility depend strongly on process parameters such as pressure difference, feed composition, and temperature, as well as the intrinsic nature of the polymer. Each selectivity contribution (diffusivity or solubility) to total selectivity can be varied by such factors, but research has mainly focused on improving selectivity by modifying the polymer chain structure.

Diffusivity (or mobility)–selectivity reflects the ability of the polymer matrix to be selective for the shape and size of penetrant molecules. Diffusivity-selectivity is governed by relative penetrant mobilities and by structural factors such as polymer chain stiffness and intersegmental polymer packing. However, in contrast to inorganic or carbon molecular sieves with a controlled molecular size, polymer membranes are seldom considered as molecular sieves. If an organic molecular sieve with high selectivity can be prepared, it will have vast advantages over zeolites or carbon molecular sieves because of its easy processability, thin-film formability, and other significant reasons. Generally, improving gas separation performance by increasing diffusivity-selectivity is more effective for small gas separations that use rigid glassy polymer membranes such as polysulfones, polycarbonates, polyimides, and polypyrrolones with narrow free volume distributions. For small gas separations such as O_2/N_2 and CO_2/CH_4 , the diffusivity-selectivity needs significant advances in its permeability-selectivity properties [99].

The solubility coefficient reflects how many gas molecules can be sorbed in polymer membranes. It depends on the condensability as well as the physical interactions of the penetrants with the polymer membrane. Solubility is determined by the concentration of the sorbed gas per unit polymer volume. Generally, the concentration as a function of pressure at constant temperature shows a sorption isotherm with a characteristic shape that is concave to the pressure axis.

Solubility-selectivity is thermodynamic in nature and is governed by the relative polymer–penetrant interactions and the relative condensability of the penetrants. Solubility-selectivity terms contribute significantly to separations of condensable vapors and polar molecules [99].

An ideal gas separation membrane must have high permeability and high selectivity. The gas permeation properties of polymer membranes have been extensively studied and a wide variety of polymers have been synthesized to be more permeable and selective. Nevertheless, there are still strong trade-off relations of gas permeability and selectivity in polymer membranes that will not easily be broken in the future. Moreover, this tradeoff behavior of polymer membranes is not yet fully comprehended theoretically. However, it is believed that this trade-off behavior for specific gas pairs is unique and related to parameters of the gas molecules.

Recently, Budd et al. [100, 101, 102] and McKeown et al., [103] reported novel polymer membranes with intrinsic microporosity, PIM. These polymers show exceptional microporous structures, high gas permeability, and high permselectivity. Their rigid but contorted molecular structures hinder polymer chain packing and create free volume coupled with chemical functionality, providing strong intermolecular interaction. These PIM polymers are unique in that they have high surface areas ($500\text{--}1000\text{ m}^2\text{ g}^{-1}$) with micropore diameters in the range of $0.6\text{--}0.8\text{ nm}$ from the fact that microporous materials containing large surface areas of $300\text{--}1500\text{ m}^2\text{ g}^{-1}$ are mostly inorganic materials such as crystalline zeolites (aluminosilicates) and activated carbons. The oxygen and carbon dioxide permeabilities of the PIMs are in the range of $190\text{--}370$ Barrers and $1100\text{--}2300$ Barrers, respectively, and the PIMs exhibit selectivities significantly higher than any other high free volume glassy polymer membranes such as PTMSP and Teflon AF series polymer membranes. These materials are good candidates for applications such as the generation of oxygen-enriched air for enhanced combustion and fermentation processes or for the removal of carbon dioxide from methane.

TZPIM membranes, which are tetrazole attached PIM membranes, demonstrate exceptional gas separation performance, surpassing the most recent upper bounds of conventional and state-of-the-art polymeric membranes for the important gas pairs, such as for example the CO_2/N_2 separation. However, a substantial hurdle exists before polymeric membranes can be used for practical CO_2 separations, such as selective CO_2 removal from flue gas, biogas refining, and natural gas sweetening. In gas mixtures, the gas selectivity is typically much lower than permselectivity from single gas permeation data because of CO_2 plasticization and/or competitive sorption effects [104].

That is, CO₂ molecules cause the polymer matrix to swell, leading to increased permeability of the slower gas beyond its pure gas permeability and resulting in reduced selectivity [19].

Recently, Patel and Yavuz reported [20] an amidoxime-functionalized PIM-1 (AO-PIM- 1) prepared by rapid reaction of the nitriles with hydroxylamine under reflux conditions, introducing ample basic nitrogen and hydroxyl groups while maintaining high surface area (4500m²/g). Structurally similar to the monoethanolamine (MEA) used in power plant CO₂ scrubbing processes; the amidoxime functionality has been integrated into sorbents, including solution-processable porous polymers, with CO₂ capture properties surpassing those of activated charcoal [105, 106]. To date, however, the gas transport properties of membranes derived from such promising amidoxime-containing polymers have not been reported [21].

Rigid chain Si-containing polynorbornenes form a new class of highly permeable membrane materials in addition to polyacetylenes and amorphous Teflons AF [107]. Interesting feature of poly (3, 4-TCNSi₂) is the trend observed for permeation of hydrocarbons. In common glassy polymers increases in the size of penetrants result in decreases in permeability. Such behavior is explained by stronger effects of diffusivity and not solubility on the permeability coefficients [108].

2.3.1 Advantage of Polymeric membrane gas separation over other technologies

There are many noteworthy advantages of using membranes for industrial processes as compared with the conventional processes, as listed below [69]:

- ✓ Being reliable for consistent production with very high selectivity,
- ✓ Because membrane processes can separate at the molecular scale up to a scale at which particles can actually be seen, this implies that a very large number of separation needs might actually be met by membrane processes.
- ✓ No requirement for phase change or chemical additives, as a result, energy requirements will be low unless a great deal of energy needs to be expended to increase the pressure of a feed stream in order to drive the permeating component(s) across the membrane.
- ✓ There are no moving parts (except for pumps or compressors), no complex control schemes, and little ancillary equipment compared to many other processes. As such, they can offer a simple, easy-to-operate, low maintenance process option.

- ✓ Modular design and ease of scale up; requirement of small footprint as well as no requirement of large space,
- ✓ High efficiency for raw materials use and potential for recycling of byproducts. Membrane processes are able to recover minor but valuable components from a main stream without substantial energy costs.
- ✓ Substantially reduced equipment size,
- ✓ Easy integration into simple automation and remote control system, making its operation simple.
- ✓ Because of the fact that a very large number of polymers and inorganic media can be used as membranes, there can be a great deal of control over separation selectivities.
- ✓ Membrane processes are potentially better for the environment since the membrane approach require the use of relatively simple and non-harmful materials.

All of the above-mentioned advantages translate into cost savings and more environmentally friendly sustainable processes.

2.3.2 Disadvantage Polymeric membrane gas separation compared other technologies

- ✗ Membrane processes seldom produce 2 pure products, that is, one of the 2 streams is almost always contaminated with a minor amount of a second component. In some cases, a product can only be concentrated as a retentate because of osmotic pressure problems. In other cases the permeate stream can contain significant amount of materials which one is trying to concentrate in the retentate because the membrane selectivity is not infinite.
- ✗ Membrane processes cannot be easily staged compared to processes such as distillation, and most often membrane processes have only one or sometimes two or three stages. This means that the membrane being used for a given separation must have much higher selectivities than would be necessary for relative volatilities in distillation. Thus the trade-off is often high selectivity/few stages for membrane processes versus low selectivity/many stages for other processes.
- ✗ Membranes can have chemical incompatibilities with process solutions. This is especially the case in typical chemical industry solutions which can contain high concentrations of various organic compounds. Against such solutions, many polymer-based membranes (which comprise the majority of membrane materials used today), can dissolve, or swell, or

weaken to the extent that their lifetimes become unacceptably short or their selectivities become unacceptably low.

- ✘ Membrane modules often cannot operate at much above room temperature. This is again related to the fact that most membranes are polymer-based, and that a large fraction of these polymers do not maintain their physical integrity at much above 100°C. This temperature limitation means that membrane processes in a number of cases cannot be made compatible with chemical processes conditions very easily.
- ✘ Membrane processes often do not scale up very well to accept massive stream sizes. Membrane processes typically consist of a number of membrane modules in parallel, which must be replicated over and over to scale to larger feed rates.
- ✘ Membrane processes can be saddled with major problems of fouling of the membranes while processing some type of feed streams. This fouling, especially if it is difficult to remove, can greatly restrict the permeation rate through the membranes and make them essentially unsuitable for such applications.
- ✘ Permeability/ selectivity tradeoff for the system
- ✘ Physical aging of the membrane material which is caused through time and reduces permeability as well as selectivity of that polymer. Most glassy polymeric membranes are affected by physical aging since they are not at thermodynamic equilibrium.
- ✘ Plasticization of polymeric membrane when exposed to gases such as CO₂. As the concentration of gas inside a polymer increases, the polymer can swell, which increases free volume and chain motion that, in turn, increases gas diffusion coefficients and decreases diffusion selectivity.

2.4 Penetrant transport mechanisms

A membrane process is a separation process that covers a broad range of problems from particles to molecules and a wide variety of membranes are available to design a process. Although the membranes may vary in material (organic vs. inorganic) and structure (porous vs. nonporous) the

basic principle of membrane separation is the same. The separation process and mass transport through the membranes is a function of the membrane being used and the constituents being separated, and subsequently the theory used to describe the process and mechanisms. However, common for all systems is the principle illustrated in Figure 2.2 where a membrane is considered a permselective barrier, or interface between two phases, and the separation process takes place due to a specific driving force transporting a compound through the membrane from the one phase to the other.

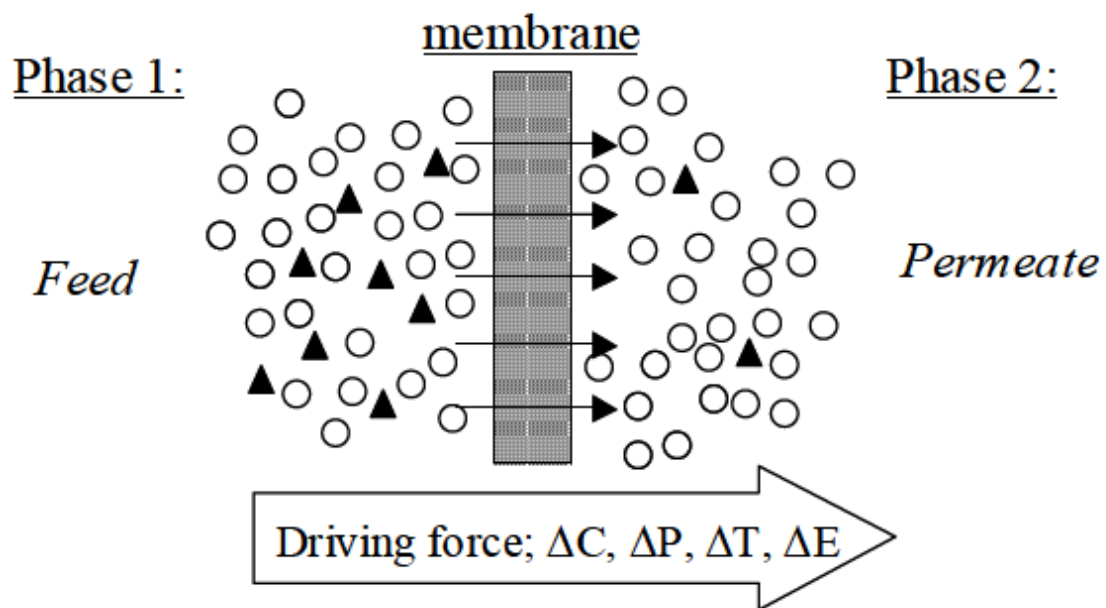


Fig. 2.2. Schematic of membrane separation process with different driving forces that are present

The separation of gas/vapor from a mixture using membranes can be achieved by any of the following three mechanisms (Figure 2.3), depending on the type of membrane used. For porous membranes, no separation can occur if the pores in the membrane structure are large enough to allow convective flow. However, when the diameters of pores are less than the mean free path of the gas molecules, Knudsen diffusion can take place. In this case, low molecular weight molecules can diffuse faster than heavier ones because of the greater interaction between these lighter species and the pore walls. Mass transport rates through Knudsen diffusion membranes can be enhanced by surface diffusion, in which molecules are absorbed onto the surface of the pores and diffuse along. The selectivity for any pair of gases is calculated by the inverse ratio of the square root of their molecular weight (Table 1). Generally Knudsen diffusion results in insufficient separation for CO_2 separation (selectivities for CO_2/N_2 and CO_2/H_2 are less than 1). Hence, a material with such pore

sizes is undesirable for making the membrane separation layer. For example, the mesoporous structure of alumina dictates a Knudsen diffusion mechanism in such materials, but alumina can find a use as a support for the membrane separation layer [109].

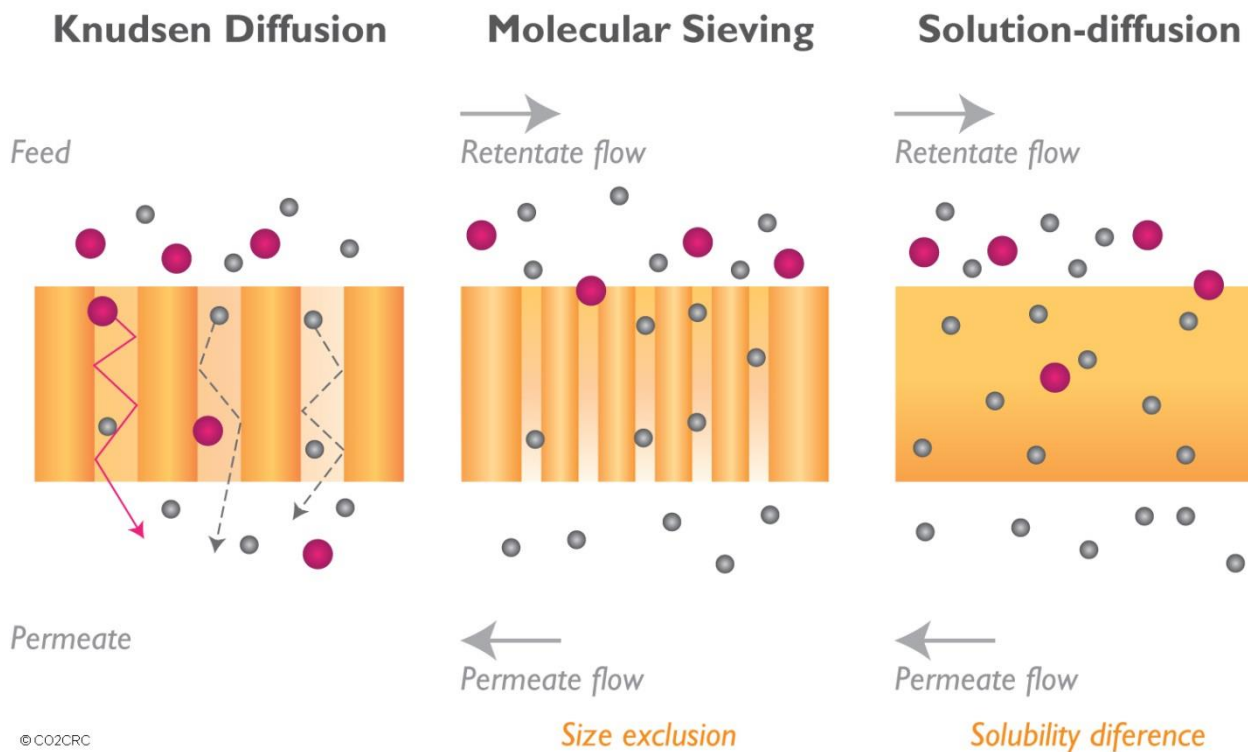


Fig. 2.3. Three different mechanisms for membrane separation [110].

Molecule	Molecular weight	Kinetic diameter (Å)
H ₂ O	18	2.65
H ₂	2	2.89
CO ₂	44	3.3
O ₂	32	3.46
N ₂	28	3.64
CH ₄	16	3.8

Table 2.1: Molecular weight and kinetic diameter of gases encountered in membrane gas separation [111].

For smaller pore sizes, molecular sieving is dominant. Large molecules in this case are restrained from passing through the pores. The size difference of molecules is used to achieve the separation.

However, a porous membrane based on the molecular sieving mechanism is difficult to commercialize, due to the difficulty of fabricating evenly distributed pore-size membranes. Further, the condensation of any vapor from the process stream will tend to block the fine pores which will significantly influence the performance of the membrane. Nevertheless, research on microporous membranes is continuing. One of the recent improvements include pyrolysis of polymeric compounds to synthesize a carbon material with a narrow pore size distribution less than 1 nm. Such a small molecular dimension makes it possible to separate gases with similar molecular size [112].

The transport mechanism exhibited by most of carbon membranes is the molecular sieving mechanism. The carbon membranes contain constrictions in the carbon matrix, which approach the molecular dimensions of the absorbing species [113].

While a porous membrane achieves separation via Knudsen diffusion, surface diffusion and molecular sieving, molecular transport through nonporous polymeric membranes occurs via a solution-diffusion mechanism [7]. The penetrant molecules dissolve into the retentate face of the membrane, diffuse through the bulk of the membrane and eventually desorb from the membrane at the permeate side due to the concentration gradient. Virtually all the modern commercialized solution-diffusion membranes are made of polymeric materials. Penetrant transport properties in this case are related to the solubility and diffusivity in the membrane.

The dependence of penetrant permeation upon both the solubility and diffusivity enables more flexibility in terms of refining the permeation properties. A physically larger molecule/compound (e.g. large organic molecules) can permeate faster than a smaller molecule if the respective solubilities are manipulated suitably in the appropriate polymer system [98]. Such a solubility selective mechanism is not possible in a Knudsen diffusion or molecular sieving process. Rubbery membranes with high permeabilities use this principle to achieve separation of higher hydrocarbons from small penetrant molecules such as nitrogen or hydrogen.

On the other hand, the separation of penetrating species in glassy polymeric membranes is dependent primarily on the penetrant's kinetic diameter. Penetrant molecules tend to move through gaps in the polymeric structure. These gaps are related to the free volume that the membrane exhibits due to the movement of polymer chains (caused by the pseudo-equilibrium in glassy polymers). A channel is "generated" between the gaps to allow penetrant molecules to "jump" from

one gap to another. The jumping motion can be considered as the way the penetrant molecules effectively diffuse through the membrane structure. The size and size distribution of the channels can be utilized to achieve selective transport [114]. As a result, diffusivity selectivity is the dominant factor in dictating glassy membranes performance and is used to separate light vapor/gases from larger molecules (e.g. CO₂ from N₂ and CH₄, and H₂ purification) [115]. Nevertheless, it should be noted that some exceptions can be found in the literature where the ultra-high permeability glassy polymers exhibit large organic vapor/small permanent gas selectivity (e.g. poly (1-trimethylsilyl-1-propyne, PTMSP [116]).

Therefore, when considering gas or vapor separation with porous membranes it is therefore important to determine which transport mechanism is dominant or controlling the mass transport.

2.5 Penetrant sorption and transport in glassy polymers

Polymer structure, pore size distribution, active layer thickness, and polymer packing morphology (symmetric or asymmetric) are important structural properties exhibited by a membrane. However, membrane performance is ultimately judged by two important characteristics: permeability and selectivity, which are directly governed by the membrane's intrinsic properties.

Permeability is a measure of the flux at which the penetrating species permeate through the membrane. It is related to the steady state flux, the chemical potential/pressure driving force, and the active layer thickness. If the active layer thickness is difficult to define, as in inorganic membranes and some hollow fiber or composite/asymmetric flat sheet membranes, permeance is also used. Permeance is independent of active layer thickness and related to permeability via:

$$\text{Permeability} = \text{Permeance} * \text{membrane thickness} \quad 2.1$$

Where Permeability is usually in Barrer ($10^{-10} \text{ cm}^3(\text{STP})\text{cmcm}^{-2}\text{s}^{-1}\text{cmHg}^{-1}$) and Permeance in GPU ($10^{-6} \text{ cm}^3(\text{STP})\text{cm}^{-2}\text{s}^{-1}\text{cmHg}^{-1}$).

In principle, the flux of the penetrant through the membrane is defined as the product of the concentration of the sorbed species in the polymer (C), and the penetrant velocity through the membrane (u). Thermodynamically, the transport of a penetrant is driven by the chemical potential

gradient across the membrane ($\partial\mu/\partial z$) against the thermodynamic resistance exhibited by the membrane (F_R).

$$J = C \cdot u = -\frac{c}{F_R} \cdot \frac{\partial\mu}{\partial z} \quad 2.2$$

Chemical potential can be defined in terms of fugacity, f :

$$\mu = \mu^{0(g)} + RT \ln(f) \quad 2.3$$

Hence the flux defined in the above equation can be expressed in terms of fugacity:

$$J = -\frac{c}{f} \cdot \frac{RT}{F_R} \cdot \frac{\partial f}{\partial z} \quad 2.4$$

Solubility (S) is defined as the concentration of penetrant sorbed in polymer divided by the fugacity in gaseous phase ($S = C/f$), while the thermodynamic diffusion coefficient (D_T) of a penetrant is defined as $D_T = RT/F_R$. The expression for flux then can be rewritten as:

$$J = -D_T \cdot S \cdot \frac{\partial f}{\partial z} \quad 2.5$$

The permeability coefficient is often defined as the product of the thermodynamic diffusivity and the solubility:

$$P = D_T \cdot S \quad 2.6$$

Hence, the permeability coefficient can be understood as the product of a thermodynamic factor and a kinetic factor. The thermodynamic factor is represented by the solubility, which is related to the critical temperature of the penetrant, polymer-penetrant interactions and also the free volume between the polymer chains [117]. The thermodynamic diffusion coefficient is the kinetic factor and strongly dependent upon the polymer-penetrant dynamics and the packing arrangement of polymer chains [118].

Fick's first law is also a common approach to describe the flux of a penetrant moving from regions of high concentration to regions of low concentration across a membrane:

$$J = -D \cdot \frac{\partial c}{\partial z} \quad 2.7$$

where D is the Fickian diffusion coefficient and is related to the thermodynamic diffusion coefficient by:

$$D = D_T \cdot \frac{c}{f} \cdot \frac{\partial f}{\partial c} = D_T \cdot S \cdot \frac{\partial f}{\partial c} \quad 2.8$$

The Fickian diffusion coefficient is equal to the thermodynamic diffusion coefficient only if $S \cdot \frac{\partial f}{\partial c}$ is equal to unity. This only occurs in ideal diffusion systems (i.e. constant solubility) where no penetrant-penetrant interactions or invariant penetrant-polymer interactions exist. In non-ideal systems where solubility varies with fugacity, unity can only be found at the theoretical limit of infinitely dilute conditions (i.e. $f = 0$).

2.5.1 Solubility

2.5.1.1 Gas sorption in glassy polymer

Gas sorption in a glassy polymer is often described by the dual mode sorption (DMS) model. This model presumes that there are two domains into which penetrant gas can sorb. Gas molecules are assumed to be absorbed directly into the polymer matrix via dissolution or adsorbed into micro-cavities within the polymer matrix. The dissolution of penetrant gas into the polymer matrix usually obeys Henry's law, which uses a linear proportional relationship between the solubility of a gas dissolving in a liquid and the applied pressure. This relationship has been found to adequately describe the concentration of gases in rubbery polymers at low concentrations [98]. The polymer matrix (the first domain) in glassy polymers is often referred as the Henry's law region whose sorption of gas penetrant follows:

$$C_D = K_D f \quad 2.9$$

Where C_D is the concentration in the Henry's law region, linearly dependent upon the Henry's law constant (K_D) and fugacity as shown in Figure 8.

The adsorption of penetrant gas in the micro-cavities with the polymer matrix usually follows the standard Langmuir relationship (Equation 2.10) and hence the second domain is often called the Langmuir region.

$$C_H = \frac{C_H' b f}{1 + b f} \quad 2.10$$

Where C_H is the concentration of penetrant gas in the micro-cavity region, dependent on the maximum adsorption capacity (C_H'), Langmuir affinity constant (b) and fugacity. The Langmuir affinity constant is the ratio of the rate coefficients of adsorption and desorption given by:

$$b = \frac{C_H}{(C_H' - C_H) f} \quad 2.11$$

A Langmuir sorption isotherm typically shows a rapid increase in concentration at low fugacity that gradually slows down until reaching a plateau, as shown in Figure 2.4.

Consequently, the concentration of penetrant gas in glassy polymer is described by the DMS model as follows, assuming that all the parameters are independent of penetrant concentration.

$$C = C_D + C_H = K_D f + \frac{C_H' b f}{1 + b f} \quad 2.12$$

The sorption isotherm described by the DMS model is the combination of the Henry's law sorption curve and the Langmuir sorption curve, and typically concave to the fugacity axis at low fugacities then approaching to a straight line as fugacity increases (Figure 2.4).

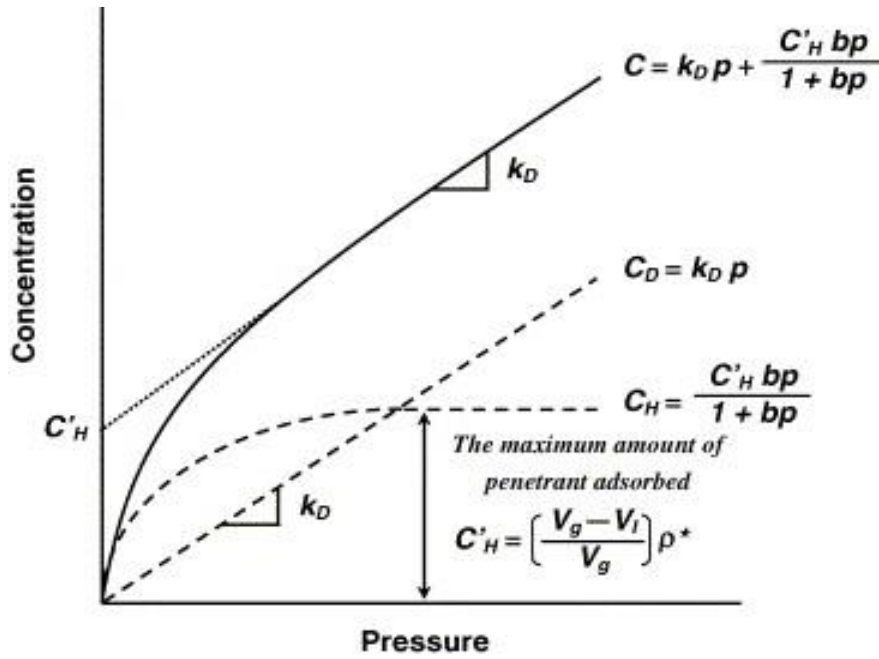


Fig. 2.4. Typical gas sorption isotherm in a glassy polymer represented by DMS model

2.5.1.2 Free volume in glassy polymer

As seen in Figure 2.4, penetrant sorption in the Langmuir regions is significantly larger than that in the Henry's law regions for low penetrant fugacities. These Langmuir regions are in fact the excess free volume that is created when polymer chains pack imperfectly in the glassy state. As illustrated in Figure 2.5, there are no packing defects within the free volume in the amorphous polymers that exist above the glass transition temperature (i.e. in rubbery state). As the temperature of the amorphous polymers decreases below the glass transition temperature (i.e. into a glassy state), the polymer segments lose the mobility to attain equilibrium and this leads to the formation of micro-cavities or microvoids within the polymer matrix [98]. In glassy polymers, the occupied volume of the polymer chains, the volume in the Henry's law region or polymer matrix region and the excess free volume (i.e. Langmuir sites or microvoid regions) are summed to form the specific volume of the polymer.

The specific volume is the reciprocal of the polymer's bulk density (ρ):

$$V = \frac{1}{\rho} \tag{2.13}$$

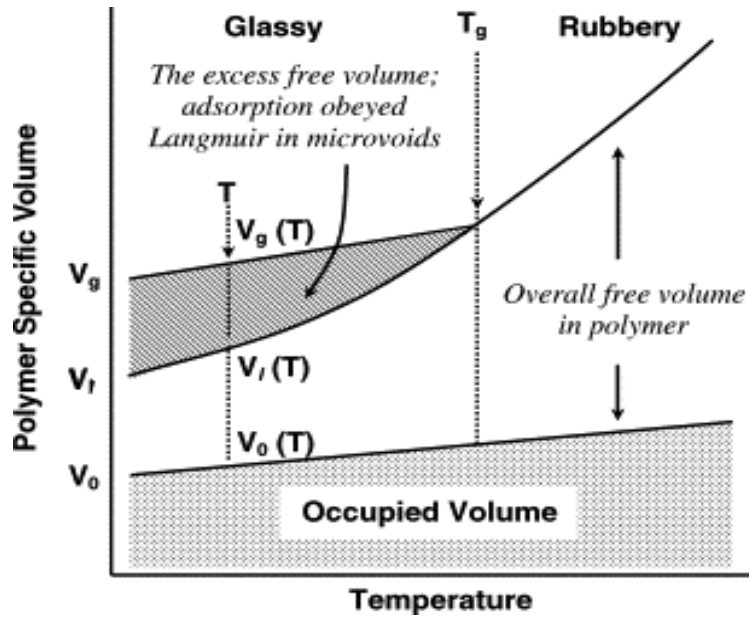


Fig. 2.5. The relationship between the polymer specific volume and temperature in amorphous polymers [119].

The fractional free volume (FFV) is well documented in the literature and is a determining factor in gas transport properties of a membrane, because it is a good measure of the space available within a polymer matrix for penetrant transport [120-123]. The free volume is simply represented as the difference between the specific volume of the polymer film (V , cm^3g^{-1}) and the volume occupied by the polymer chains (V_0 , cm^3g^{-1}). FFV is then expressed as:

$$FFV = \frac{V - V_0}{V} \quad 2.14$$

The occupied volume of the polymer chains is determined via a simple and popular approach proposed by Bondi [124], using the calculation of the van der Waals volume (V_W , cm^3g^{-1}) of the repeat unit of polymers and a group contribution method. Because V_W is estimated from the average atomic volume, it is not absolute and can vary with intermolecular forces, types of bonding and sometimes quantum mechanical factors. These variations are then corrected by the group contribution method which allows for the estimation of the polymer's molar volume [125]. Bondi's approach also postulates that

$$V_0 = 1.3V_W \quad 2.15$$

The factor 1.3 was derived by Bondi [124] based on the packing densities of molecular crystals at absolute zero. It was assumed to apply to all structures and functional groups.

Besides this group contribution theory, it should be noted that information on polymer's free volume magnitudes can also be obtain in other ways including X-Ray diffraction studies which experimentally estimate the mean spacing between polymer chains [98], and Positron Annihilation Lifetime Spectroscopy (PALS) which provides information on microvoid size, total void volume and the size distribution [126].

2.5.1.3 Competitive sorption in multi component system

When more than one penetrant component is present in the system, different types of penetrant molecules will compete against each other for adsorption sites. Koros et al. [127, 128] extended the dual mode sorption theory for multi-component systems to account for such competitive sorption effects. This approach assumes that the Henry's Law component of the polymer matrix behaves ideally and competitive sorption effects are only exhibited in the Langmuir sorption sites. The concentration of gas B within the membrane when two or more components are present is therefore:

$$C_B = C_{DB} + C_{HB} = k_{DB}f_B + \frac{c'_{HB}b_Bf_B}{1+b_Af_A+b_Bf_B+b_Cf_C+\dots} \quad 2.16$$

where b_A and b_C are the Langmuir affinity constant for component A and C respectively. The concentration of each component is reduced compared to the single gas case (Equation 2.11) and is heavily dependent on the relationship between the Langmuir affinity constants and fugacity of all components.

2.5.2 Diffusivity

Diffusion is the process in which penetrants are transported from one part of the membrane to the other as a result of random molecular motion driven by chemical potential/concentration/fugacity gradients. The diffusivity or diffusion coefficient is a proportionality constant that characterizes the relationship between the molar flux of the penetrant and the concentration gradient.

Diffusivity depends on the size of the penetrant molecules, the size of the microvoids and the size distribution of these voids in the polymer. Since FFV is the indication of the proportion of space between polymer chains (i.e. microvoid size and size distribution), it can be also correlated to the diffusivity of a penetrant according to Fujita's free volume theory [123, 129- 131]:

$$D = A_D \exp(-B_D/FFV) \quad 2.17$$

where A_D and B_D are constants. This correlation can be applied to structurally related polymers or a single polymer system with high accuracy [131].

2.5.3 Permeability

In the absence of chemical reaction between the gas and polymer, the diffusion of dissolved penetrant is the rate-limiting step in this process. The one-dimensional flux of gas A through the film in the x-direction (Fig. 2.5) can be described by Fick's Law [132].

$$N_A = -D \frac{dC_A}{dx} + w_A(N_A + N_P) \quad 2.18$$

where D is the gas diffusion coefficient in the film, C_A is the local concentration of dissolved gas and w_A is the weight fraction of gas A in the film; N_P is the flux of the membrane, which is typically taken to be zero. Consequently, the above equation reduces to, [133]

$$N_A = -\frac{D}{1-w_A} \frac{dC_A}{dx} \quad 2.19$$

The steady-state permeability of gas A, P_A , through a film of thickness l is defined as [132-134],

$$P_A \equiv \frac{N_A l}{p_2 - p_1} \quad 2.20$$

where p_2 and p_1 are the upstream (i. e., high) and downstream (i. e., low) pressures, respectively. Permeability coefficients are commonly expressed in Barrers, where

1 Barrer = $1 \times 10^{-10} \text{ cm}^3$ (STP) $\text{cm}/\text{cm}^2 \text{ s cmHg}$. Combining (2.19) and (2.20) and integrating from $x = 0$ ($C = C_2$) to $x = l$ ($C = C_1$), one obtains:

$$P_A = D_A \frac{C_2 - C_1}{p_2 - p_1} \quad 2.21$$

where D_A is the concentration-averaged effective diffusion coefficient in the range C_1 – C_2 :

$$D_A = \frac{1}{C_2 - C_1} \int_{C_1}^{C_2} \frac{D}{1 - w_A} dC = \frac{1}{C_2 - C_1} \int_{C_1}^{C_2} D_{eff} dC \quad 2.22$$

where D_{eff} is the local effective diffusion coefficient.

In general, it can be challenging to measure the average gas diffusivity directly. Instead, gas permeability and gas solubility are often measured independently, and gas diffusivity is inferred from these measurements, as described below. For simplicity, experiments are often designed so that $p_1 \ll p_2$ and, consequently, $C_1 \ll C_2$. In this limit, (2.21) reduces to:

$$P_A = D_A \times S_A \quad 2.23$$

where $S_A = C_2/p_2$ is the apparent sorption coefficient or solubility of penetrant A in the polymer. Therefore, by measuring the gas permeability at an upstream pressure of p_2 and solubility at a pressure of p_2 , one can calculate the average gas diffusivity D_A . As indicated in (2.22), this diffusion coefficient is an average over the concentration range 0– C_2 . The local effective diffusion coefficient D_{eff} , characterizing the penetrant diffusivity in the polymer at a penetrant concentration of C_2 , can be evaluated using an equation obtained by taking the derivative of both sides of (2.21) with respect to C [136].

$$D_{eff}(C_2) = \left(P_A + p \frac{dP_A}{dp} \right)_{p_2} \left(\frac{dp}{dC_2} \right)_{p_2} \quad 2.24$$

this requires the pressure dependence of the permeability and solubility to calculate D_{eff} .

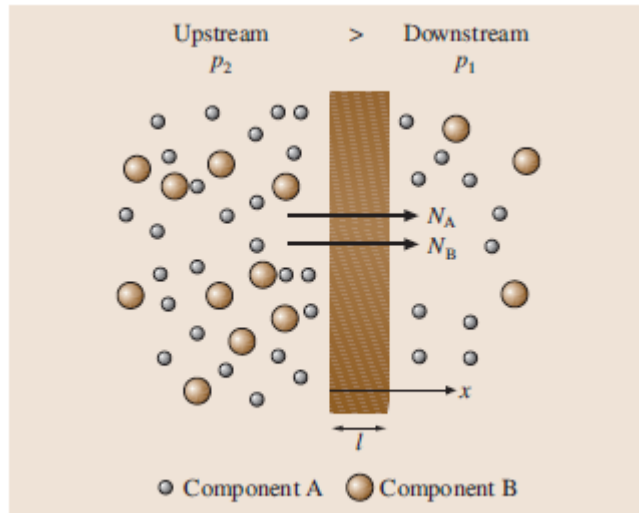


Fig. 2.6. Transport of gas A and B across a membrane [135].

2.5.4 Selectivity

A common parameter characterizing the ability of a polymer to separate two gases (e.g., A and B) is the ideal selectivity, $\alpha_{A/B}$: [137]

$$\alpha_{A/B} = \frac{P_A}{P_B} \quad 2.25$$

By combining Eqs. (2.23) and (2.25), permeability selectivity can be written as a product of solubility and diffusivity selectivity:

$$\alpha_{A/B} = \frac{D_A S_A}{D_B S_B} \quad 2.26$$

Like permeability, the ideal selectivity is often treated as a material property of a polymer.

Another measure of the ability of a membrane to separate a particular gas mixture is the separation factor, α^* , where x_i is the concentration of gas i in the feed and y_i is the concentration of gas i in the permeate [137]:

$$\alpha^*_{A/B} = \frac{y_A/y_B}{x_A/x_B} \quad 2.27$$

This value is less commonly reported in the membrane materials literature because it depends more sensitively on operating conditions (e.g., upstream and downstream pressure and feed gas composition) than $\alpha_{A/B}$. Thus, the separation factor is not a material property of the polymer being used as the membrane. However, when the upstream pressure is much greater than the downstream pressure, the separation factor becomes equal to the ideal selectivity. This relationship can be shown by recognizing that the mole fraction of component A produced in the permeate, y_A , is related to the flux of A and B as follows:

$$y_A = \frac{N_A}{N_A + N_B} \quad 2.28$$

An analogous relation may be written for component B. Substituting Eq. (2.28) into Eq. (2.27) and using the definition of permeability in Eq. (2.20) to solve for flux, the following expression is obtained:

$$\alpha^*_{A/B} = \alpha_{A/B} \frac{p_2 - p_1 \left(\frac{y_A}{x_A}\right)}{p_2 - p_1 \left(\frac{y_B}{x_B}\right)} \quad 2.29$$

Therefore, when the upstream pressure, p_2 , is much greater than the downstream pressure, the downstream pressure p_1 (e.g., if $p_1 = 0$ (i.e. vacuum)), $\alpha^*_{A/B} = \alpha_{A/B}$.

2.6 Physical aging

Glassy polymers are non-equilibrium materials having excess free volume due to kinetic constraints on polymer segmental motion that prevent such materials from coming completely to equilibrium properties (e.g., specific volume) once they are below their glass transition temperature. However, even in the kinetically constrained glassy state, polymers undergo at least local scale segmental motions, and these motions act to gradually increase the density of the polymer (and, therefore, reduce its free volume) toward the thermodynamic equilibrium value [138]. Physical aging slows over time for two reasons: (1) as the excess free volume gradually decreases the driving force for physical aging is diminished, and (2) as free volume is reduced, polymer chain mobility decreases, which decreases segmental motions available to assist in reorganizing the polymer chains. Physical aging reduces gas permeability and alters other physical properties of polymers (e.g., specific volume, enthalpy, entropy, etc.) [139-146]. The observed decrease in permeability, usually

accompanied by an increase in selectivity, is seen as a reduction in membrane flux over time. Recently, it has become widely recognized that physical aging also depends on the thickness of the polymer under study, particularly when the thickness becomes of the order of less than 1 micron. Gas separation membranes are often believed to be on the order of approximately 0.1 mm thick, making the effects of thickness on aging a relevant field of study [140].

Eq. (30) presents the most common framework used to describe physical aging [138,140]

$$\frac{dV}{dt} = \frac{-(V-V_{\infty})}{\tau} \quad 2.30$$

where the rate of change in the specific volume, V , of a polymer with time depends on the departure of the polymer's specific volume from its equilibrium value, V_{∞} , and the characteristic timescale for relaxation of the specific volume toward equilibrium, τ . The characteristic relaxation time is related to the mobility of the polymer chains, and it is typically taken to be a function of the specific volume of the polymer and temperature [140]. Additionally, the dependence of physical aging on sample thickness is typically accounted for by allowing s to vary with thickness, suggesting that molecular mobility of polymer chains near free interfaces may be greater, at least initially following the beginning of an aging experiment, than that of polymer chains in bulk polymer [140]. The fractional free volume is directly related to a polymer's specific volume, as discussed in Section 2.5.1.2. Therefore, as a polymer ages and fractional free volume decreases, gas permeability also decreases, albeit at slower and slower rates as time goes on, due to the self-retarding nature of physical aging. Because the losses in permeability and densification due to physical aging come from relaxation of the polymer matrix, they are thermally reversible, so losses in permeability (i.e., increases in density) can be restored by heating the polymer above its T_g [147].

Because of the relationship between free volume and physical aging, the aging of high free volume polymers has been a point of interest in the literature. In particular, the aging of PTMSP, one of the most permeable polymers known, has been widely studied [148-153]. Many of these studies have documented a rapid loss in gas permeability as a function of time, but the permeability of PTMSP films is also affected by contaminants, such as vacuum pump oil, that can lead to discrepancies in these measurements. In a study accounting for this contamination, PTMSP films with thicknesses of approximately 100 μm still showed significant physical aging [150]. Permeabilities of CH_4 , O_2 , and N_2 decreased by more than 20% over roughly 200 days. These films were first preconditioned in

methanol, increasing the initial free volume, which increases the driving force for physical aging [150]. In contrast, Pfromm and Dorkenoo found no loss in permeability in an 85 μm PTSMP film that was not pretreated with methanol; however, thin films with thicknesses of 1 and 3 μm showed 76% and 38% losses in N_2 permeability, respectively [140]. These results show the complexity of physical aging and the importance of membrane preparation conditions in physical aging studies.

The dependence of physical aging on thickness on physical aging has become a growing area of study. Physical aging rates increase substantially, as tracked both by gas transport and optical properties, as films approach sub-micron thicknesses [154-165]. For example, in polysulfone, significant deviation from the aging behavior in bulk films is seen once films become thinner than roughly 10 μm , while thicker films age at rates similar to bulk films [157].

2.7 Temperature dependence of transport parameters

Barrer [166] was the first one who showed that the diffusion of small-size molecules in rubbery polymers is a thermally activated process. A great number of data in literature suggest that the transport coefficients (namely P, D and S) depend on temperature, at a given pressure, via Arrhenius's and Van't Hoff laws on a narrow range of temperatures [167]:

$$S(T) = S_0 \exp\left(-\frac{\Delta H_S}{RT}\right) \quad 2.31$$

$$D(T) = D_0 \exp\left(-\frac{E_D}{RT}\right) \quad 2.32$$

$$P(T) = P_0 \exp\left(-\frac{E_P}{RT}\right) \quad 2.33$$

The pre-exponential terms represent the limit values of the various coefficients of transport for an infinite molecular agitation ($T \rightarrow \infty$). E_P represents the apparent activation energy for the permeation process and is equal to the sum of E_D , the apparent activation energy of the diffusion process, and ΔH_S , the heat of the solution needed for the dissolution of a permeant mole in the matrix:

$$E_P = E_D + \Delta H_S \quad 2.34$$

These parameters depend on the morphology of the polymer matrix: amorphous or semi crystalline structure, value of the temperature relative to the characteristic temperatures [168,169] such as T_g and T_f , etc. According to Gee [170], the heat of the solution, ΔH_S , may be expressed as:

$$\Delta H_S = \Delta H_{cond} + \Delta H_1 \quad 2.35$$

where:

- ΔH_{cond} is the molar heat of condensation, this term is always negative and small for gases [171];
- ΔH_1 is the partial molar heat of mixing. This is a small and positive term, which can be estimated from the cohesive energy densities of the penetrant and the polymer by using Hildebrand's theory [172].

For gases well above their critical temperature (such as H_2 , N_2 , O_2 at room temperature), ΔH_{cond} is very weak and, so, ΔH_S is governed by ΔH_1 . As the interactions are negligible, this term will be positive and S will increase with temperature [173]. For more condensable gases and vapours (e.g. CO_2 , SO_2 , NH_3 and hydrocarbons), ΔH_S is negative due to the ΔH_{cond} 's strong contribution and, for a given system, a decrease of the solubility will be observed with a temperature increase. This expresses the fact that the penetrant has more and more difficulties in condensing in the polymer when the temperature is raised. It is worth noting that by using the above relation, a positive value for ΔH_1 (endothermic solution) is always obtained. However, if one considers polymer-gas systems in which the molecular interactions are particularly energetic, ΔH_1 's value can become negative (exothermic solution) and cannot be calculated any more by means of this formula.

The activation energy represents physically the energy level that a molecule should reach to make a jump between one position and another one; it is always a positive quantity. As a consequence, D is an increasing function of the increased temperature. This effect may be expressed in terms of an increase in free volume directly related to the bulk expansion of the polymer due to the increased segmental motions and hence, the diffusion process of molecules is facilitated. Then, the value of the activation energy is all the more high as the cohesive forces between chains are strong. On the other hand, for a given polymer, the activation energy E_D increases with the penetrant size (it needs more space), and reaches an asymptotic limit when the penetrant mobility becomes comparable to that of the polymer segments [174, 175]. Experimentally, this theory was verified on numerous

penetrant-polymer systems [176] and the determined activation energies are included between 10 and 100 kJ/mol. Pre-exponential factor D_0 has an entropic character [177, 178] and takes into account the length jump and increases with the penetrant size. However, for a given polymer and at a fixed temperature, the diffusion coefficient always decreases with the diffusing molecule size.

2.8 Objective of the research

One important application of gas separation membranes is the capture of CO_2 from natural gas sweetening processes, pre- and post- combustion flue gases, and other possible carbon emission sources. The implementation of such gas separation systems poses significant challenges. One of them is the effect of one gas on the other gas sorption and permeation which deviates these properties from the ideal properties. This variation in transport properties of gases in polymers interests to get the real solubility and permselectivity rather than ideal solubility and permselectivity which doesn't represent the actual system in the market. Promising polymeric membranes for gas separation technology has been examined to study the solubility behavior of mixed gas CO_2 and CH_4 .

This literature review has shown that the performance of polymer of intrinsic microporosity membranes in dry gas service as well as gas sorption and transport phenomena is well understood. However, there no studies that have determined the mixed gas sorption and its transport properties with their effects on the solubility of other gas species. No results have been obtained under different molar fraction mixture and at different temperature because it is particularly difficult to perform this type experiments under such conditions in a laboratory.

Mathematical model developed in our group long time ago for single gas sorption also estimates the mixed gas sorption results with a good agreement with experimental results. This model can be used as a substitute in the absence of tedious and tiresome experimental results. Dual mode sorption model is also used to represent the data which expressed it very well so that this model can be used in the absence of experimental data.

Therefore the focus of this thesis is to:

- ✓ Describe the experimental methods and techniques used to obtain results presented in this thesis. This is detailed in Chapter 3.

- ✓ Carry out and analyze mixed gas solubility results for different polymers especially for polymers of intrinsic microporosity and its derivatives at different molar fraction and temperature. Here the results for solubility selectivity for both ideal and real case are examined. This work is detailed in Chapter 4 and 5.
- ✓ Study modeling of pure and mixed gas sorption experiments at different molar fraction and temperature with an increasing pressure up to 33 atm using Nonequilibrium Lattice fluid Model (NELF) and dual mode sorption model (DMSM). This is detailed in chapter 6.
- ✓ Show the effect of heat treatment, which increases the physical aging of polymeric membranes, on transport properties at different temperature. Chapter 7 provides an account for this study.
- ✓ Calculate and show the difference between transient and steady state diffusivity which are calculated from pure gas sorption and pure gas permeation experiment respectively. This study is presented in Chapter 8.
- ✓ Finally, consider the overall conclusions and suggestions for further work in Chapter 9.

3 Experimental methods

3.1 Introduction

This chapter describes the experimental methods and techniques used to acquire results presented in this thesis. It outlines the raw materials used in this work, as well as detailing the methods used for preparing membrane, and film drying. These preparation protocols were followed for each membrane sample fabricated for this study. Techniques for obtaining physical properties including membrane thickness and membrane density are shown.

Moreover, methodologies for determining membrane sorption, transport and permeation properties are described, including a detailed description of the mixed gas sorption measurement apparatus. The heat treatment procedure for the membranes studied in this work is also presented here.

It should be noted that this chapter aims to provide a basic description of all the methods and techniques so that all work reported herein could be reported. These descriptions however, are not intended to be the complete operating procedures, as these have been well described in the open literature.

3.2 Materials and membrane preparation

3.2.1 Polymers and polymer synthesis

Membranes were fabricated from a number of polymers of intrinsic microporosity and its derivatives and Polynonene. PIM-1, Tetrazole containing PIM (TZPIM-1) and Amidoxime-functionalized PIM-1 (AO-PIM-1) are the PIM based membranes that are examined in this work. These polymers were the focus of the thesis because of their promising results for gas separation industry.

Polymerization of PIM-1 was carried out in a Radleys LARA reactor equipped with an anchor-type stirrer. The glass reactor body was dried overnight at 100°C before use. 5,5', 6,6'-Tetrahydroxy-3,3,3',3'-tetramethyl-1,1'-spirobisindane (44.950 g, 0.1320 mol) and tetrafluoroterephthalonitrile (26.418 g, 0.1320 mol) were added to a 1-L vessel and the reactor flushed with nitrogen. Anhydrous dimethylformamide (DMF, 846 cm³) was added by double-ended needle under nitrogen. A stream of nitrogen was bubbled through the pale brown solution as it was stirred (300 rpm) at room temperature for 1 h, then the contents of the reactor were heated to 65°C over 30 min, under a nitrogen purge. The stirring rate was increased to 500 rpm and anhydrous K₂CO₃ (155 g, 1.123 mol, 8.51 mol equiv.) was added. An exotherm was noticed immediately after the addition (to 73°C), and an immediate color change to yellow was apparent. After 2 h, the stirring rate was reduced to 300 rpm, and the reaction mixture was then stirred at 65°C under a nitrogen purge for 68 h. The reaction mixture was cooled to 20°C then filtered, and the filter cake washed with DMF (300 cm³), acetone (300 cm³) and water (1 L). The yellow solid was stirred with water (4 L) in a 5-L vessel for 30 min. The solid was filtered off, and washed with water (2 L) and acetone (700 cm³). The filter cake was then washed with 1,4-dioxane (2 L in 100 cm³ portions), with frequent stirring. The solid was rinsed with acetone (700 cm³), and 10% water in acetone (semi-pure yield 57.77 g, 95.0%). To purify the batch further, the PIM-1 was washed on a sinter with water (4 L), acetone (600 cm³), 1,4-dioxane (4 L in 200 cm³ portions), acetone (600 cm³), water (1 L) and acetone (400 cm³), then dried overnight at 95 °C (final yield 55.53 g, 91.4%) [183,184]. The structure of PIM-1 is shown in Fig. 3.1.

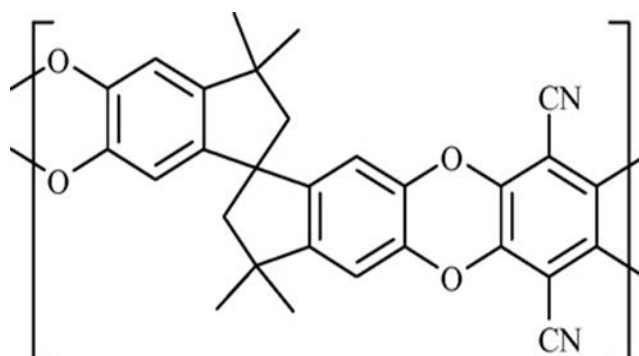


Fig. 3.1. Structure of PIM-1 polymer.

In order to synthesize TZPIM, PIM-1 was dissolved in NMP (1-3 g in 20 mL of solvent). NaN_3 and anhydrous ZnCl_2 with different mol equiv. versus the nitrile groups were added, and the mixture was stirred at 120 °C for different reaction times according to the conversion required (See Table 3.1) [180]. After cooling to 60 °C, 15 mL of diluted HCl (1:50 by volume in water) was added, and the reaction mixture was maintained at this temperature for 3 - 5 h. The PIMs thus obtained were then precipitated into excess 1 M HCl, filtered, washed on the filter with dilute HCl and water, and dried in a vacuum oven at 120°C. Elem. Anal. Calculated for $\text{C}_{29}\text{H}_{22}\text{N}_8\text{O}_4$ (the fully-substituted tetrazole TZPIM-3 from the 8 d reaction): N, 20.50%; Found: N, 19.14%. We used TZPIM-1 for this thesis work. The structure of TZPIM is shown on Fig 3.2 below.

Sample No	-CN/ NaN_3 / ZnCl_2	Reaction time	Conversion	M_n
PIM-1	/	/	0	58,000
TZPIM-1	1 : 4 : 2	2 d	55%	52,000
TZPIM-2	1 : 4 : 4	2 d	70.5%	45,000
TZPIM-3	1 : 4 : 4	8 d	100%	34,000

Table 3.1. Properties of PIM-1 and TZPIM films modified under different conditions

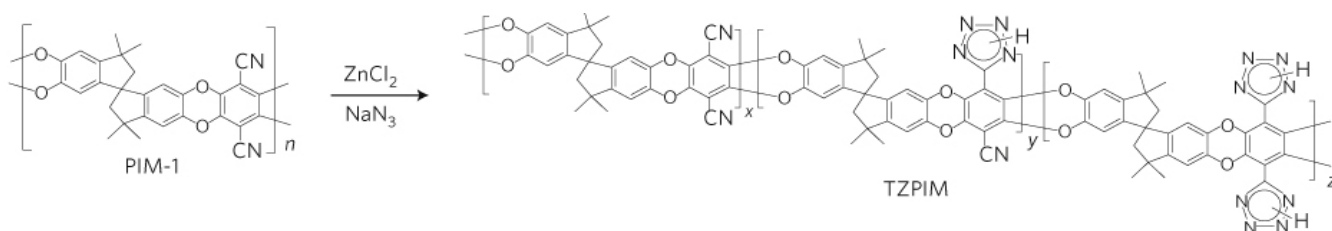


Fig. 3.2. Conversion of PIM-1 to TZPIM via the T2C3U cycloaddition reaction between aromatic nitrile groups and sodium azide, producing a tetrazole functional group [180].

The amidoxime-functionalized PIM-1, AO-PIM-1, (Fig. 3.3) was synthesized as previously reported [20] by dissolving 0.6g PIM-1 in 40mL THF and heating to 65°C under N₂. 6.0mL of hydroxyl amine were added drop wise and the mixture was refluxed at 69°C for 20h. The polymer was precipitated by addition of ethanol, filtered and washed thoroughly with ethanol, and then dried at 110°C for 3h to yield an off-white powder. Complete conversion of the nitriles to amidoxime groups was demonstrated previously for AO-PIM-1 prepared by this procedure [20, 21].

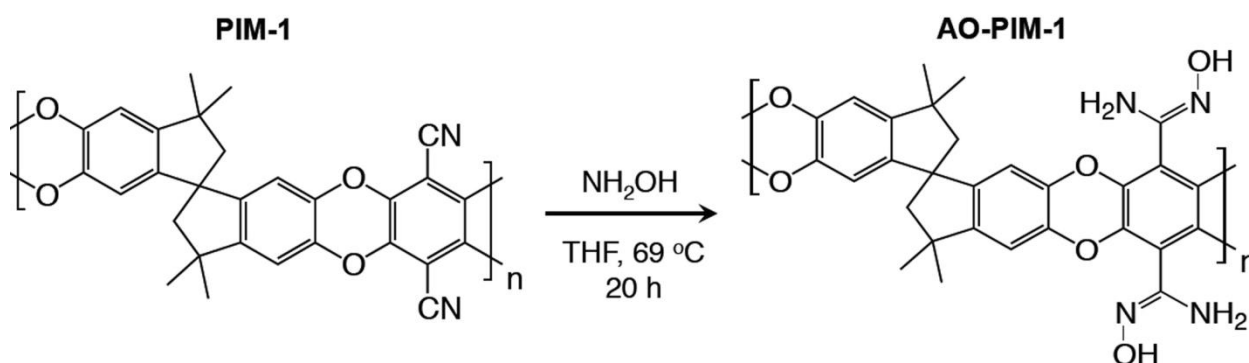


Fig. 3.3. Synthetic scheme for amidoxime-functionalized PIM-1(AO-PIM-1) [21].

Polynonene is polymerized by in a typical procedure (the example is given for ratio 3, 4-TCNSi₂/Pd (OAc)₂/B (C₆F₅)₃=3000/1/150), the 0.06M toluene solution of Pd (OAc)₂ (0.1 mL, 0.000556 mmol) and monomer (0.48 mL, 1.67 mmol) were introduced into round bottom glass ampule (5-10 mL) equipped with a magnetic stirrer preliminary purged in vacuum and filled with argon. Polymerization was initiated by adding of 0.09M toluene solution of B (C₆F₅)₃ (0.94 mL, 0.084 mmol). The reaction mixture was continuously stirred for 24h at ambient temperature. The polymers were precipitated by acidified ethanol (ethanol: HCl=10:1), separated, washed by several portions of ethanol and dried in vacuum. It was twice reprecipitated by ethanol from toluene solution and dried in vacuum at 80-90°C up to a constant weight [182]. The structure of the polymer is as given on Fig 3.4.

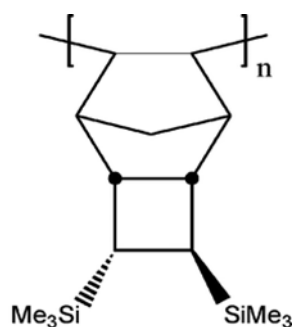


Fig. 3.4. Structure of poly (3, 4-TCNSi₂)

3.2.2 Gas supply and analysis

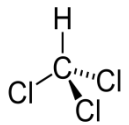
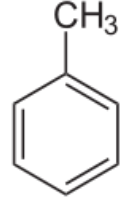
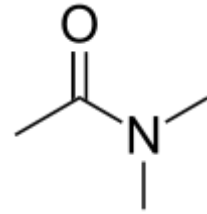
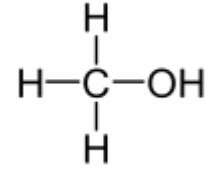
Gases were purchased from two companies, SIAD and RIVOIRA, and used without further purification.

Name	Supplier	Purity
Nitrogen, N ₂	SIAD	≥ 99.9%
Oxygen, O ₂	SIAD	≥ 99.5%
Methane, CH ₄	RIVOIRA	≥ 99.5%
Carbon dioxide, CO ₂	SIAD	≥ 99.5%
Helium, He	SIAD	≥ 99.998%

Table 3.2: Gas suppliers and purities used in this thesis work

3.2.3 Solvent analysis

Solvents were used as received from the suppliers, with purities detailed below.

Name	Structure	Supplier	Purity
Chloroform		SIGMA-ALDRICH	≥ 99.5%
Toluene		SIGMA-ALDRICH	≥ 99.7%
DMAc (Dimethylacetamide)		SIGMA-ALDRICH	≥ 99.5%
Methanol		SIGMA-ALDRICH	≥ 99.9%

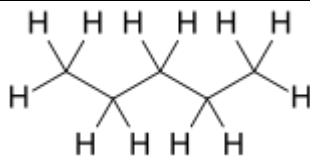
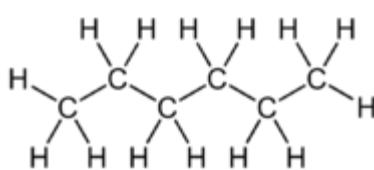
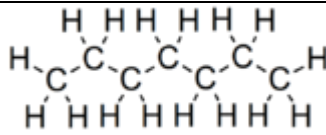
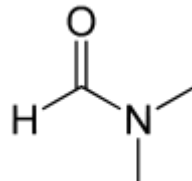
Pentane		SIGMA-ALDRICH	$\geq 99.0\%$
Hexane		SIGMA-ALDRICH	$\geq 95\%$
Heptane		SIGMA-ALDRICH	$\geq 99.0\%$
DMF (Dimethylformamide)		FLUKA	$\geq 99.5\%$

Table 3.3. List of solvent suppliers and purity

3.2.4 Preparation of dense polymeric films

PIM-1 ($M_w = 53000$ Da) membrane was prepared with solvent evaporation method from a filtered ca. 2.0 wt.% chloroform solution, which was poured into a FEP-coated Petri dish and partially covered. Chloroform (Riedel de Haen, stabilized, 99.0-99.4%) evaporated from the solution after ca 3 days under the ambient air conditions; the membrane was then placed into a vacuum oven (70 °C, vacuum) for 24 hours. Mass of the membranes was checked over time until it was found to be time-invariant. The polymer was then submerged in liquid methanol for 2 hours, cut into pieces and dried under vacuum for 12 hours at 70 °C. This method of preparation of the membrane is a modification of that of M. Guiver et al. [179], in which the final drying is performed under air at 70 °C. The procedure is shown in Figure 3.5.

Dense polymer films of TZPIM for gas sorption measurements were prepared from 1-2 wt% solutions in DMAc. Solutions tetrazole-modified PIM were filtered through 0.45 μm polypropylene filters and then poured onto Teflon Petri dishes in a vacuum oven at 80°C and allowed to evaporate slowly for 1 day. After several washes in water, the membranes were soaked in methanol and dried in a vacuum oven at 120°C for 24 h

The membrane film for AO-PIM-1 is produced by dissolving the polymer in a solution of dimethylacetamide (DMAc) (2–3% w/v) and then filtered with 1.0- μm PTFE cartridges. Isotropic films of AO-PIM-1 were obtained by slow evaporation of the solvent at 45°C from a Teflon petri dish. After 2 days, the dry membranes (80–100 μm) were soaked in methanol for 24h at ambient conditions, air-dried, and then heated at 120°C for 24h under high vacuum to remove any DMAc trapped in the micropores.

Polynonene membranes were prepared by evaporating toluene from c.a. 1 wt. % solution of exo, endo-3, 4-bis(trimethylsilyl) tricyclononene [182], abbreviated as Poly (3, 4-TCNSi₂), in a Teflon FEP-coated Petri dishes. When toluene evaporated, the membrane was kept under vacuum at 35 °C for 1 day and then used for measurements. The membrane produced is with the thickness of (85 \pm 10) μm .

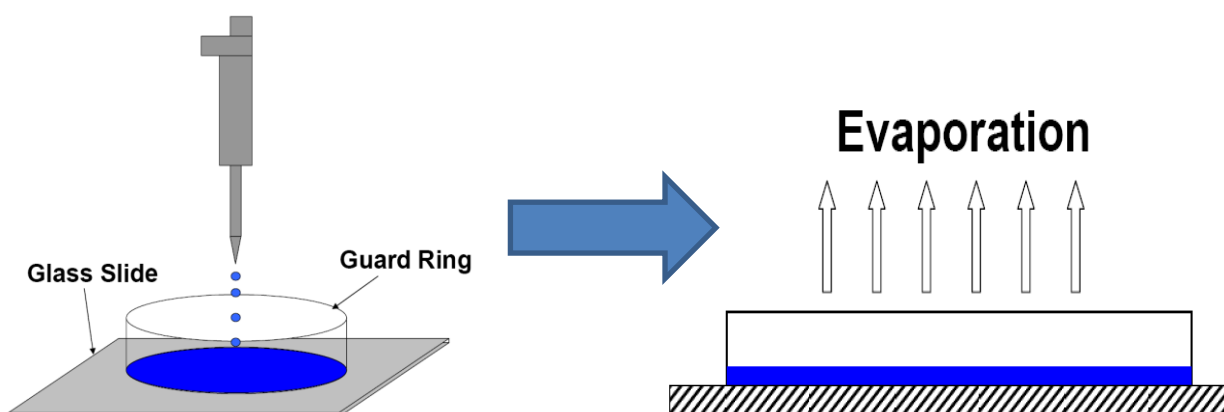


Fig. 3.5. Solution casting/solvent casting procedure.

3.3 Measurement of Physical properties

3.3.1 Membrane thickness

The thickness of the membrane is measured using Varner caliper having an accuracy of 0.001. The measurement is taken at 10 different internal positions of the given membrane film and the average is taken as the thickness of the sample. The variation of each sample is used to calculate the standard deviation of the measurement from the average value. The thickness considered in this thesis work is in the range of 50-110 μm .

The central part of the membrane film is considered during the measurement of thickness. This is because the peripheral part is thicker than the inside part. The sample for the measurement of sorption and permeation is also taken from the inside part as can be seen from Figure 3.6. The circular shaded area is 5mm wide.

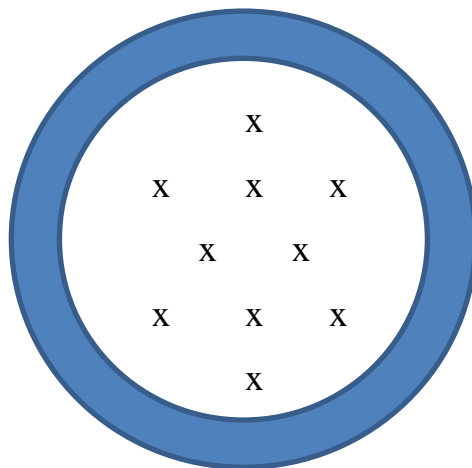


Fig. 3.6. The location pattern of thickness measurement, where the circular shaded edge is 5 mm wide.

3.3.2 Membrane density

The buoyancy technique is a standard displacement technique for measuring bulk membrane densities and is adopted widely in the literature [185-187]. Dense membrane samples were weighed using a Mettler Toledo AB204-5 top loading balance. Samples were weighed in air (W_{air}) and then in solvent ($W_{solvent}$). Water is used as a solvent to measure the density of PIM-1 and Heptane is used for the density measurement of TZPIM-1. The density of the polymeric film was then calculated by:

$$\rho_{polymer} = \left(\frac{W_{air}}{W_{air} - W_{solvent}} \right) \rho_{solvent}$$

3.4 Heat treatment of Polymers

Heat treatment which is applied to the membranes to enhance the physical aging is applied using a vacuum oven. The process starts from room temperature and the temperature increases slowly to the temperature of heat treatment. Then the sample stays at this temperature for 24 hr under high vacuum. The temperature decreases slowly to room temperature to reduce the effect of quenching

due to sudden drop of temperature. The sample then put in the sorption equipment and put under vacuum overnight at the temperature of experiment.

3.5 Measurement of Penetrant transport properties

3.5.1 Experimental set-up

Sorption experiments were performed using a self-developed pressure decay apparatus, which was designed in a similar way as that introduced by Sanders et al. [188]. The schematic picture of the setup is shown in Fig. 3.7, the experimental methods of measurements were described in paper [189] published in our group and presented also here un section below. The apparatus was constructed of stainless steel combined with aluminium face-seal gaskets (Swagelok). The apparatus was equipped with the Honeywell STJE absolute pressure gauges of the full-scales of 500 psia and with the gas chromatograph Varian CP-4900 Micro-GC equipped with the capillary column (Varian PoraPLOT U, length 10 m, inner diameter 0.32 mm) and with the thermal conductivity detector. The column was maintained at 80 °C, the column-inlet helium pressure was maintained at 90 kPa. The main part of the apparatus, which is separated from the surroundings with the valves V1, V5 and V6, was fully submerged in a water bath so that the pressure gauges remained above the water surface. The temperature of the water was maintained at the temperature of the experiment with the Techne TE-10D circulator and checked with a mercury thermometer having the same precision. The oil-sealed rotary vacuum pump Edwards RV3 was used.

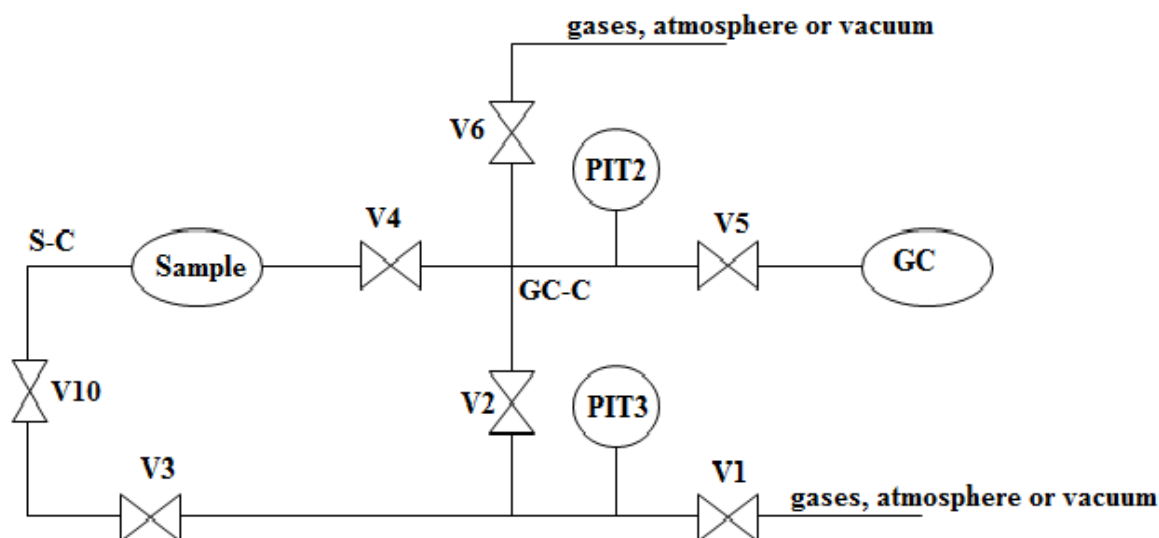


Fig. 3.7. Schematic drawing of pressure decay used for pure and mixed gas sorption experiment

Pure gas CO₂ and CH₄ permeability in the films was investigated by means of a closed-volume manometric apparatus, already described elsewhere [190, 191]. The device contains two identical permeation cells which can operate simultaneously, both placed in an incubator with PID temperature control to within $\pm 0.1^\circ\text{C}$. The schematic diagram of permeation equipment used for this work is shown in Figure 3.8.

The permeation system is composed of a high-pressure, upstream section and a low-pressure, downstream side, which are separated by a leak-proof tightened stainless steel cell where a circular sheet of sample is placed; a constant pressure difference is maintained across the sample and the amount of mass permeated is calculated from the otherwise negligible pressure increase in the downstream volume. Before each experiment, the samples were kept under vacuum for a minimum of 12 h at the temperature of the experiment, in order to ensure that any residual gaseous or vapour components within the sample were evacuated.

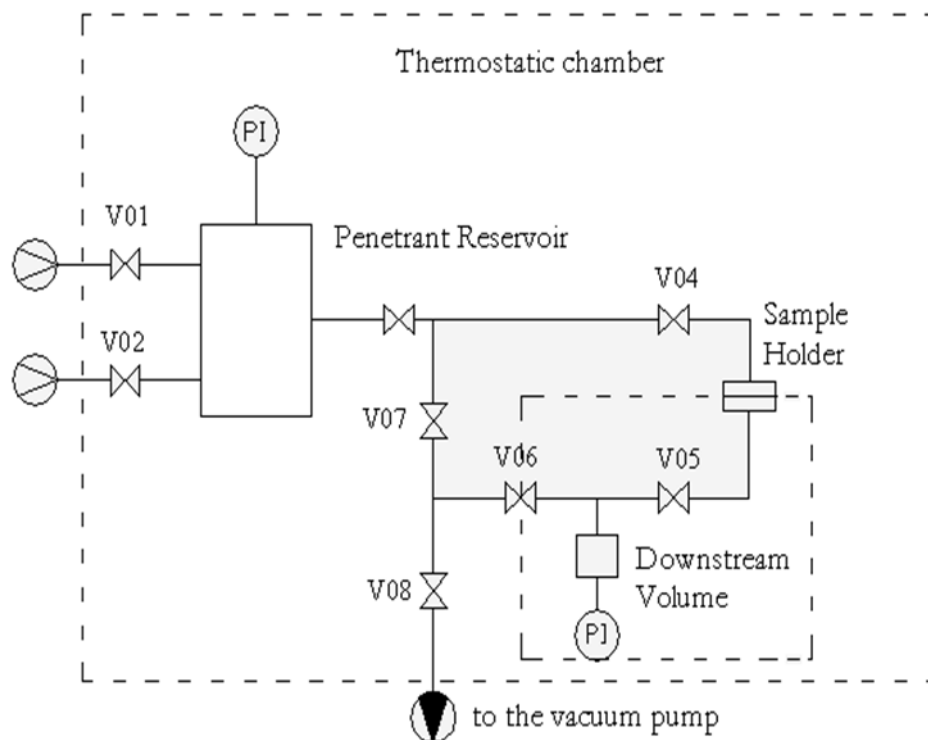


Fig.3.8. Layout of permeation apparatus.

3.5.2 Pure gas sorption measurement

The whole apparatus was kept under vacuum for at least twice the equilibration time before every pure gas sorption experiment. A series of pure-gas integral sorption steps was conducted by expanding the measured gas from the chamber V2456 (separated with valves V2, V4, V5, V6) into the evacuated volume with the sample (separated with V4, V7). Pressure track was acquired with the gauge PIT 2. When the time-invariant pressure was reached, the apparatus was vented to the atmosphere and evacuated. Sorption of pure methane and carbon dioxide was found to be reproducible within the experimental accuracy when prolonged time of desorption under vacuum was applied and when high pressure experiment (with methane and with carbon dioxide) was conducted before the pure methane and before carbon dioxide sorption experiment. Reproducibility of sorption of carbon dioxide was checked within the entire time of experiment (ca. 4 months), as the pure carbon dioxide sorption experiment is a part of the experimental procedure, and was found to be reproducible within the maximum experimental accuracy which is 20%.

3.5.3 Mixed gas sorption measurement

The whole apparatus was kept under vacuum for at least three hours before every mixed gas sorption experiment. Four methods of measurement were used in order to measure the sorption of mixed gases under all combinations of pressure and molar fraction of carbon dioxide in the gaseous phase. The methods were described in detail earlier [189]; schematic description is provided here.

In the first method, carbon dioxide was filled into V2456 and the volume with the sample was kept under vacuum. The separating valve (V4) was then quickly opened and gradually closed when time-invariant pressure was reached. The volume V2456 was then evacuated and filled with methane up to the desired pressure and V4 was then opened. The equilibration was terminated with the fast closure of V4 when time-invariant pressure was reached, but never earlier than 38 hours. The equilibrium gaseous mixture was then expanded into the helium-purged and evacuated volume that is separated with valves V1, V2 and V7. The sample chamber and V2456 were then evacuated, V4 was closed and a sequence of three samples was taken through V2 into V2456. The pressure of each sample in V2456 was set to 3 psia; helium was then added to the total pressure of 35 psia. The mixture was incubated for one hour and analyzed by means of the gas chromatograph. The method

of quantification of molar fractions of the components of the gaseous mixture was described in earlier work [189].

The second method stands for the modified first method, in which the expansion of carbon dioxide from V2456 into the sample chamber is replaced with the direct equilibration of pure carbon dioxide in the sample chamber up to the desired pressure. The valve V4 is then gradually closed and the next steps follow the first method.

The third method consists of a modification of the second method, in which carbon dioxide is firstly equilibrated with the sample and V4 is gradually closed. The volume V2456 is then filled with carbon dioxide or with methane up to the desired pressure. The second gas is then added into V2456 up to the desired time-invariant pressure. The valve V4 is then opened and the next steps follow those of the first and second method.

The fourth measuring method consists of a modification of the third method, in which methane is equilibrated firstly with the polymer at the desired pressure and V4 is gradually closed. The mixture of desired pressure and composition is then prepared as in the third method. The valve V4 is then opened and the next steps follow those of the previous methods.

3.5.4 Pure gas permeability measurement

Single gas permeability was measured on a constant volume, variable pressure (CVVP) gas permeation apparatus as detailed in Minelli et al [190, 191] (Figure 3.8). The feed gas was supplied at a fixed temperature and pressure to the membrane cell. The permeate side of the membrane consists of a known calibrated volume which was initially evacuated. Before determining the permeability, the known calibrated volume was isolated from the vacuum to evaluate the rate of air leaking from the ambient through fittings between tubes and valves, by monitoring the rate of pressure increase in the calibrated volume (under zero pressure drop). The feed gas at desired pressure was then preheated before proceeding to the membrane cell. The pressure increase in the permeate side due to the permeation of gas across the membrane was monitored. Permeability is then calculated using:

$$P = \left(\frac{\partial p_d}{\partial t} \right)_{t \rightarrow \infty} \frac{V}{RT} \frac{l}{A(p_u - p_d)}$$

Where

p_u is upstream pressure

p_d is downstream pressure

R is universal gas constant

T is temperature of the system

V is downstream volume

l is thickness of the membrane sample

The fickian diffusion coefficient is calculated from time lag using the following formula;

$$D = \frac{l^2}{6t_L}$$

Where

l Membrane thickness

t_L Time lag found from tangent of steady state pressure gradient towards time axis.

Solubility coefficient in this experiment can be calculated from solution-diffusion model described in section 2.5.3 from permeability and diffusivity coefficients calculated above.

4 Mixed gas sorption in PIM-based polymers

4.1 Introduction

Due to their good performance, PIM-based polymeric membranes are promising for natural gas sweetening, CO₂ capture and many other applications. Among the most important features of PIM-1 are: (i) relatively high gas permeability with good perm selectivity, which leads to data points on or above Robeson's upper bound [18] for several important gas pairs and help to define the recently revised upper bounds [79]; (ii) extremely high solubility coefficients (iii) large free volume as measured by independent probe methods; (iv) low activation energies of permeation; and (v) strong sensitivity of the transport parameters to the protocol of film-forming procedure.

In this chapter pure and mixed gas sorption of CO₂ and CH₄ at different temperature and pressure is discussed. Three PIM- based membranes are considered in this work, Polymer of Intrinsic microporosity-1 (PIM-1), Tetrazole containing polymer of intrinsic microporosity-1 (TZPIM-1) and Amidoxime functionalized polymer of intrinsic microporosity (AO-PIM-1). As cast polymer film membranes are used for the sorption experiment as discussed in the Chapter 3 of this thesis work.

Solubility selectivity which is the main property measuring for high free volume glassy polymers is discussed with comparison between the polymer considered at different temperature and pressure. Solubility selectivity is the ratio between the solubility coefficients of highly sorbed polymer (in our case CO₂) to that of less soluble gas (CH₄) as explained in chapter 3.

Finally temperature dependence of solubility in PIM-based polymers is considered for discussion. Comparison of pure and mixed gas sorption of CO₂ and CH₄ in these polymers is also the part of this chapter. Finally depending on the results found in this chapter conclusion will be drawn.

4.2 Pure gas sorption in PIM-based polymers

Sorption results are represented using well-known solubility isotherms which are concave in shape towards the pressure axis. Pure CO₂ sorption in PIM-1 membrane is shown in Fig 4.1a and pure

CH₄ sorption result is shown in Fig 4.1b at 25°C. The same type of isotherms are obtained at different temperature and for different polymers studied in this thesis work.

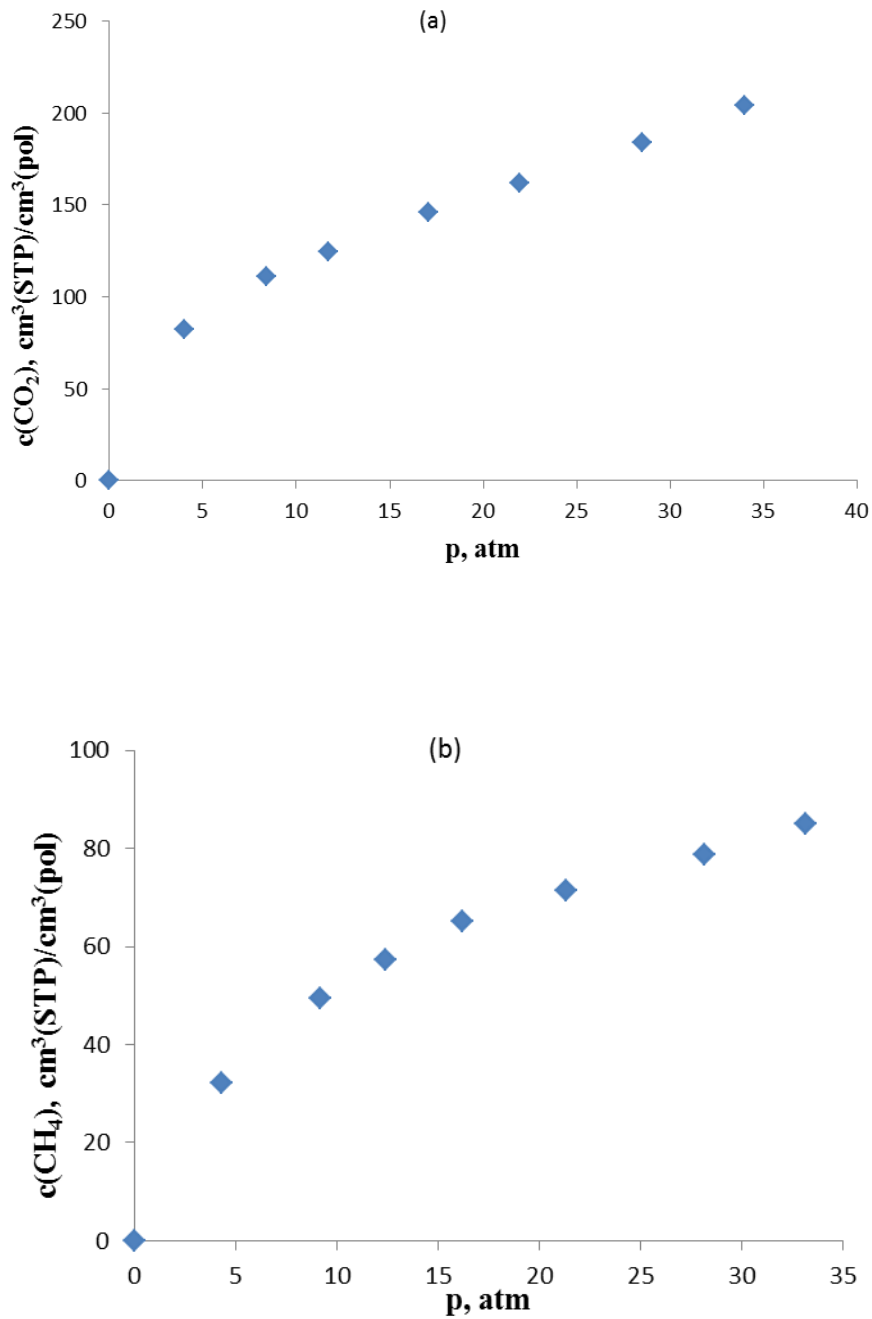


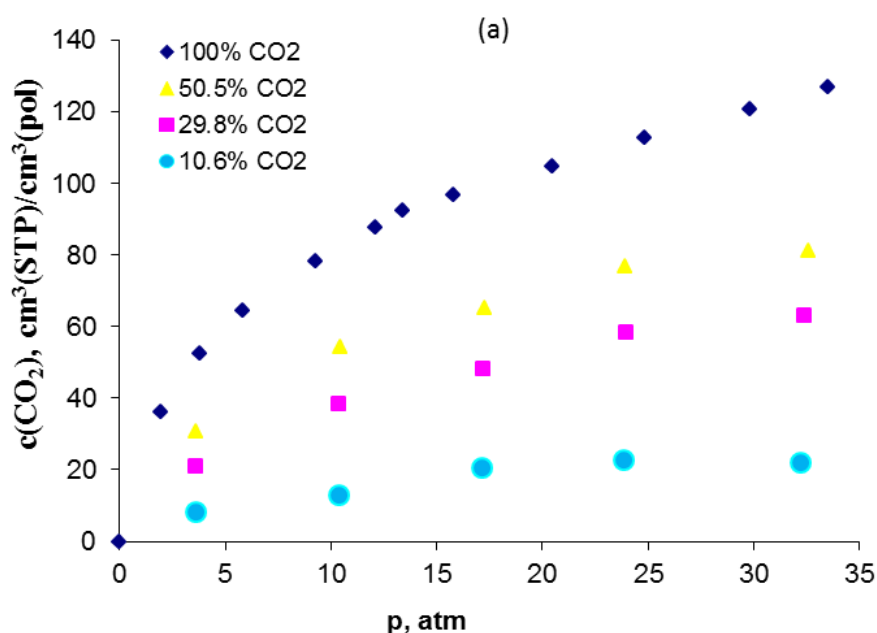
Fig 4.1 (a). Pure CO₂ gas sorption (b), Pure CH₄ sorption in PIM-1 at 25°C.

4.3 Mixed gas sorption in PIM-based polymers

Mixed gas sorption of carbon dioxide and methane at three different gas composition of $y_{CO_2} = 0.109 \pm 0.006$, $y_{CO_2} = 0.313 \pm 0.002$ and $y_{CO_2} = 0.509 \pm 0.001$ at two temperatures, 25°C, 35°C and 50°C, and pressure up to 33 bar has been measured. Here we present only the results at 35°C for TZPIM-1 and AO-PIM-1, and at 50°C for PIM-1 simplicity and the results at the other temperatures follow the same trend as that of 35°C.

The solubility isotherms of carbon dioxide and methane are shown in Fig 4.2 and 4.3 respectively at 35°C for TZPIM and AO-PIM-1 and at 50°C for PIM-1, in the entire three polymers considered. For all polymers the isotherms show the well-known concave shape towards the pressure axis.

The results of mixed gas experiments confirm that for all polymers, the solubility of both gases is lower in mixed gas conditions than for the pure gases, with larger decreases the further we are from pure gas conditions.



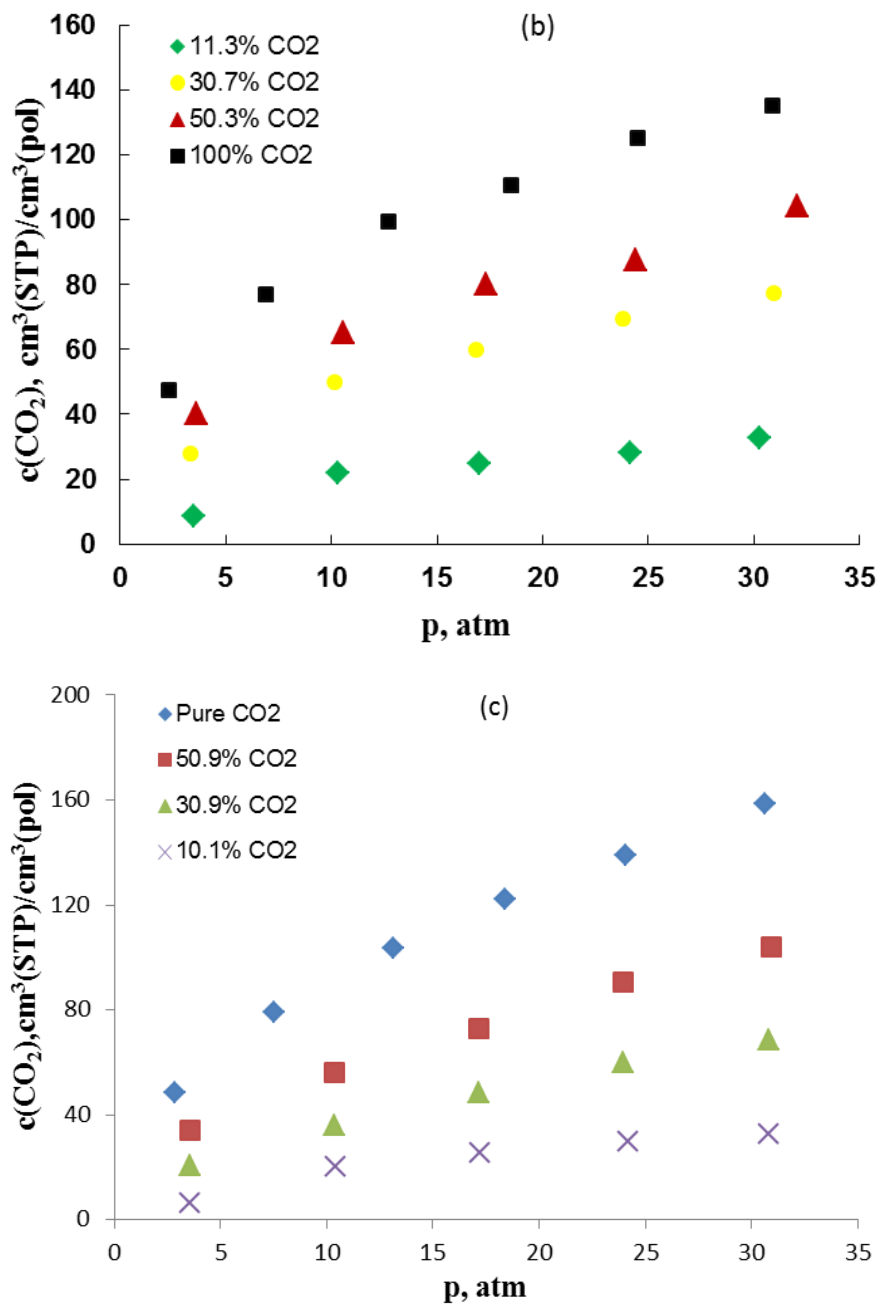
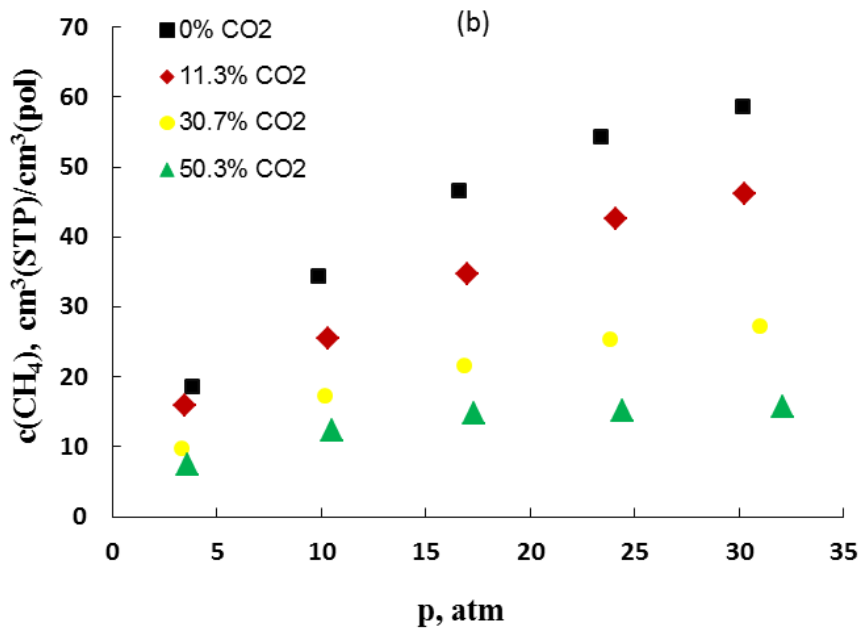
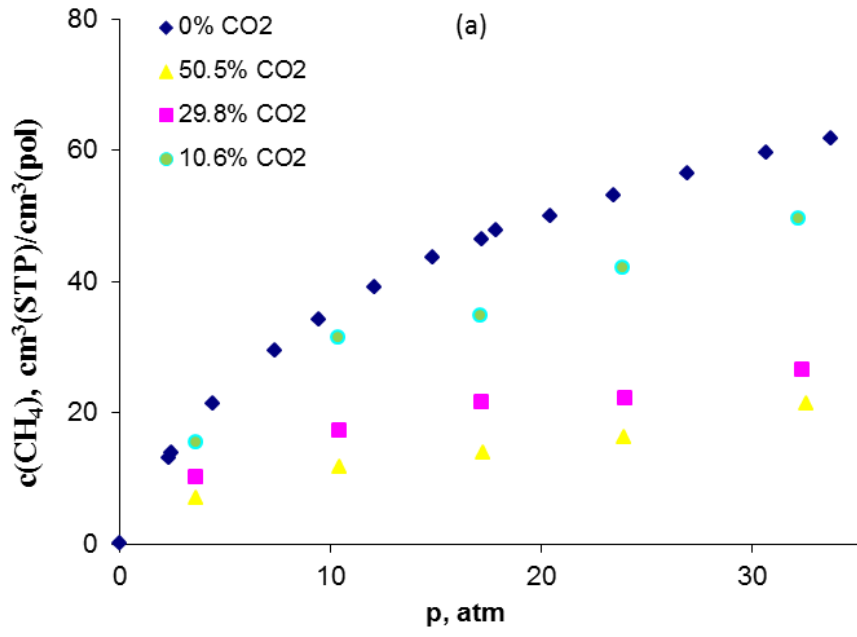


Fig 4.2. Pure and Mixed gas CO₂ Sorption a) in PIM-1 at 50°C b) TZPIM at 35°C and c) in AO-PIM-1 at 35°C.



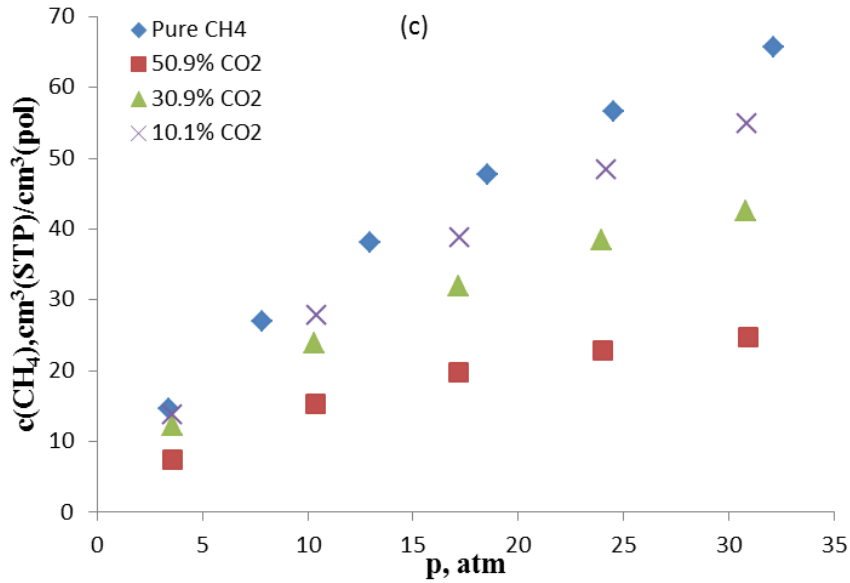
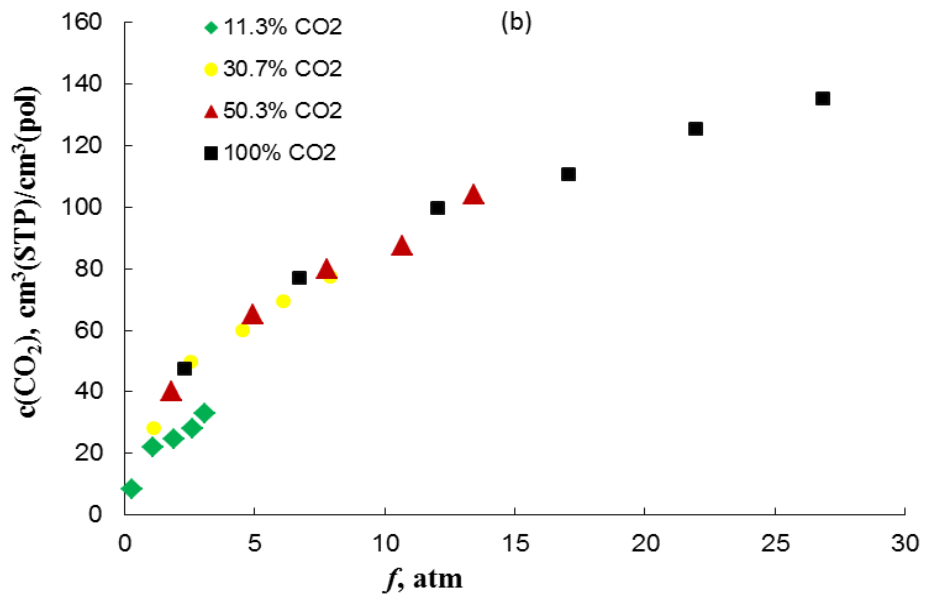
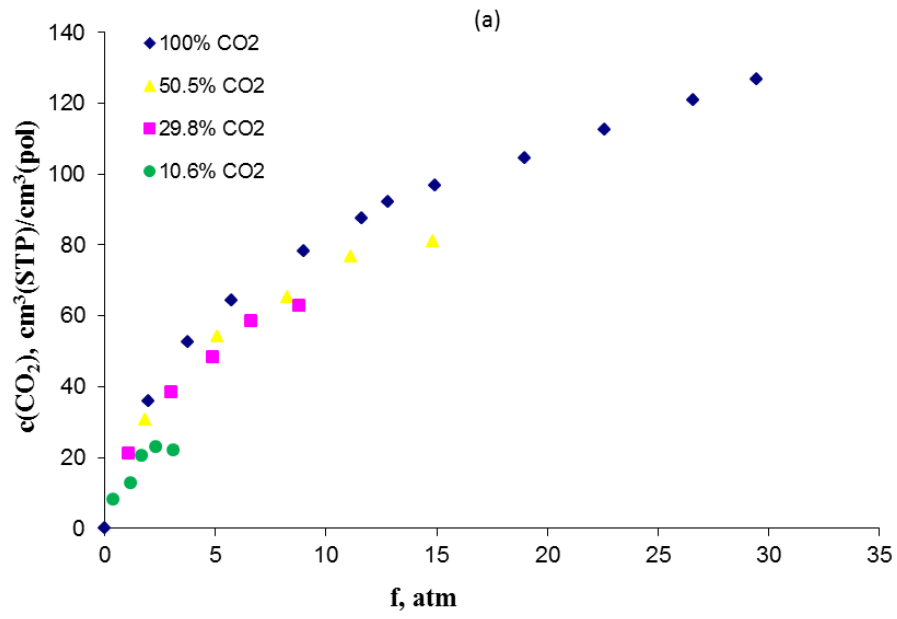


Fig 4.3. Pure and mixed gas CH₄ Sorption a) in PIM-1 at 50°C b) TZPIM at 35°C and c) in AO-PIM-1 at 35°C.

The effect of presence of one of the gas on the other gas solubility is clearly visible on Fig 4.4 for CO₂ and Fig 4.5 for CH₄ for the three polymer considered in the experiment PIM-1 (a), TZPIM (b) and AO-PIM-1 (c). The figures give the solubility of the two gases as a function of their fugacity, respectively. The variation of solubility of gas due to the presence of the other gas is more pronounced for CH₄ than CO₂. Mixed gas solubility of methane varies significantly with feed gas composition besides methane fugacity, while on the contrary mixed gas solubility of CO₂ is a function of CO₂ fugacity and is somehow less sensitive to gas phase composition, for all polymer considered and temperatures inspected. Indeed that confirms the behavior already observed at 35°C in a previous work [223]. From this result we can conclude that carbon dioxide influences the solubility of methane more than methane influences carbon dioxide solubility. This competitive nature, which to some extent favors the CO₂ with respect to CH₄ solubility, is of great interest since it increases the separation performance of the membrane.



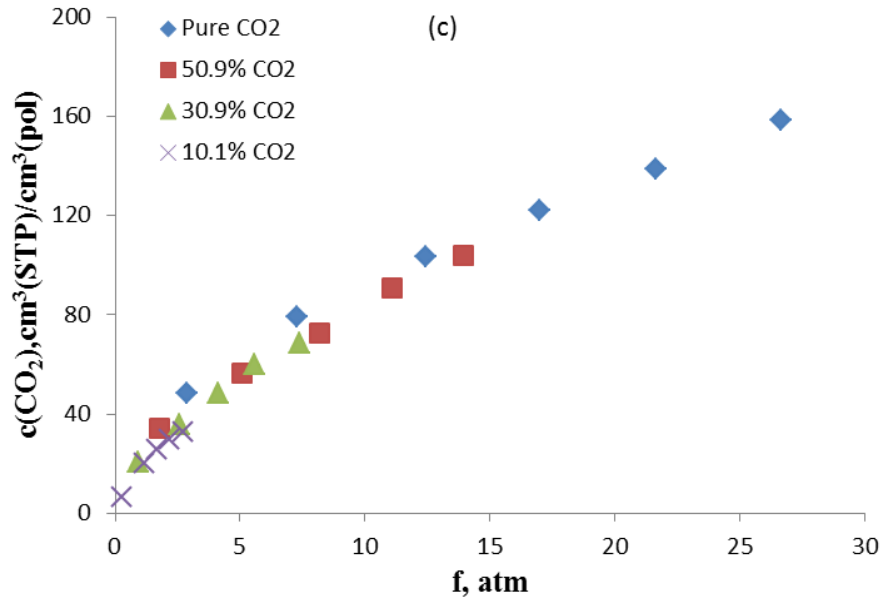
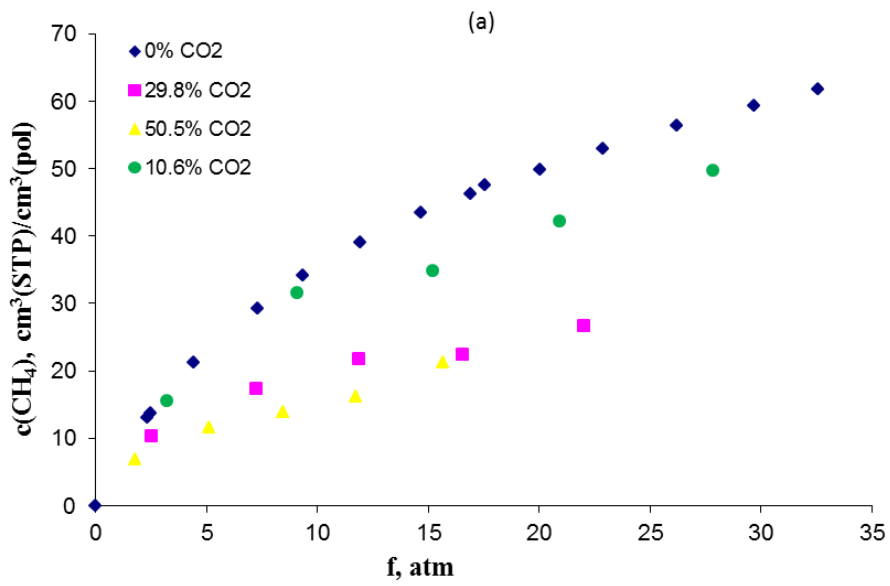


Fig 4.4. Pure and mixed gas CO₂ Sorption versus fugacity of CO₂ a) in PIM-1 at 50°C b) TZPIM at 35°C and c) in AO-PIM-1 at 35°C



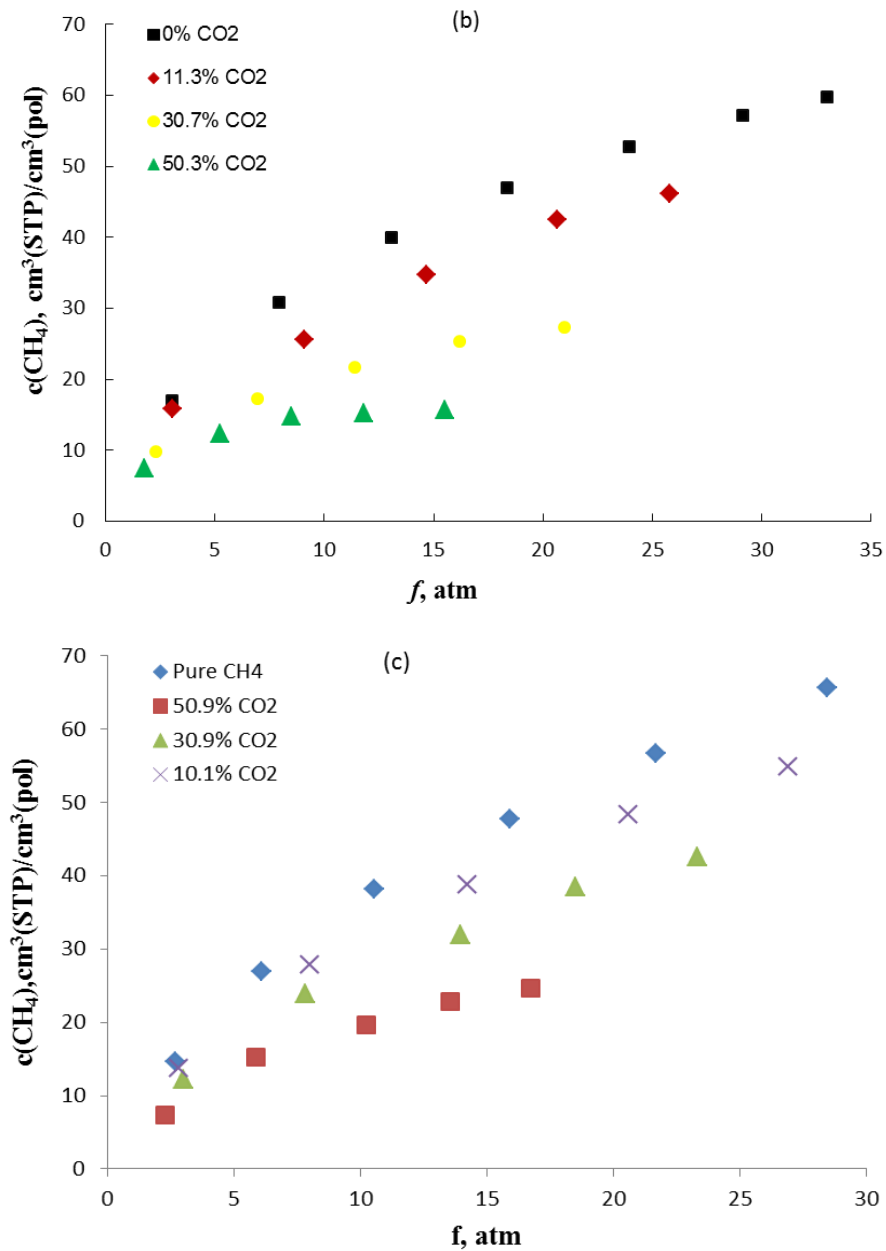
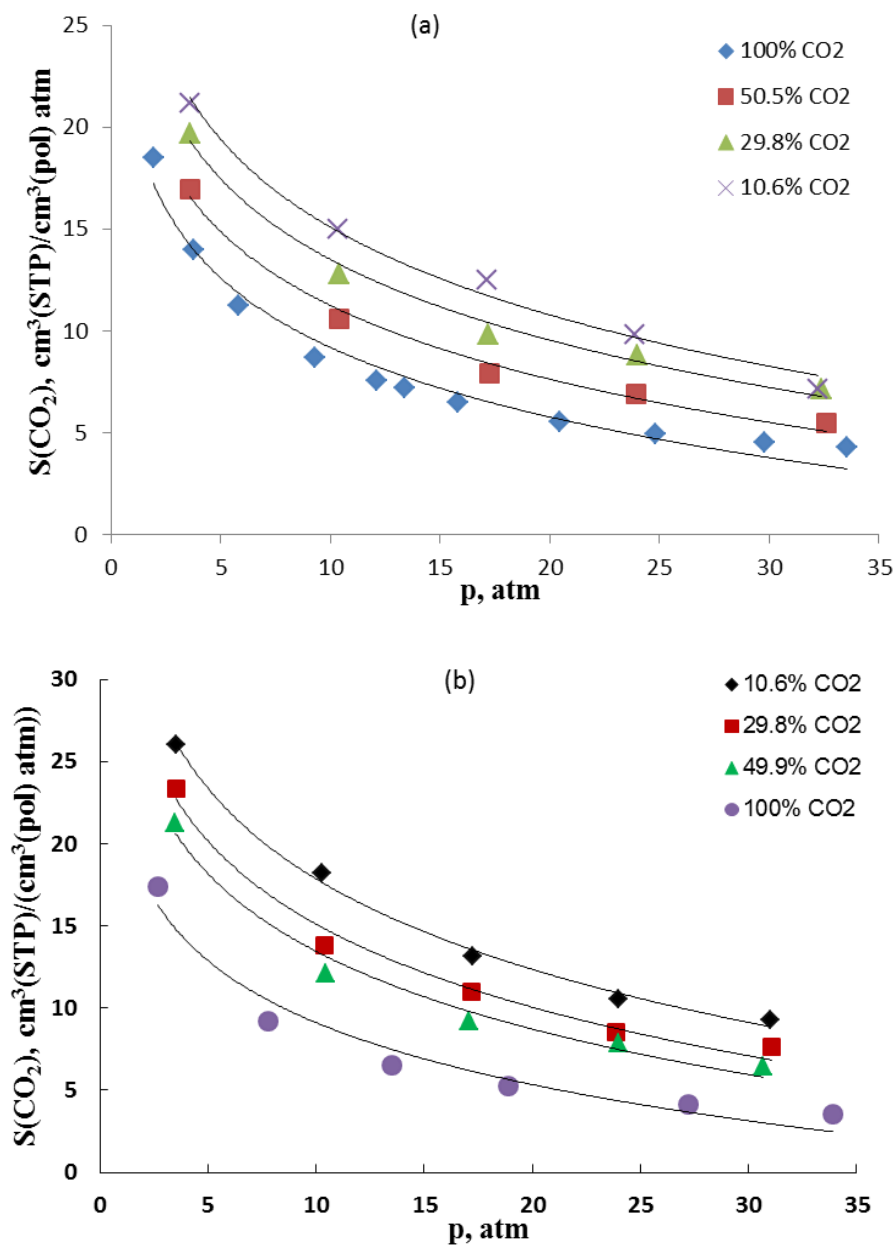


Fig 4.5. Pure and mixed gas CH₄ Sorption versus fugacity of CH₄ a) in PIM-1 at 50°C b) TZPIM at 35°C and c) in AO-PIM-1 at 35°C

4.4 Pure and mixed gas solubility coefficient

The solubility coefficient is calculated from the ratio of sorbed concentration of the gas to its fugacity; mixed gas solubility coefficients of CO₂ are plotted in Figure 4.6 versus total pressure for

the three polymer inspected at a given temperature. The corresponding plots obtained for CH₄ are presented on Figure 4.7. The results show that for both CO₂ and CH₄ solubility coefficients decrease with total pressure at all temperatures and polymers studied, they depend significantly on the pressure rather than on molar fraction of the mixture.



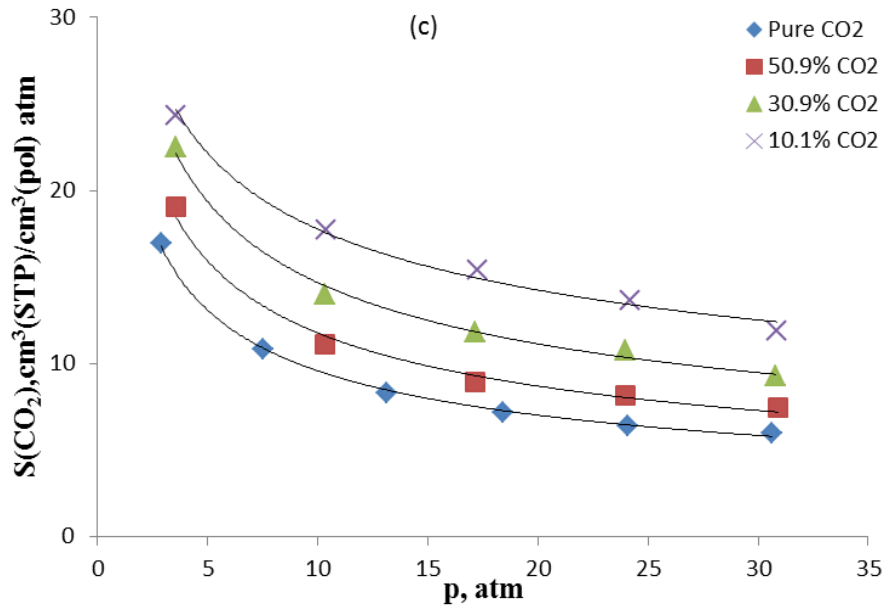
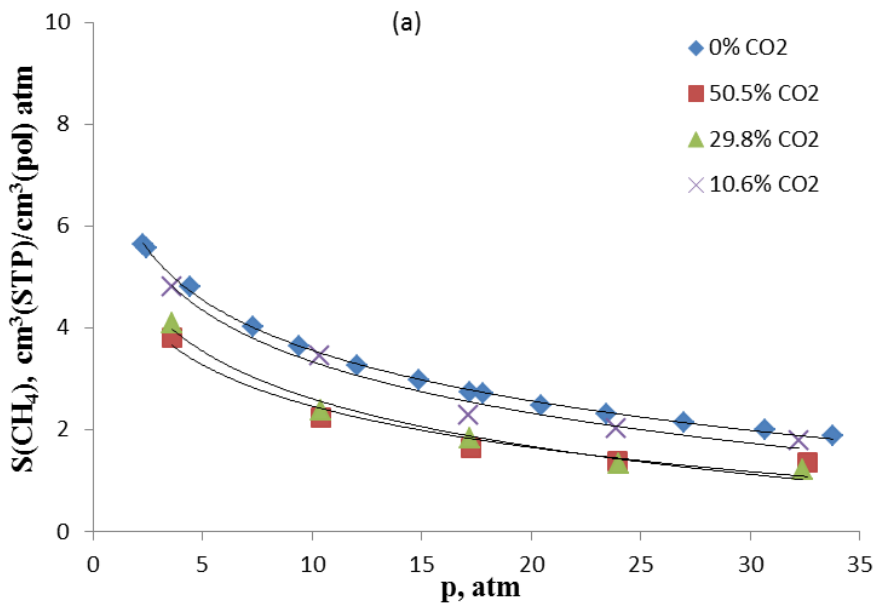


Fig. 4.6 Solubility coefficient of CO₂ versus total pressures for a) PIM-1 at 50°C, b) TZPIM at 50°C and c) AO-PIM-1 at 35°C.



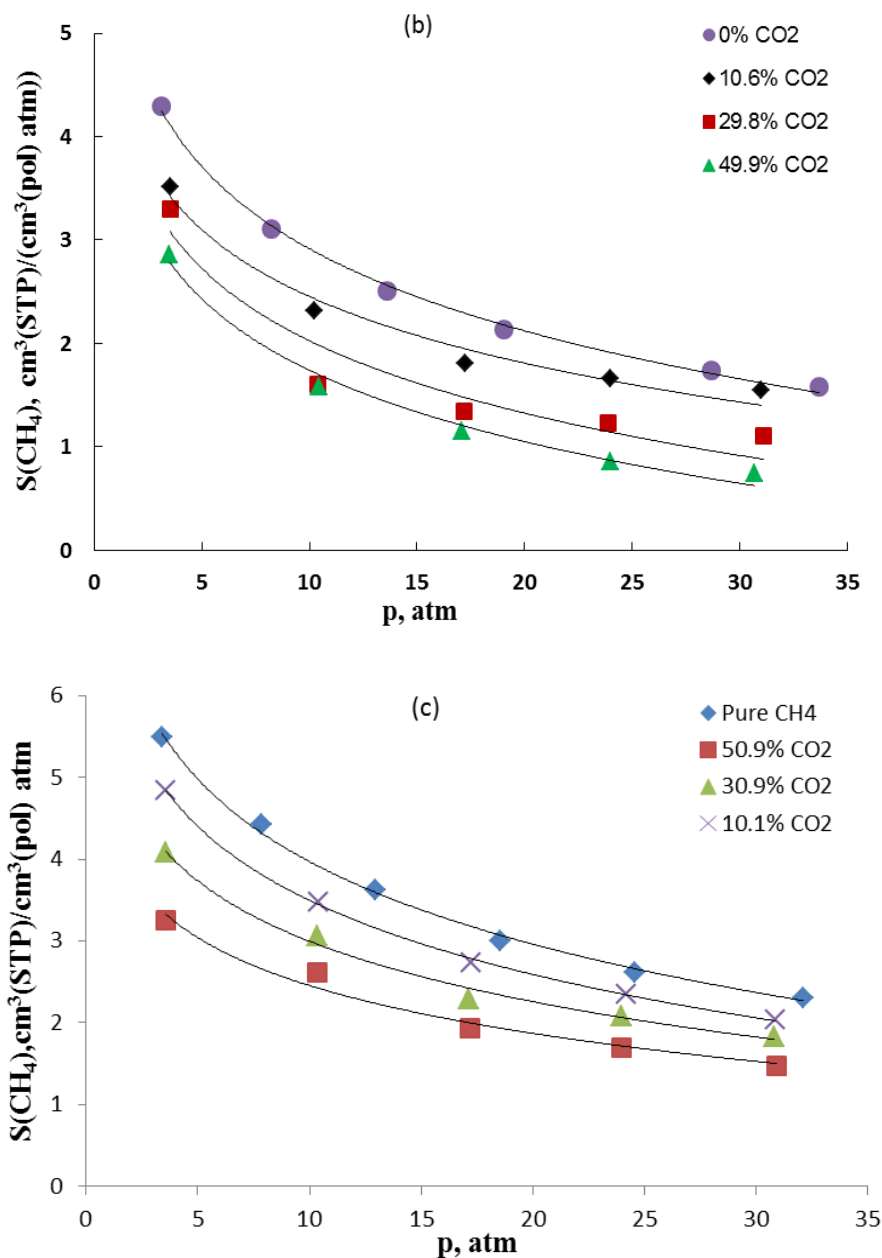
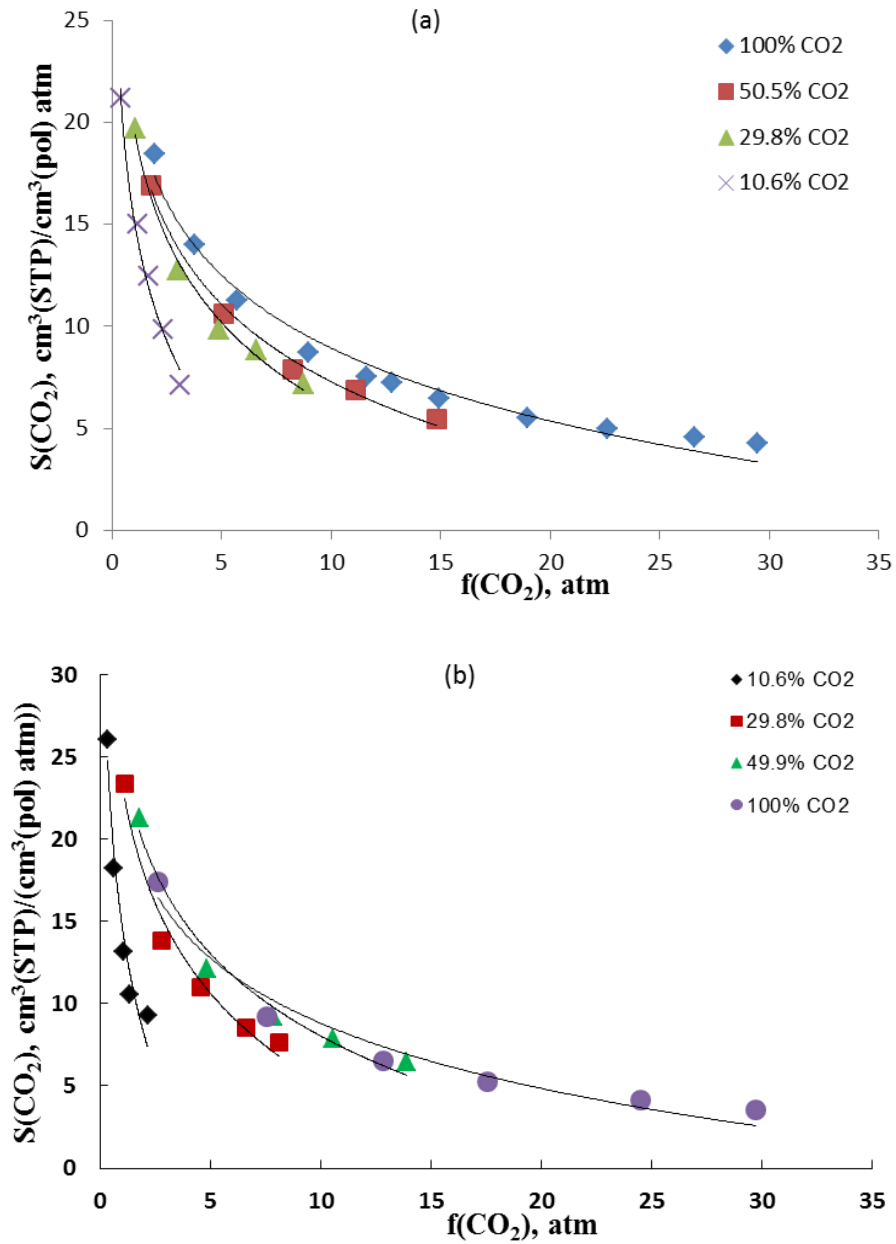


Fig. 4.7 Solubility coefficient of CH₄ versus total pressures for a) PIM-1 at 50°C, b) TZPIM at 50°C and c) AO-PIM-1 at 35°C.

An alternative, possibly more direct representation of the solubility coefficient behaviour of the two gases is presented on Fig 4.8 and Fig 4.9 by reporting the experimental values versus gas fugacities for all the three PIM-based polymers. These results show that the solubility coefficients of the two gases decrease with both gas fugacities with a logarithmic trend. Solubility coefficient of CO₂ decreases with increasing of CO₂ fugacity but it increases with increasing the molar fraction of CO₂

in the gas mixture at a fixed CO₂ fugacity. Solubility coefficient of CH₄ follows a similar trend as the solubility coefficient of CO₂ with respect to both CO₂ fugacity and molar fraction.



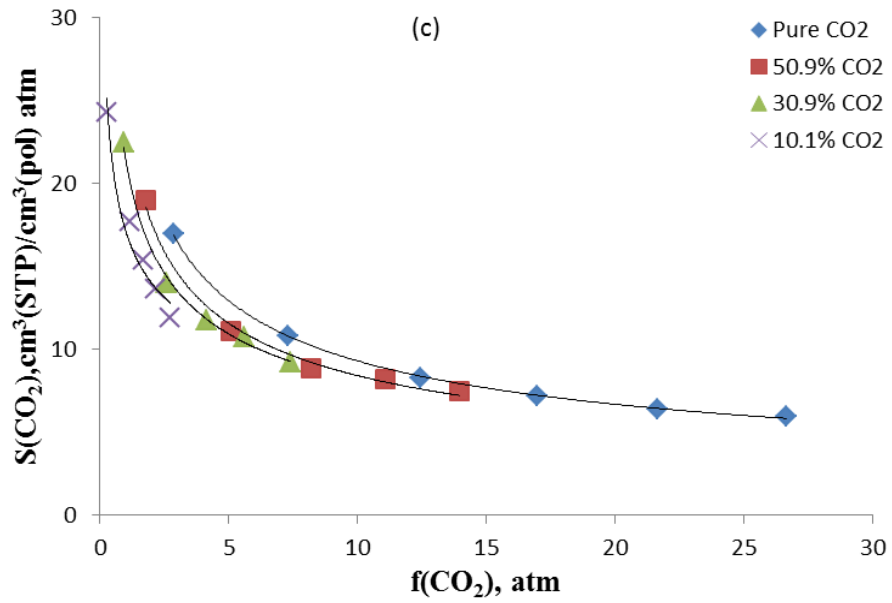
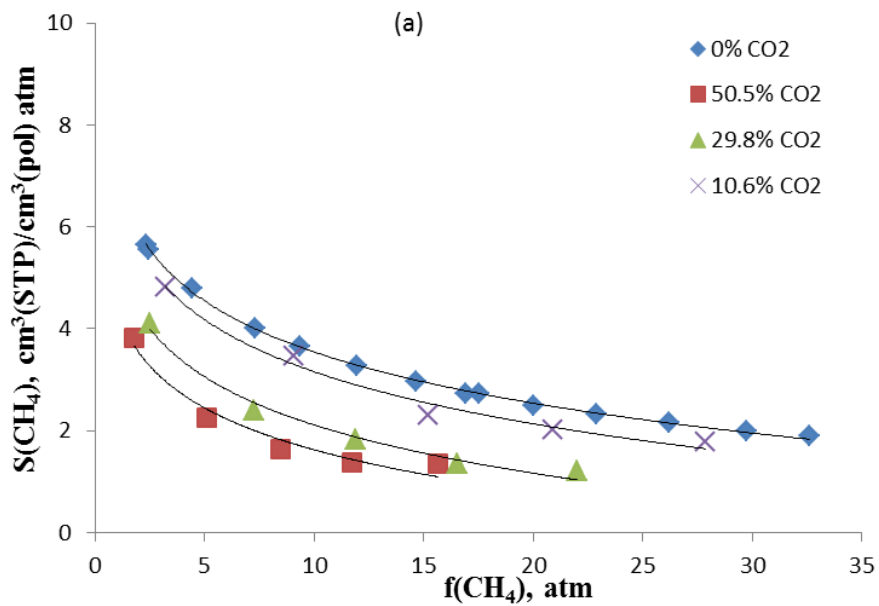


Fig. 4.8 Solubility coefficient of CO₂ versus CO₂ fugacity of the gases for a) PIM-1 at 50°C, b) TZPIM at 50°C and c) AO-PIM-1 at 35°C.



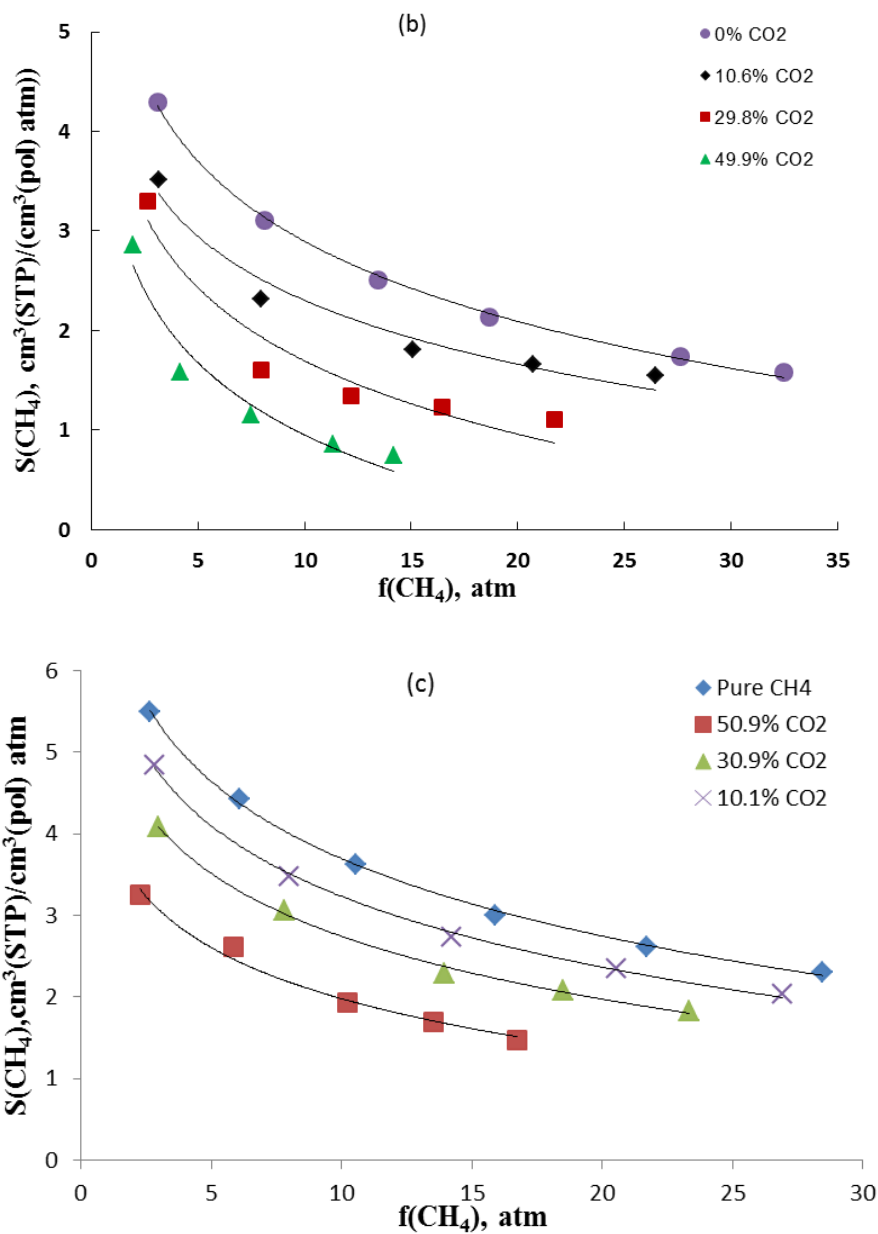
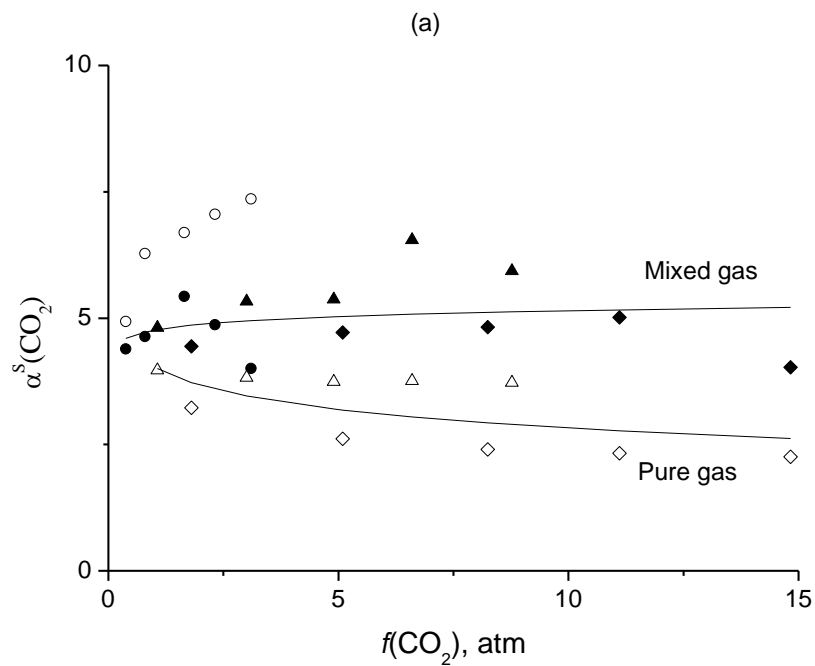


Fig. 4.9 Solubility coefficient of CH_4 versus CH_4 fugacity for a) PIM-1 at 50°C , b) TZPIM at 50°C and c) AO-PIM-1 at 35°C .

4.5 Solubility selectivity of PIM-based polymers

Pure gas and mixed gas solubility selectivity of CO_2/CH_4 mixture is calculated from pure and mixed gas solubility coefficients of CO_2 and CH_4 respectively at each pressure. These results are presented on Fig 4.10 for all PIM-based membranes. The Figure shows mixed gas and pure gas solubility selectivity versus fugacity of CO_2 . From the graph it can be seen that the pure gas solubility

selectivity is decreasing with respect to fugacity of CO₂. Interestingly, the mixed gas solubility selectivity has an increasing or constant behavior with respect to fugacity of CO₂. These is due to competition of the two gases in the mixture experiment which is absent in the pure gas experiment. In the mixed gas case the polymer favours CO₂ more than CH₄, which increases the solubility coefficient of CO₂ and while that of CH₄ remains the same as the pure one so solubility selectivity becomes higher.



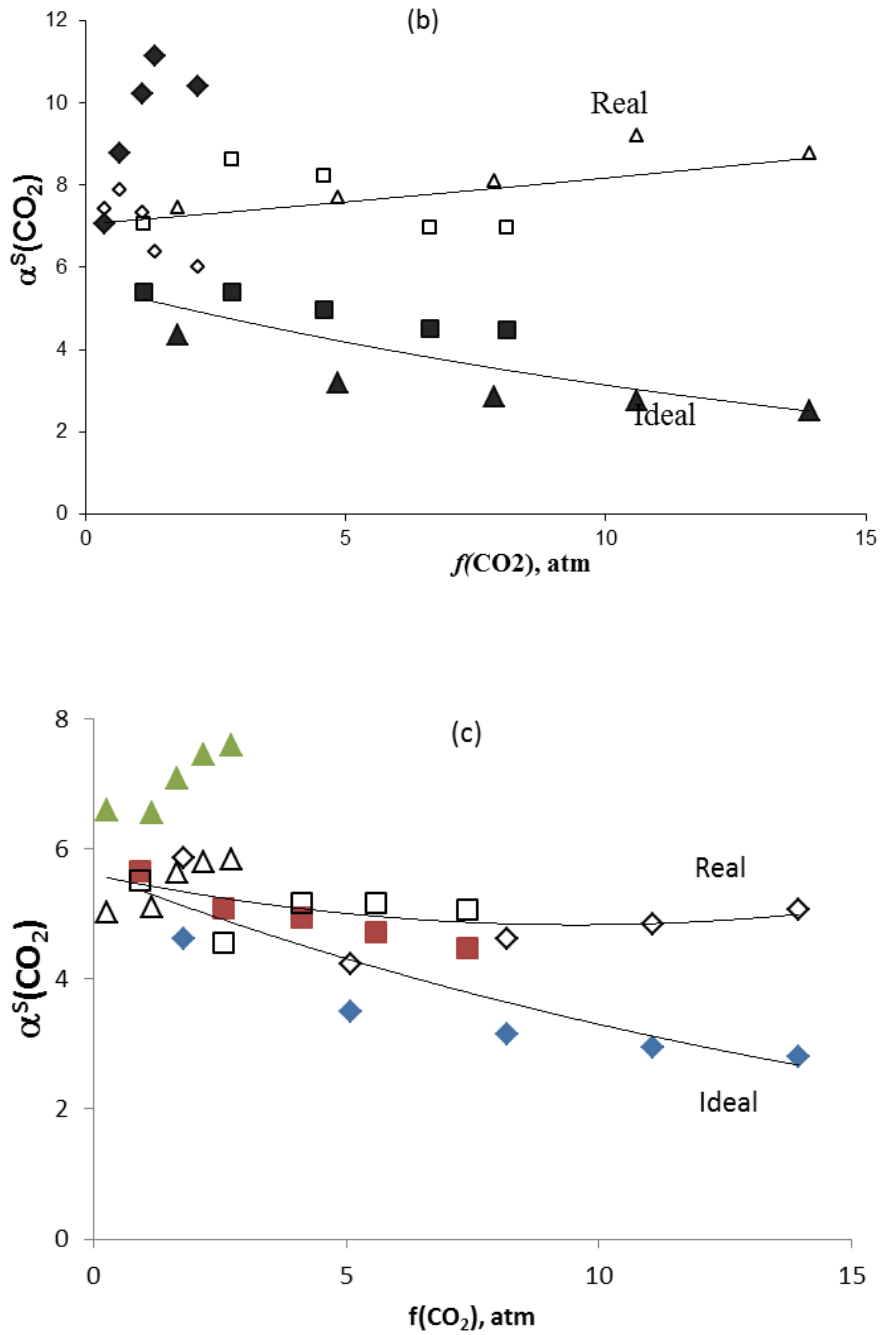
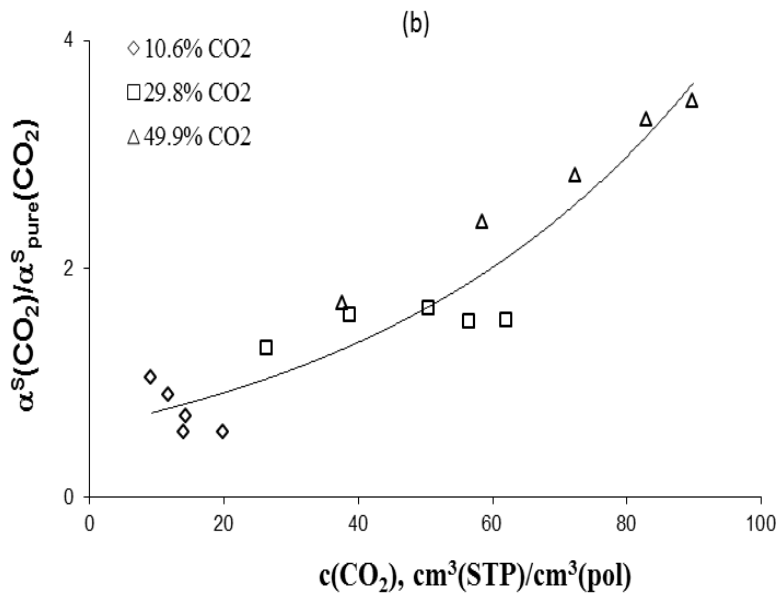
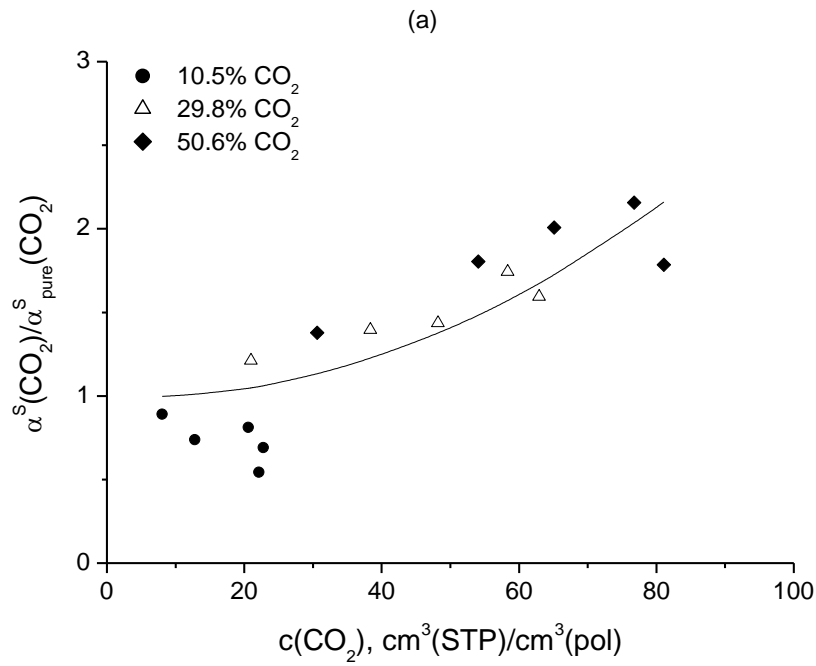


Fig. 4.10 Real and Ideal CO₂/CH₄ solubility selectivity versus CO₂ fugacity for a) PIM-1 at 50°C, b) TZPIM at 50°C and c) AO-PIM-1 at 35°C.

In a clearer way to show the effect of mixed gas condition on solubility selectivity, pure and mixed gas solubility selectivities are given as a ratio in Fig 4.11. Interestingly, solubility selectivity ratio has shown monotonous dependence on sorbed concentration of CO₂. This dependence is seen with a

mastercurve which works in all molar fraction of CO₂ and pressure range. The mastercurves are represented in Eq 4.1 for PIM-1, Eq 4.2 for TZPIM and Eq 4.3 for AO-PIM-1. These mastercurves show that solubility selectivity is highly influenced by sorbed CO₂ molecules.



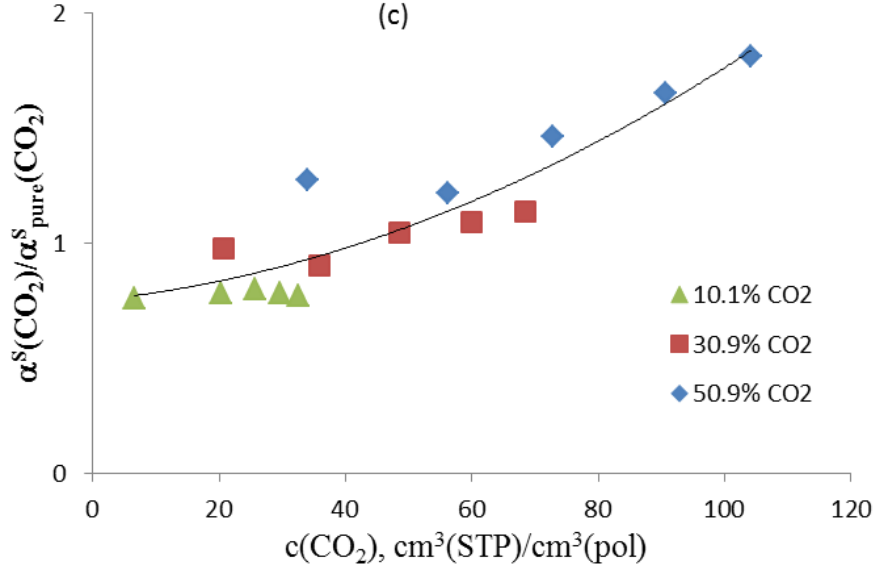


Fig. 4.11 The Ratio of Real and Ideal CO₂/CH₄ solubility selectivity versus CO₂ concentration for a) PIM-1 at 50°C, b) TZPIM at 50°C and c) AO-PIM-1 at 35°C.

$$\frac{\alpha^S(\text{CO}_2 / \text{CH}_4)}{\alpha_{\text{pure}}^S(\text{CO}_2 / \text{CH}_4)} = 2.0 \times 10^{-4} c(\text{CO}_2)^2 - 1.9 \times 10^{-3} c(\text{CO}_2) + 1.0; R^2=0.72 \quad 4.1$$

$$\frac{\alpha^S(\text{CO}_2 / \text{CH}_4)}{\alpha_{\text{pure}}^S(\text{CO}_2 / \text{CH}_4)} = 4.0 \times 10^{-4} c(\text{CO}_2)^2 - 7.6 \times 10^{-3} c(\text{CO}_2) + 1.0; R^2=0.88 \quad 4.2$$

$$\frac{\alpha^S(\text{CO}_2 / \text{CH}_4)}{\alpha_{\text{pure}}^S(\text{CO}_2 / \text{CH}_4)} = 2.0 \times 10^{-4} c(\text{CO}_2)^2 - 7.0 \times 10^{-3} c(\text{CO}_2) + 1.0; R^2=0.80 \quad 4.3$$

4.6 Comparison of pure and mixed gas solubility in PIM-based polymer

Sorption results of pure carbon dioxide and pure methane in different PIM-1 based polymers are compared at temperature of 35°C as can be seen on Figure 4.12. The result shows that pure CO₂ sorption is almost the same for all three polymers at 35°C at lower pressure but there is a small difference as the pressure increases above 15 atm. The solubility of CO₂ in TZPIM is smaller than both AO-PIM-1 and PIM-1 above 15 atm as can be seen on Fig 4.12a. As can be seen on Fig 4.12b pure CH₄ sorption in PIM-1 is higher than pure CH₄ sorption of TZPIM and AO-PIM-1. This is

because the two modified polymers (TZPIM and AO-PIM-1) has high tendency of absorption towards CO₂ which will decrease the solubility of CH₄.

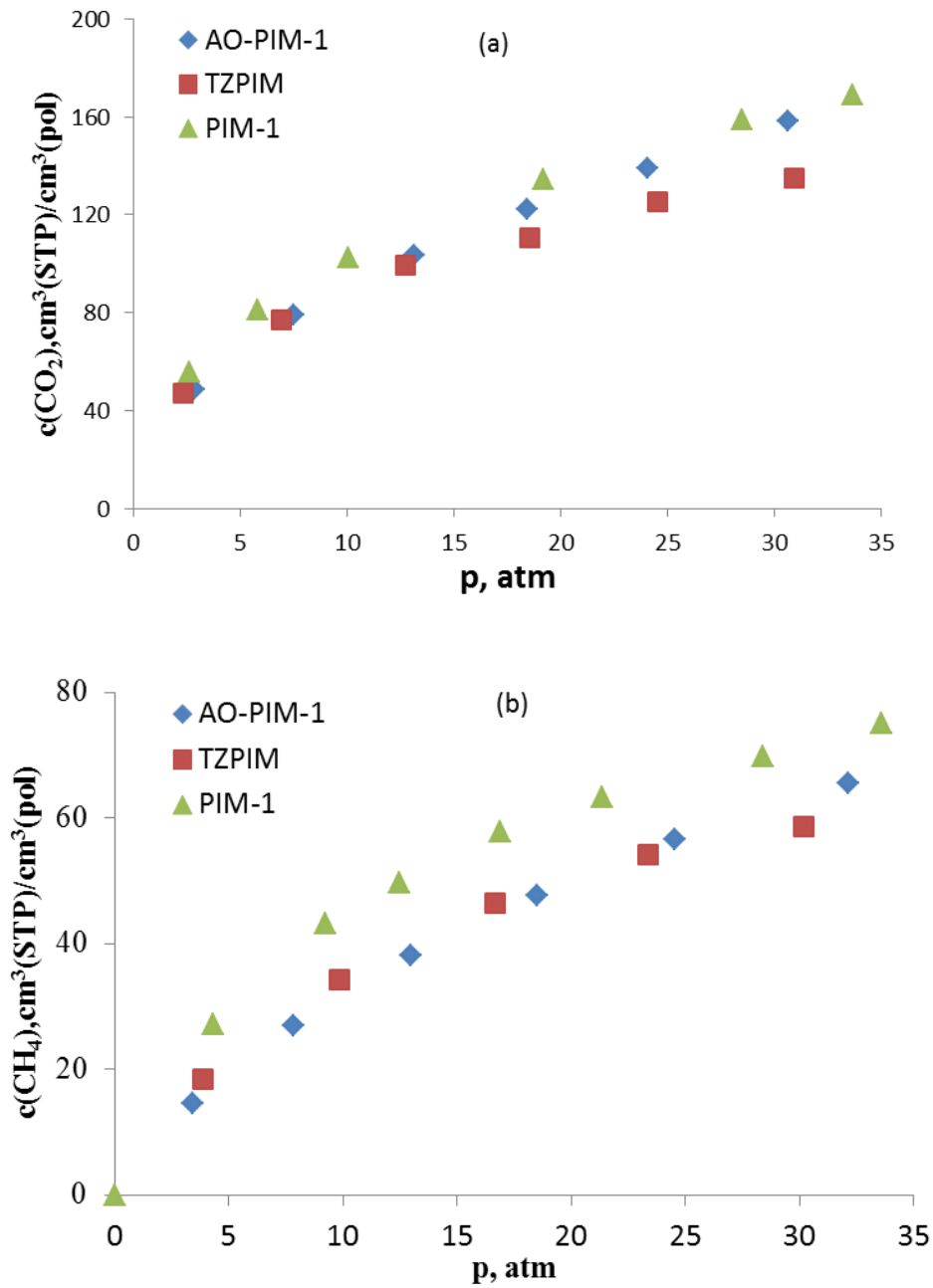


Fig. 4.12 Pure gas sorbed concentration comparison of PIM-1, TZPIM-1 and AO-PIM-1 at 35°C; a) CO₂, b) CH₄

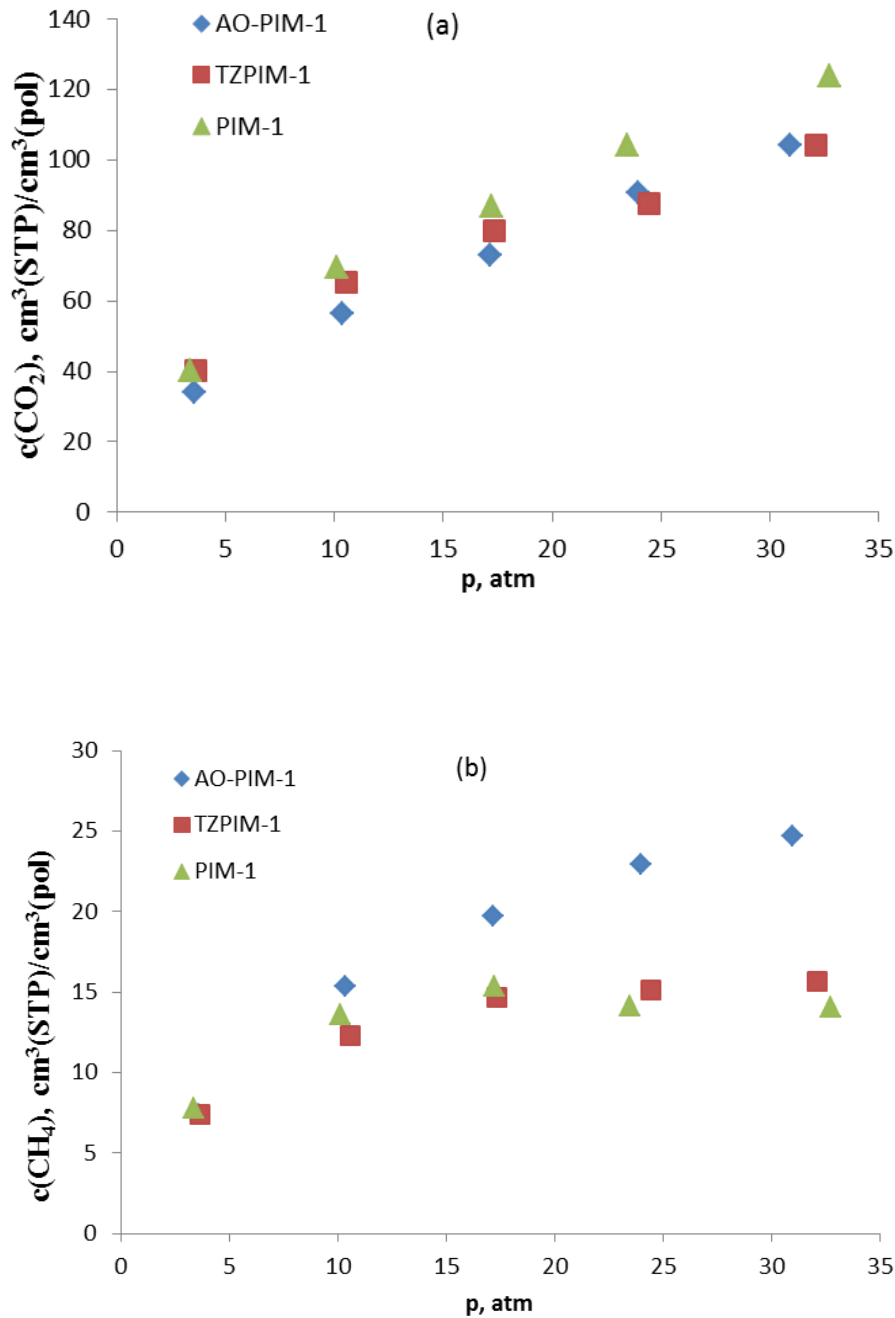


Fig. 4.13 Mixed gas sorbed concentration comparison of PIM-1, TZPIM-1 and AO-PIM-1 at 35°C; a) CO₂, b) CH₄

Ideal and real solubility selectivity is also compared for these membranes. Ideal solubility selectivity of TZPIM-1 membrane is higher than both solubility selectivity of PIM-1 and AO-PIM-1. As can be seen on Fig 4.14a the second higher solubility selectivity AO-PIM-1 followed by that of PIM-1.

Real solubility selectivity of TZPIM is again higher than that of both AO-PIM-1 and PIM-1 as shown on Fig 4.14b. Though the ideal solubility selectivity of AO-PIM-1 is higher than the ideal

solubility selectivity of PIM-1, the reverse is true for the real solubility selectivity as can be seen on Fig 4.14b.

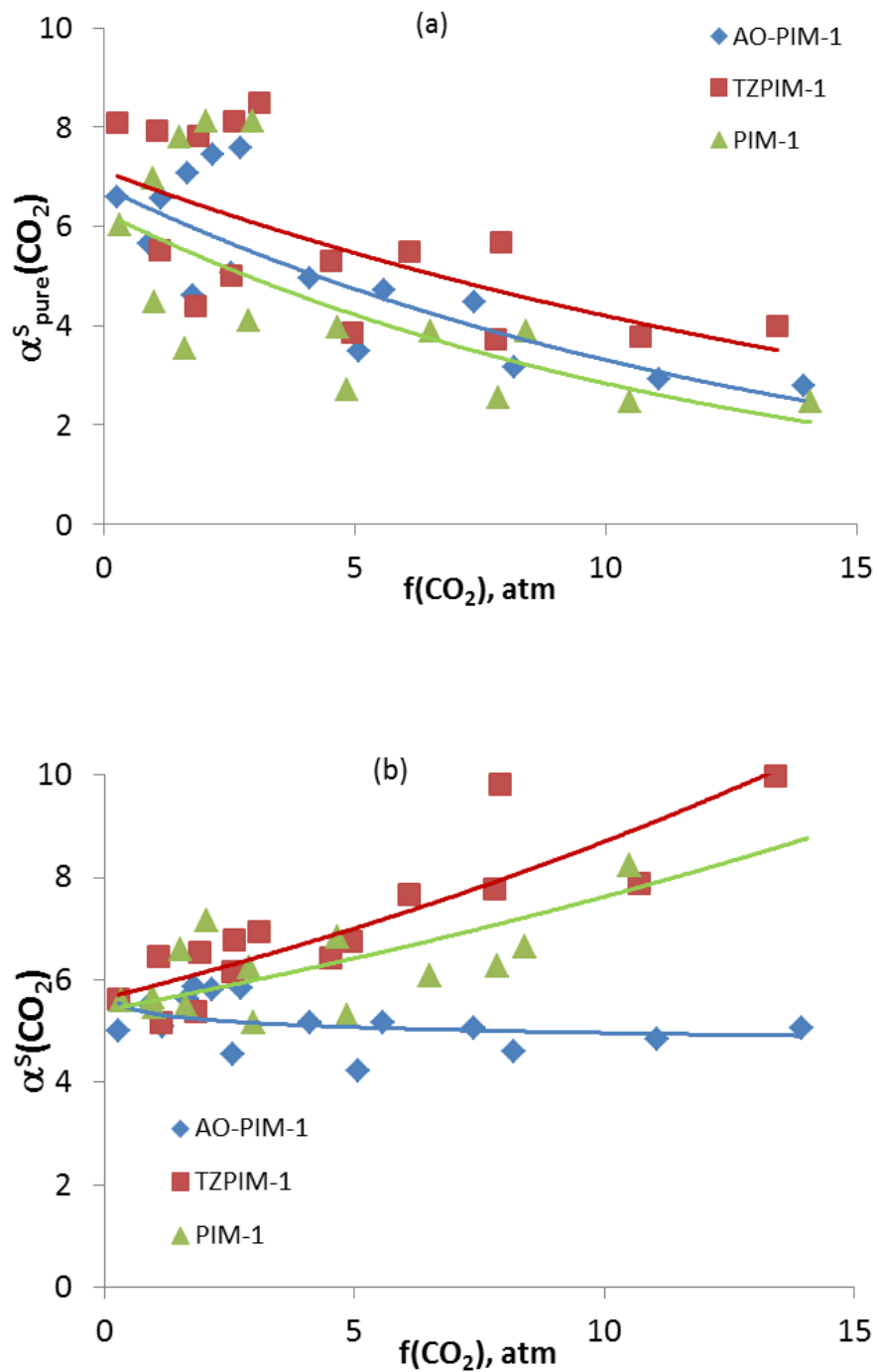


Fig 4.14 Real and Ideal Solubility selectivity of PIM-1, TZPIM-1 and AO-PIM-1 at 25°C; a) Ideal, b) Real

4.7 Temperature dependence of sorption in PIM-based polymers

Pure gas sorption experiments of both carbon dioxide and methane in PIM-1 at two temperature show that the solubility decreases with increasing temperature as shown in the Fig 4.15. The same results are obtained for the other membranes. This explains that the solubility follows Van't Hoff trend as shown in the Fig 4.16. Enthalpy of sorption calculated from the slope of graph of solubility at infinite dilution versus the inverse of temperature is tabulated in table 1.

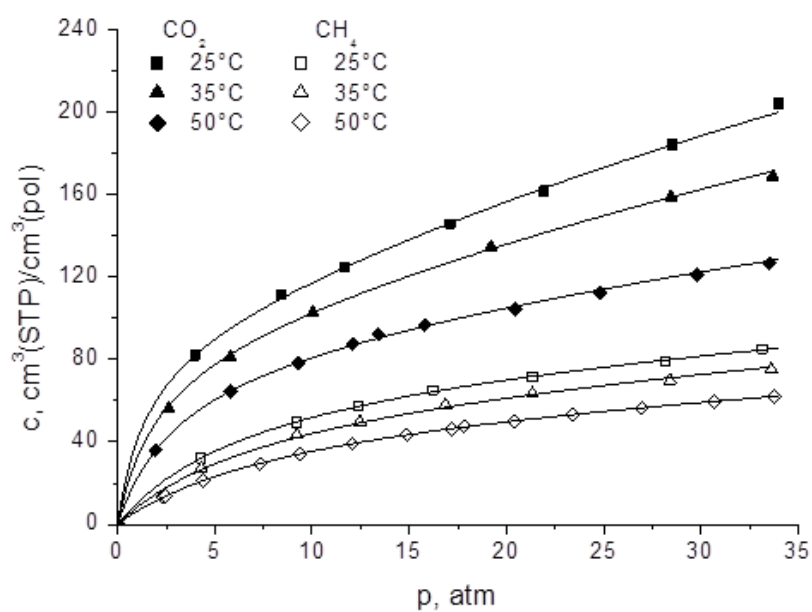


Fig 4.15: Pure gas sorption of CO_2 and CH_4 at 25°C, 35°C [223], 50°C.

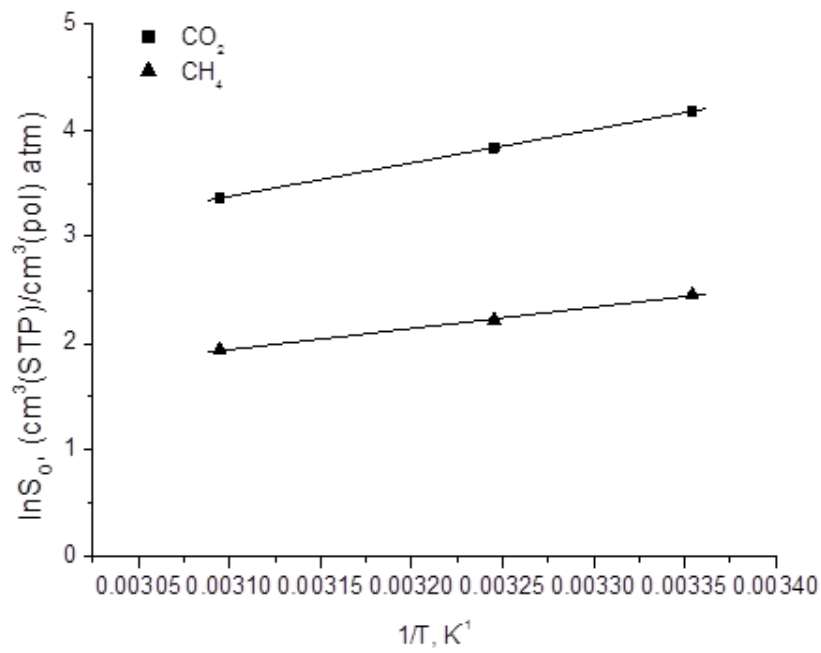


Fig 4.16: Logarithm of solubility of pure CO₂ and pure CH₄ versus inverse temperatures (results at 35°C are taken from [223])

On Fig 4.17, the selectivity ratio is presented as a function of molar concentration of CO₂ at three different temperatures 25°C, 35°C [23] and 50°C for PIM-1. The result shows that there is an increase in the selectivity ratio with increasing of temperature.

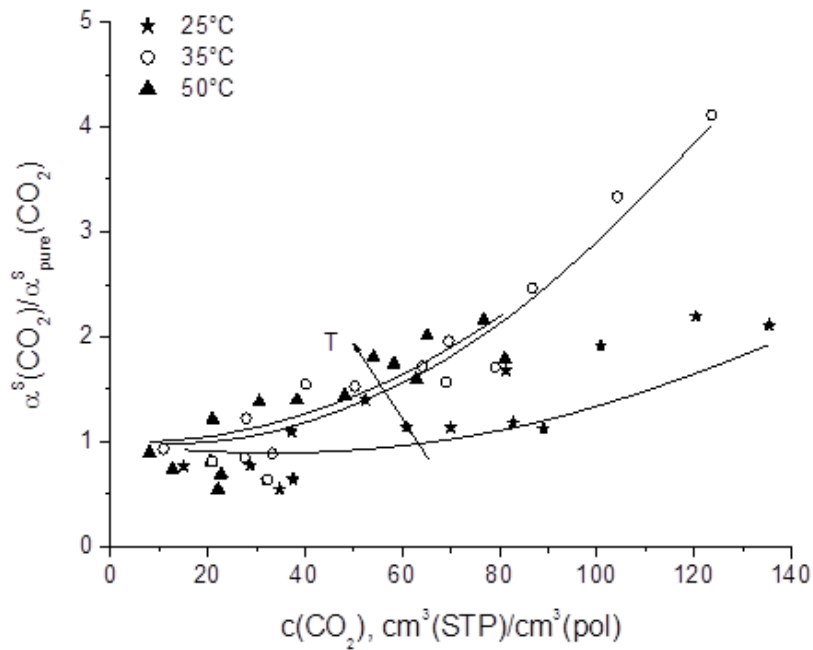


Fig 4.17: Ratio between mixed and pure gas selectivity coefficient, versus CO_2 molar concentration at 25°C, 35°C [23] and 50°C.

4.8 Conclusions

Mixed gas solubility experiment of CO_2 and CH_4 was carried out at three temperatures, 25°C, 35°C and 50°C for three PIM-based membranes, by varying pressure at three constant molar fraction of CO_2 , 10.9% ± 0.59 , 31.3% ± 0.24 and 50.9% ± 0.13 . From the results it is observed that the real solubility selectivity was increased from the ideal results. This is because the solubility coefficient of both CO_2 and CH_4 decreased due to the presence of the other gas with higher decrease of solubility coefficient of CH_4 compared to the solubility coefficient of CO_2 .

Pure gas Solubility selectivity increases with solubility coefficient of CO_2 for higher molar fraction of CO_2 whereas it decreases with solubility coefficient of CO_2 for lower molar fraction of CO_2 . Pure gas solubility selectivity of TZPIM-1 is higher than that of AO-PIM-1 and PIM-1. Mixed gas

solubility selectivity of TZPIM-1 is again higher than both PIM-1 and AO-PIM-1 membrane. But real solubility selectivity of AO-PIM-1 is lower than that of PIM-1 though the reverse is true for the ideal solubility selectivity.

5 Mixed gas sorption in Polynonene polymer

5.1 Introduction

Addition polymerization (AP) of norbornene and its derivatives has been first accomplished nearly 20 years ago [192]. However, relatively little has been reported on the membrane parameters of these polymers, though their rigid chains as manifested in high glass transition temperatures can imply interesting properties [193-195].

Introduction of proper pendant groups in monomer unit of addition polynorbornene is the way to get polynorbornenes with desired properties. However, the appearance of substituents in norbornene molecules resulted in a decrease of the catalytic activity as monomers [196,197]. In the case of ring-opening metathesis polymerization (ROMP) this effect is softened to some extent by substantial thermodynamic driving force in the process appeared as a result of opening highly strained bicyclic norbornene skeleton. AP is not so thermodynamically favorable process. It is well-known that in the case of AP the introduction of substituents, especially bulky or functional groups, leads to a dramatic decrease in activity of norbornene derivatives in the presence of all tested catalysts [198-201]. Probably, this is one of the reasons for limited number of publications devoted to AP of silyl-substituted norbornenes.

Interesting feature of poly (3, 4-TCNSi₂) and poly-(3-TCNSi) is the trend observed for permeation of hydrocarbons. In common glassy polymers increases in the size of penetrants result in decreases in permeability. Such behavior is explained by stronger effects of diffusivity and not solubility on the permeability coefficients. For all addition Si-containing polynorbornenes (PTMSN and its structure analogues) solubility controlled permeation is characteristic, that is, the changes of P and the solubility coefficients S are similar for penetrants series: P values increase when the critical temperature of the penetrants increases. Such behavior has been reported for several but not all polyacetylenes [202] (and not for amorphous Teflons AF7). It can be caused by weak size sieving ability of polyacetylenes having unusually large free volume and its specific spatial distribution (open porosity) as was confirmed by computer simulation [203]. In this section pure and mixed gas solubility coefficient of CO₂ and CH₄ in polynorborene membrane is presented. Solubility selectivity of CO₂/CH₄ mixture in polynonene membrane is presented in section 5.3 of this chapter. Finally, solubility selectivity result of CO₂/CH₄ mixture of polynorborene is compared with that of PIM-based polymers.

5.2 Pure gas sorption in Polynonene polymers

Pure gas sorption of both CO₂ and CH₄ in polynonene membrane has shown the concave shown solubility isotherm as discussed in chapter 4 of this thesis work. Pure gas CO₂ solubility is always higher than that of pure gas solubility of CH₄ in any membrane. The results are shown in Fig 5.1a for pure CO₂ sorption and Fig 5.1b for pure CH₄ sorption.

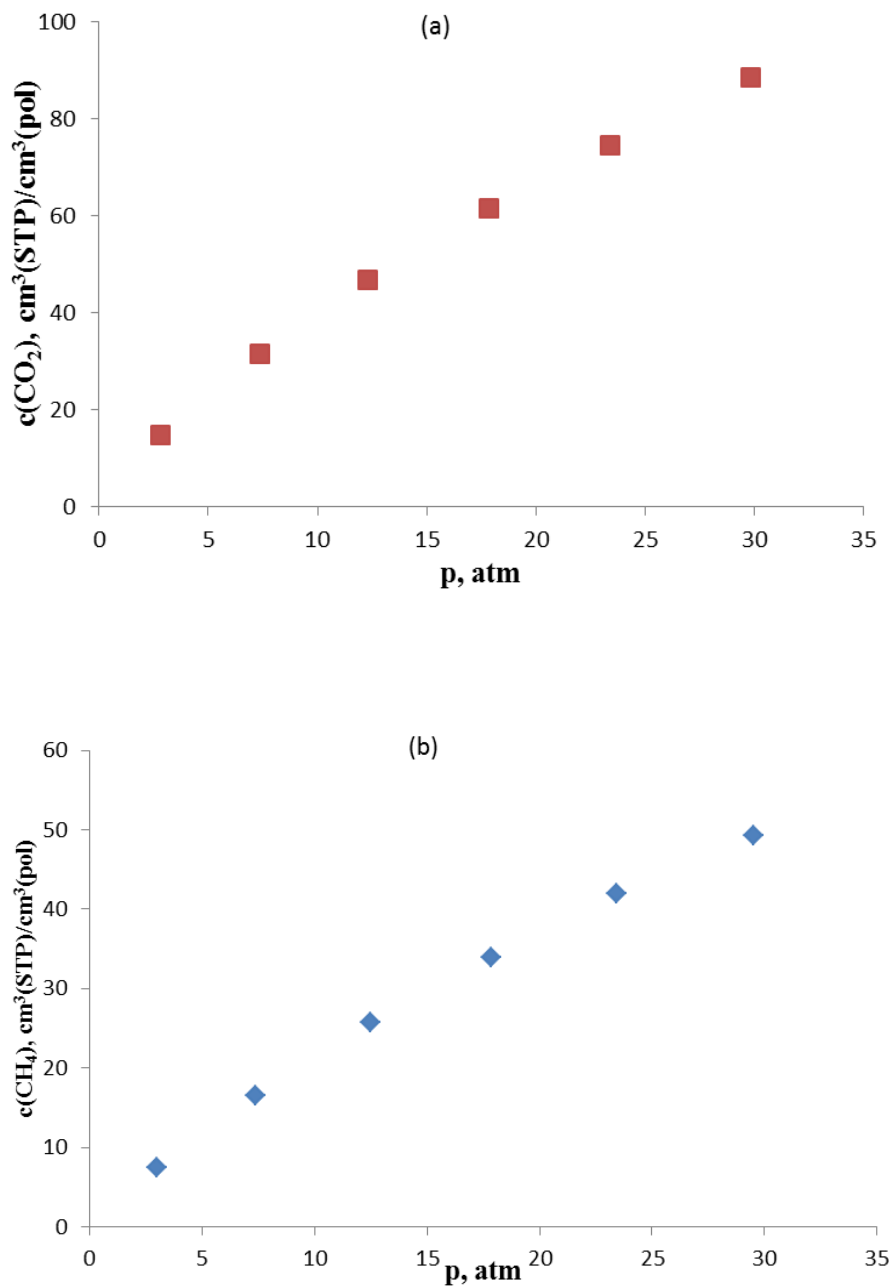


Fig 5.1 (a) Pure CO₂ gas sorption, (b) Pure CH₄ sorption in Polynonene at 35°C.

5.3 Mixed gas sorption in Polynonene polymers

Sorption isotherms of carbon dioxide under pure gas and mixed gas conditions in polynonene membrane are shown in Fig 5.2a. The corresponding results for methane under the pure gas and mixed gas conditions are shown in Fig. 5.2b. There is a decrease in mixed gas sorption compared to pure gas sorption due to the presence of the other gas in the system. This competitive effect finally increases the mixed gas solubility selectivity of the system.

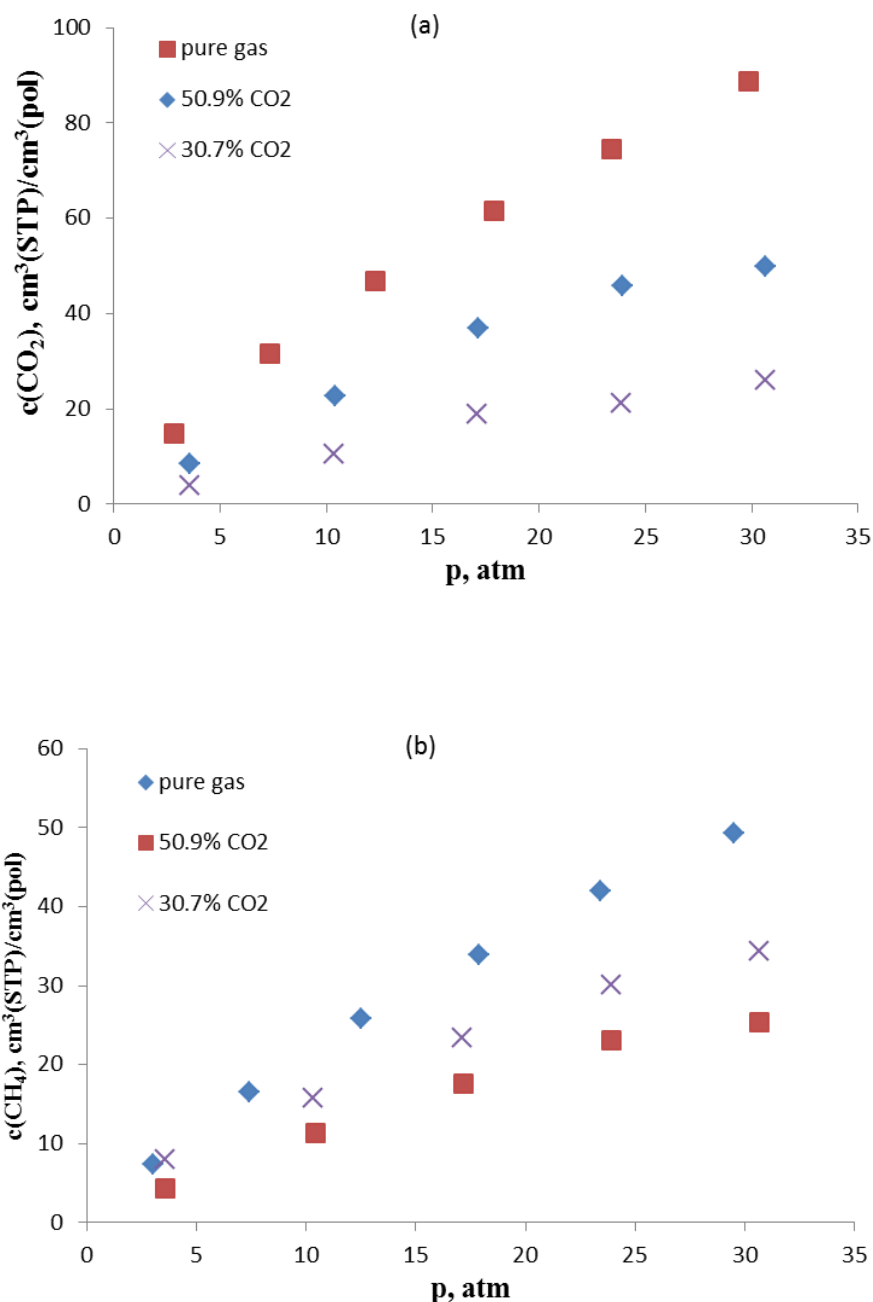


Fig 5.2. Pure and mixed gas in Polynonene membrane at 35°C a) CO₂, b) CH₄.

To see clearly the effect of mixed gas, solubility isotherms of the gases are plotted with respect to their respective fugacity. The results are shown on Fig 5.3a for CO₂ and Fig 5.3b for CH₄. As can be seen on the figure below the sorbed concentration of both CO₂ and CH₄ in polynonene membrane doesn't vary with the presence of the other gas in the system. The behavior observed in experimental analysis is proved by two models used to characterize the polymers Non-equilibrium Lattice Fluid (NELF) and Dual mode sorption model (DMS).

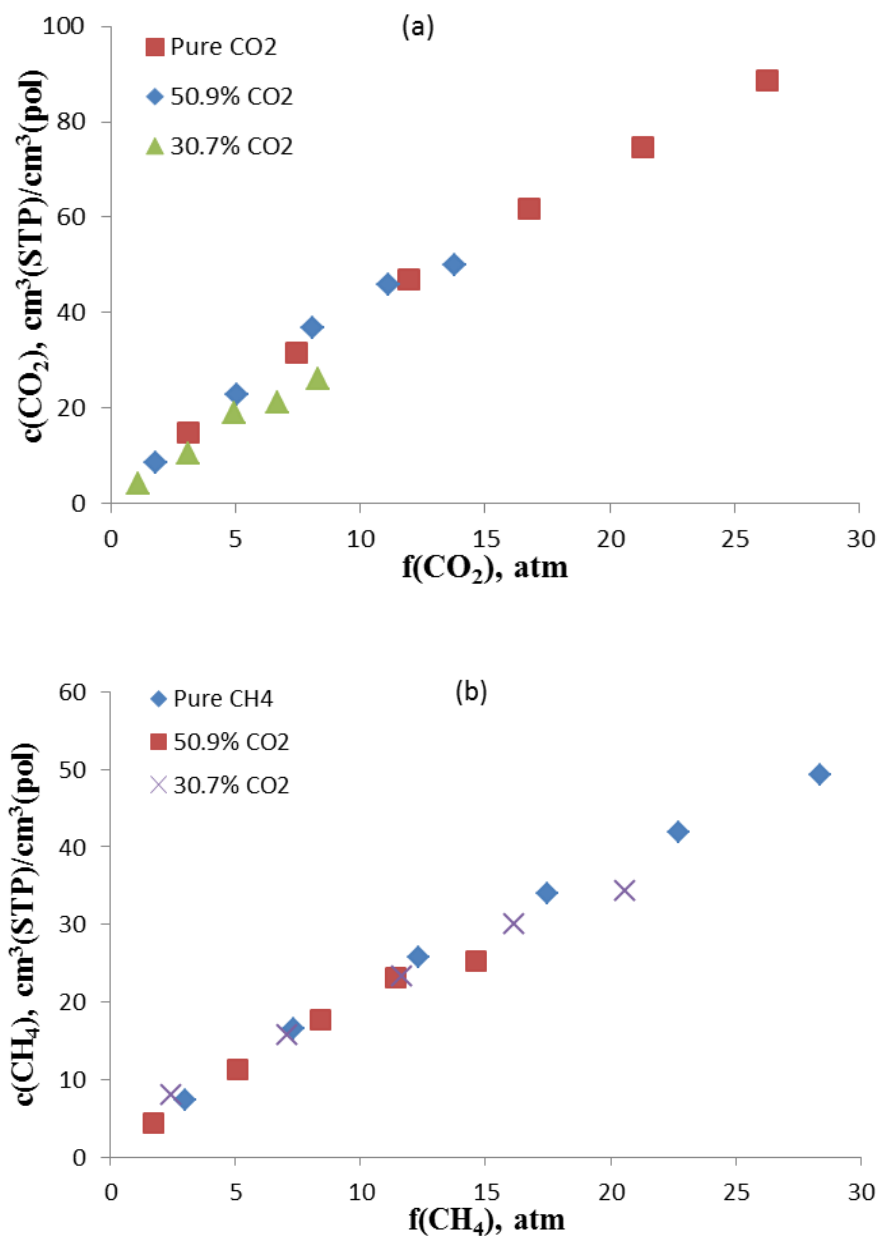
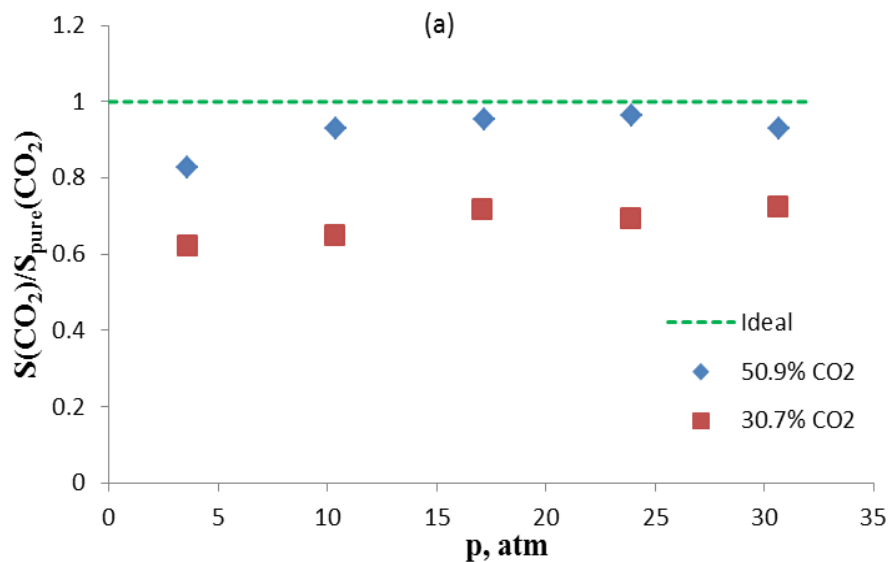


Fig 5.3. Pure and mixed gas sorption versus fugacity of gases at 35°C; a) CO₂, b) CH₄

In order to present in a more direct way the mixed gas effect, we have reported the ratio between actual solubility coefficient and its pure gas value. Deviations from unity immediately quantify the deviations from the ideal pure gas behavior. Fig 5.4a shows solubility coefficients ratio for CO₂ at 35°C, while Fig 5.4b shows solubility coefficients ratio of CH₄ at 35°C in polynonene membrane.

The results show that all solubility coefficient ratios are below unity which means that for both gases there is always a solubility depression from the pure gas case due to mixed gas conditions. This is because of the competition between the two gases in the mixture, which lowers the solubility of the other gas compared to the pure gas solubility coefficient. The solubility coefficient ratio is more varying with respect to molar fraction of CO₂ than is with respect to total pressure, as it can be seen from the figure.



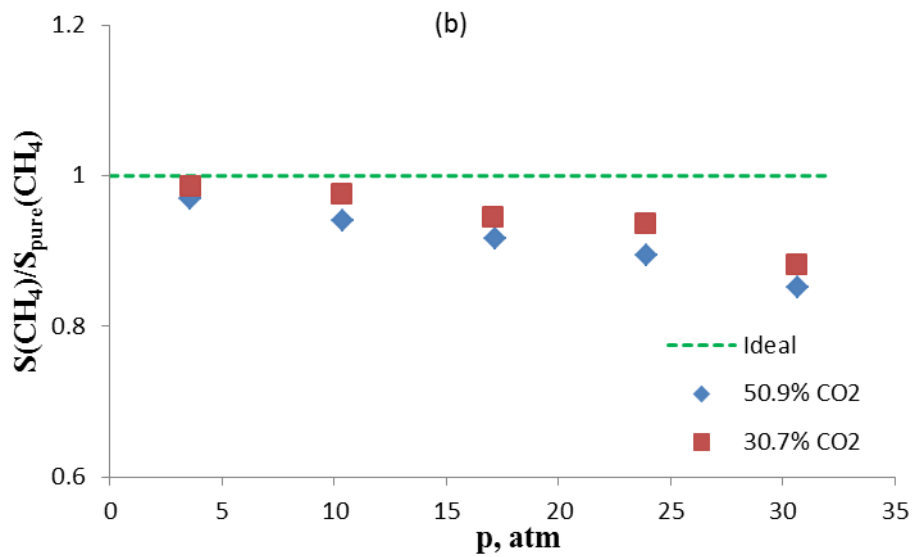
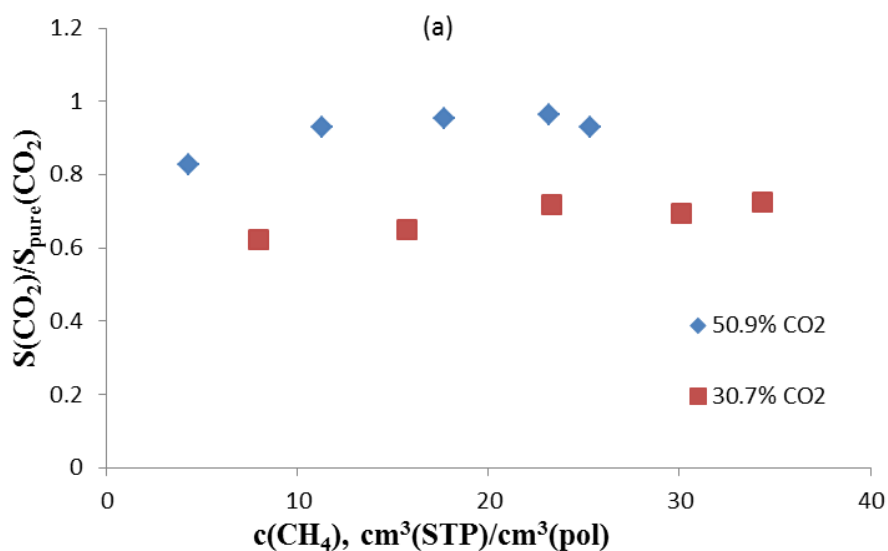


Fig 5.4. Ratio between mixed and pure gas solubility coefficient of a). CO₂, b) CH₄, versus total gas pressure at 35.0°C for different molar fractions of CO₂ in the gas mixture.

Another way to present these data is to plot solubility coefficient ration with respect to concentration of co-sorbent gas. The results are shown in Fig 5.5a and b. It can be seen from the plot that solubility coefficient ratio of CO₂ doesn't vary with respect to concentration of CH₄ as can be seen on Fig 5.5a. But there is a decreasing trend for solubility coefficient of CH₄ with respect to concentration of CO₂. This shows that the presence of CH₄ in the mixture system doesn't affect solubility of CO₂ that much while the presence of CO₂ in the system decreases the solubility of CH₄ as can be seen from the graph.



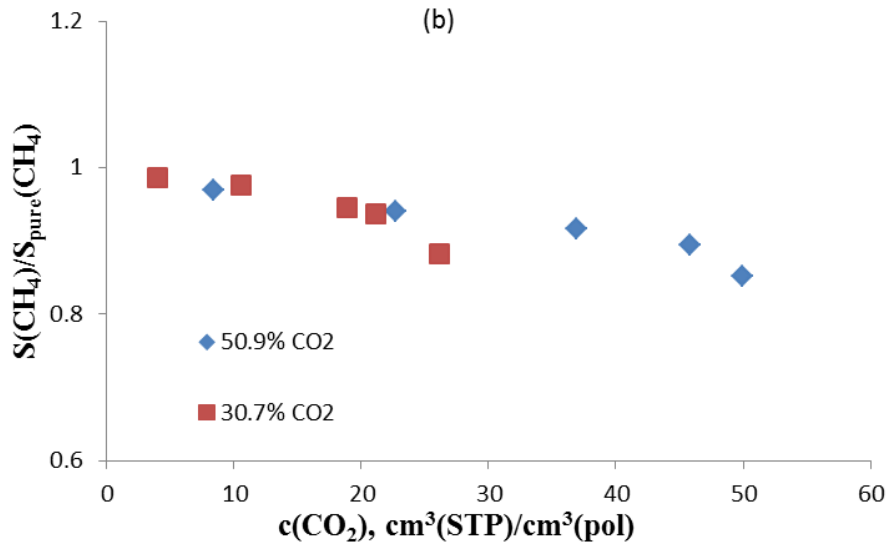


Fig 5.5. Ratio between mixed and pure gas Solubility coefficient S of (a) CH_4 , (b) CO_2 , versus 2nd component molar concentration at 35°C .

5.4 Solubility selectivity of Polynonene polymers

Pure gas solubility selectivity polynonene is presented on Fig 5.6a. From the result it can be seen that pure gas solubility selectivity follow a constant trend with respect to total pressure for 30.7 molar percent of CO_2 in the mixture, while it shows a small decrease for 50.9 molar percent of CO_2 . Pure gas solubility selectivity increases with decreasing of molar concentration of CO_2 .

Mixed gas solubility selectivity is plotted against total pressure as can be seen on Fig 5.6b. The results show that there is a constant trend of mixed gas solubility selectivity with respect to total pressure for 50.9% CO_2 , while it increases for 30.7% CO_2 . Mixed gas solubility selectivity increases with increasing of molar concentration of CO_2 .

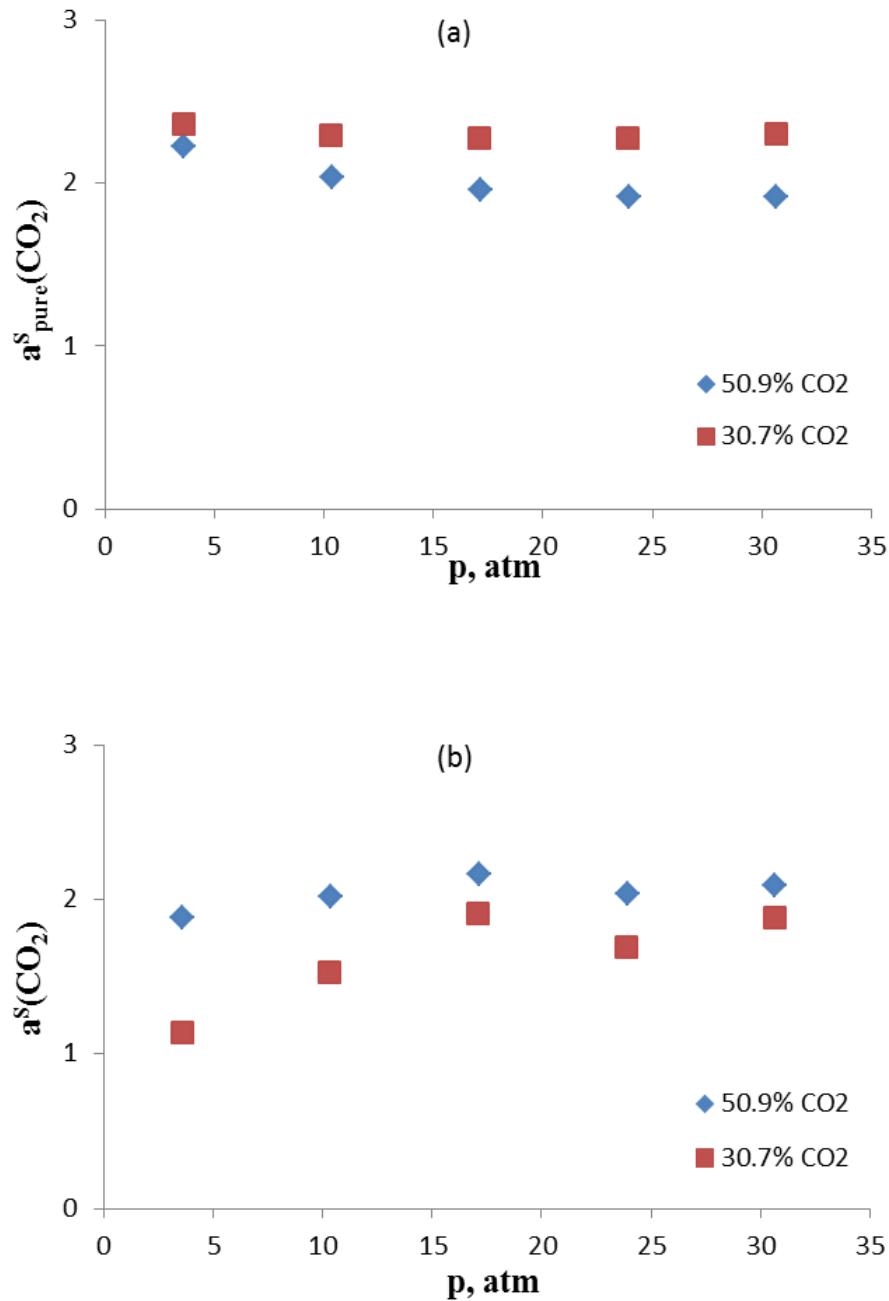


Fig 5.6. (a) Pure-gas (ideal) and (b) mixed-gas (real) solubility-selectivity for the CO₂-CH₄ mixture in Polynonene at 35°C, for different molar fractions of CO₂ in the gas mixture, versus total pressure

5.5 Comparison of solubility of polynonene with that of PIM-based polymers

In this section solubility and solubility selectivity of polynonene membrane and that of PIM-based membranes are compared. The results are shown on Fig 5.7a and b. From the result it can be seen that CO₂ pure gas solubility in polynonene membrane is lower than CO₂ pure gas solubility in PIM-based membranes. Fig 5.7b shows CH₄ pure gas solubility in Polynonene, PIM-1, TZPIM-1 and

AO-PIM-1 membrane. The result reveals that CH₄ pure gas solubility in polynonene membrane is also lower than CH₄ pure gas solubility in PIM-based membranes. But the difference between the pure CO₂ solubility in polynonene and PIM based membranes is higher than the difference between pure CH₄ solubility in polynonene and PIM-based membranes which reveals that the solubility selectivity of polynonene membrane is lower than that of PIM-based membranes.

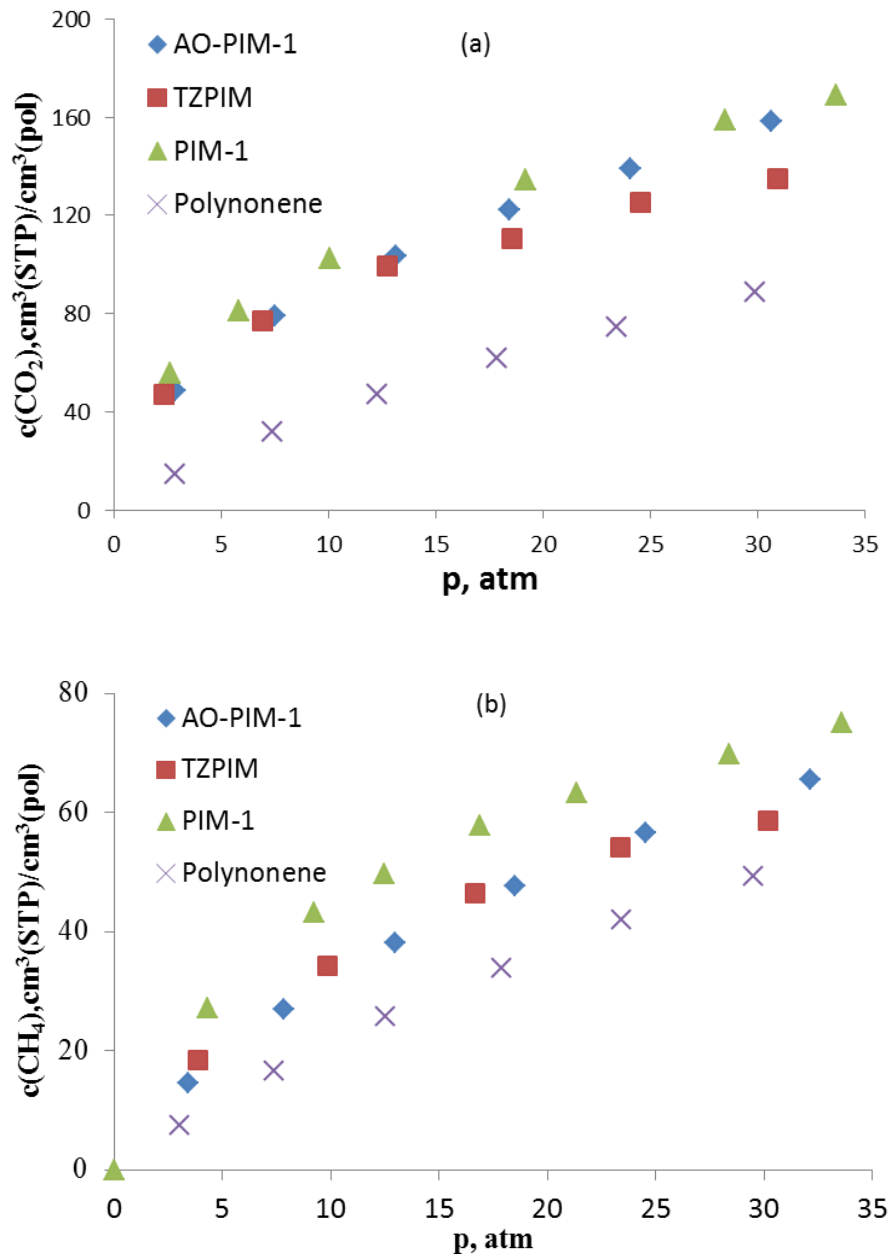


Fig. 5.7. Pure gas sorption comparison between polynonene and PIM-based membranes at 35°C; a). CO₂ and b).CH₄

Mixed gas solubility of CO₂ and CH₄ at 50.9 molar percent of CO₂ is also compared for polynonene and PIM-based membranes. The results are shown on Fig 5.8a, and b. From the plot of 5.8a, we can see that mixed gas solubility of CO₂ is lower for polynonene membrane as compared to the PIM-

based membrane. This result has the same trend with that of pure CO₂ solubility in these polymers as explained above. On the contrary mixed gas solubility of CH₄ for polynonene membrane is higher than that of PIM-1 and TZPIM-1 above 15 atm and it is lower than the results of PIM-1, TZPIM-1 and AO-PIM-1 below 15 atm. CH₄ mixed gas solubility of polynonene is the same with that of AO-PIM-1 above 15 atm as can be seen on Fig 5.8b.

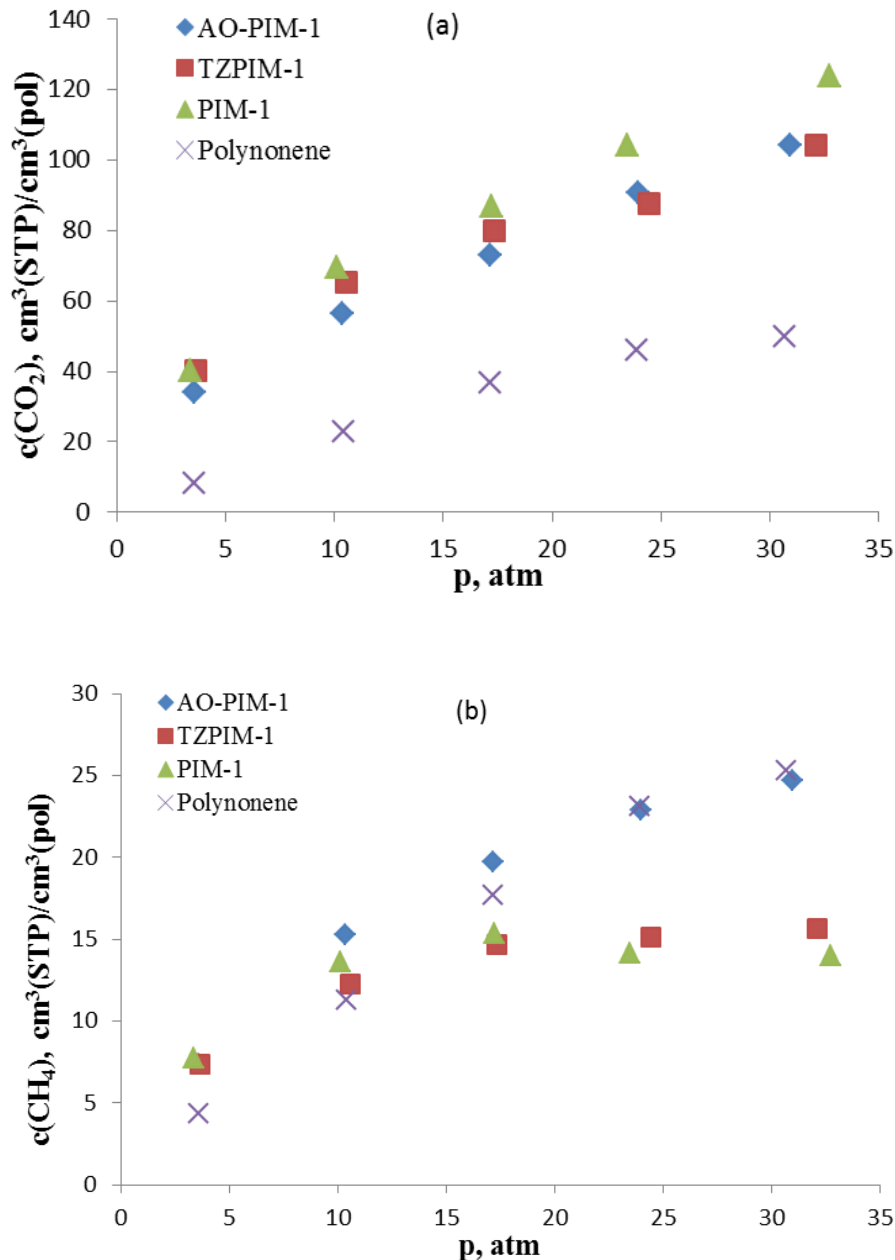
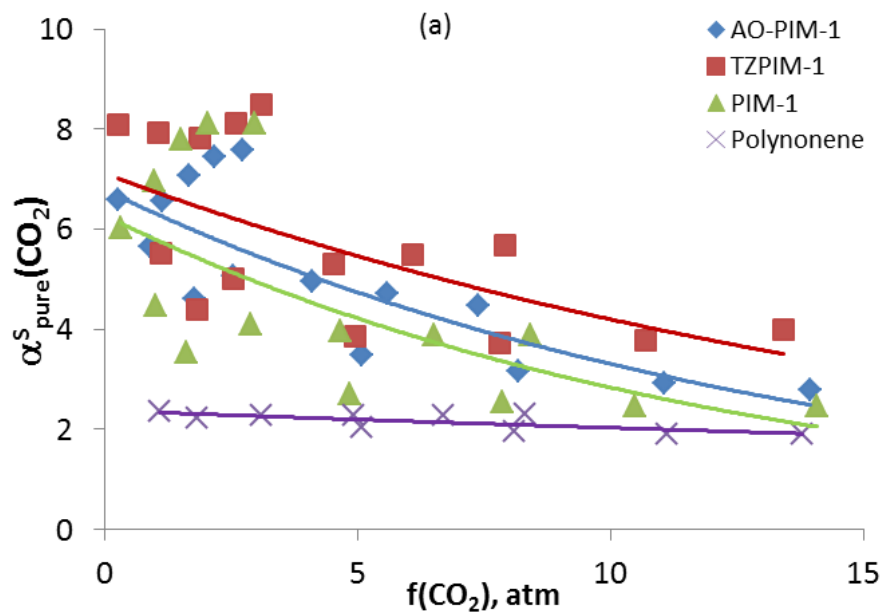


Fig. 5.8. Mixed gas sorption comparison between polynonene and PIM-based membranes at 35°C and 50.9% CO₂; a). CO₂ and b).CH₄

Solubility selectivity of polynonene membrane for CO₂/CH₄ mixture is also compared with PIM-based membranes. The results are plotted against total pressure as shown on Fig 5.9. It can be seen from the plot that both pure gas and mixed gas solubility selectivity of Polynonene is lower than the corresponding results of PIM-based polymers. Pure gas solubility selectivity of polynonene membrane shows a constant trend with respect to fugacity of carbon dioxide while the mixed gas solubility selectivity shows a slight increase with respect to fugacity of carbon dioxide.

When we compare the variation of pure gas solubility selectivity of polynonene with that of PIM-based membranes and variation of mixed gas solubility selectivity of polynonene membrane and PIM-based membrane, the latter is higher; this is because the methane mixed gas solubility of Polynonene is almost comparable to that of methane solubility in PIM-based membrane in mixed gas which will reduce the mixed gas solubility selectivity even more than pure gas solubility selectivity.



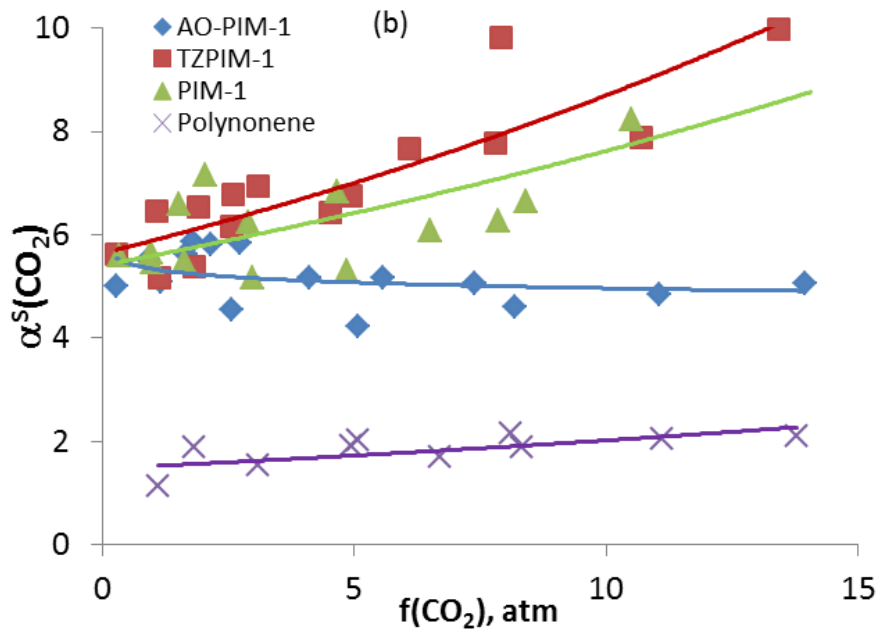


Fig 5.9. a) Pure gas solubility selectivity, b) mixed gas solubility selectivity of glassy polymers versus fugacity of CO₂ at 35°C

5.6 Conclusions

Finally we can conclude that Polynonene membrane has lower pure gas and mixed gas solubility than the corresponding results of PIM-based membranes. Both pure gas and mixed gas solubility selectivity of polynonene membrane are lower than pure gas and mixed gas solubility selectivity of PIM-based membranes. The methane mixed gas solubility of polynonene membrane is comparable with that of PIM-based membranes while carbon dioxide mixed gas solubility is lower than PIM-based membranes which make the final result of mixed gas solubility selectivity much smaller than the mixed gas solubility selectivity of PIM-based membranes.

There is a slight increase of mixed gas solubility selectivity of polynonene membrane with respect to fugacity of carbon dioxide but pure gas solubility selectivity follows a constant trend with respect to fugacity of carbon dioxide.

6 Modeling of mixed gas sorption in glassy polymers

6.1 Introduction

In this chapter, sorption of pure and mixed gas of carbon dioxide and methane in different polymeric membrane material is parameterized using two well-known models. The first model studied here is Dual mode sorption model (DMS) at different temperature and composition of mixture. Non-equilibrium lattice fluid (NELF) model is also studied in detail to parametrize sorption of pure and mixed gas sorption of carbon dioxide and methane in PIM-1, TZPIM-1, AO-PIM-1 and Polynonene.

A gas sorption isotherm in a glassy polymer is generally concave to the pressure axis. This behavior is characteristic for dual-mode sorption composed of Henry's law dissolution in an equilibrium region and Langmuir-type sorption in a non-equilibrium region [204-206]. This non-equilibrium region is directly related to the excess free volume or unrelaxed free volume in a glassy polymer [207]. The excess free volume reflects the non-equilibrium structure of a glassy amorphous polymer, which results from quenching the polymer from the rubbery to the glassy state. To date, various researchers have reported evaluation of the excess volume and related properties, such as gas sorption or dilation of glassy polymers [208–215]. For example, Paterson and Yampol'skii summarized solubility data of gases in a wide variety of glassy polymers [216].

The NELF model is based on the use of an expression for the Gibbs free energy of the non-equilibrium glassy mixture, which derives from the lattice fluid theory developed by Sanchez and Lacombe (1978), by using the polymer density as an internal state variable. Formulation of NELF model and several comparisons with experimental data will be considered by Doghieri et al [217-220]. Simply based on the knowledge of pure penetrant and pure polymer PVT properties and on knowledge of the polymer volume, the model can indeed predict the solubility of pure and mixed components in a non-equilibrium glassy polymer.

6.2 Dual mode sorption model

6.2.1 Basic concept

Permeation of a gas molecule in a dense polymer film is usually governed by a solution-diffusion mechanism. The permeability, P , is the product of diffusivity, D , and solubility, S , when the downstream pressure is significantly lower than the upstream pressure,

$$P = DS \quad 6.1$$

Rubbery polymers are in a hypothetical thermodynamic equilibrium liquid state and their gas solubility obeys Henry's law. On the other hand, glassy polymers are typically assumed to be in a non-equilibrium state containing two components; a hypothetical liquid state and a solid state. Over the past three decades, sorption of gas molecules in glassy polymers has been described and analyzed by the dual-mode sorption model [204–206]. This model is based on two types of sorption sites that obey (i) Henry's law dissolution and (ii) Langmuir-type sorption. The former is related to dissolution of gases into rubbery polymers and low molecular weight liquids. The latter is related to Langmuir-type sorption in porous solids. The Langmuir sorption site in a glassy polymer corresponds to holes or "microvoids" which arise due from the non-equilibrium nature of glassy polymers.

The dual-mode sorption model for pure component is expressed by:

$$c = k_D f + \frac{C_H f}{1 + b f} \quad 6.2$$

Where f is fugacity of the pure gas, k_D is the Henry's law constant, C_H is the Langmuir sorption capacity and b is the Langmuir affinity constant.

Based only on parameters of pure gases in the polymer, the concentrations of each compound of a binary mixture in the polymer were estimated from equations [189];

$$c_i = k_{D1} f_i + \frac{C_{H1} f_i}{1 + b_1 f_i + b_2 f_2}$$

$$\frac{c_1}{c_1 + c_2} = \frac{f_1}{f_1 + f_2}$$

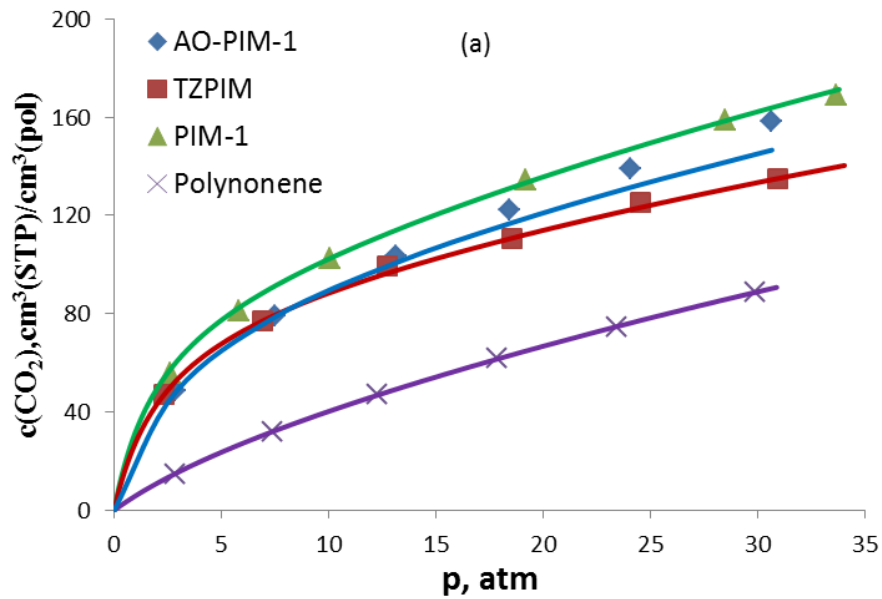
6.3

Where f_1 and f_2 are fugacities of gas 1 and gas 2 in the gaseous binary mixture.

6.2.2 Dual mode sorption model for pure gas sorption

Dual mode sorption model for sorption experiment in different polymeric membrane at different temperature was carried out to see whether the system of pure and mixed gas sorption can be parametrized and the results are predicted.

Pure gas sorption of carbon dioxide and methane in PIM-1, TZPIM-1, AO-PIM-1 and polynonene at 35°C is presented on Fig 6.1 with the corresponding dual mode sorption model results. From the figure it can be seen that dual mode sorption model represents the experimental results quit well. The Dual mode parameters used for the modeling are presented on Table 6.1.



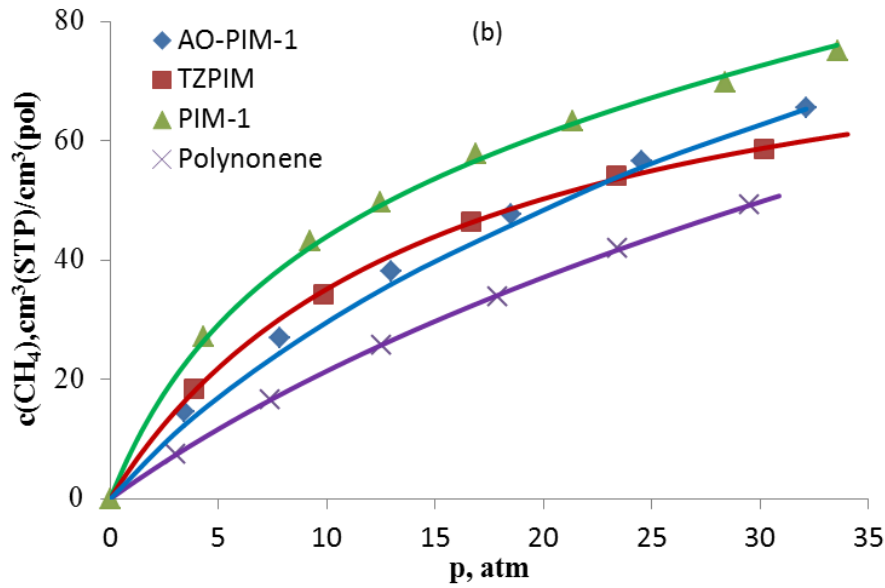


Fig.6.1. Dual mode model results of pure gas sorption in different membranes at 35°C; a) CO₂, b) CH₄

Membrane	CO ₂			CH ₄		
	K _D , cm ³ (STP)/cm ³ (pol) atm	C _H , cm ³ (STP)/cm ³ (pol)	b, atm ⁻¹	K _D , cm ³ (STP)/cm ³ (pol) atm	C _H , cm ³ (STP)/cm ³ (pol)	b, atm ⁻¹
PIM-1	3.081	88.5	0.4882	0.7137	66.4	0.127
TZPIM-1	2.158	83.99	0.437	0.0004	90.19	0.065
AO-PIM-1	2.663	84.46	0.3243	0.817	60.34	0.067
Polynonene	2.603	26.98	0.139	0.706	64.56	0.029

Table 6.1. Dual mode parameters for pure CO₂ and pure CH₄ at 35°C.

Dual mode sorption model is studied at different temperature for PIM-1 and TZPIM-1 up to the pressure range of 30 atm. The results for PIM-1 are presented on Fig 6.2. It can be revealed that dual mode sorption model predicts the experimental results at different temperature correctly. Solubility decreases with increasing of temperature and the result is well represented with the model. Dual mode parameters for PIM-1 at different temperatures are presented in table 6.2.

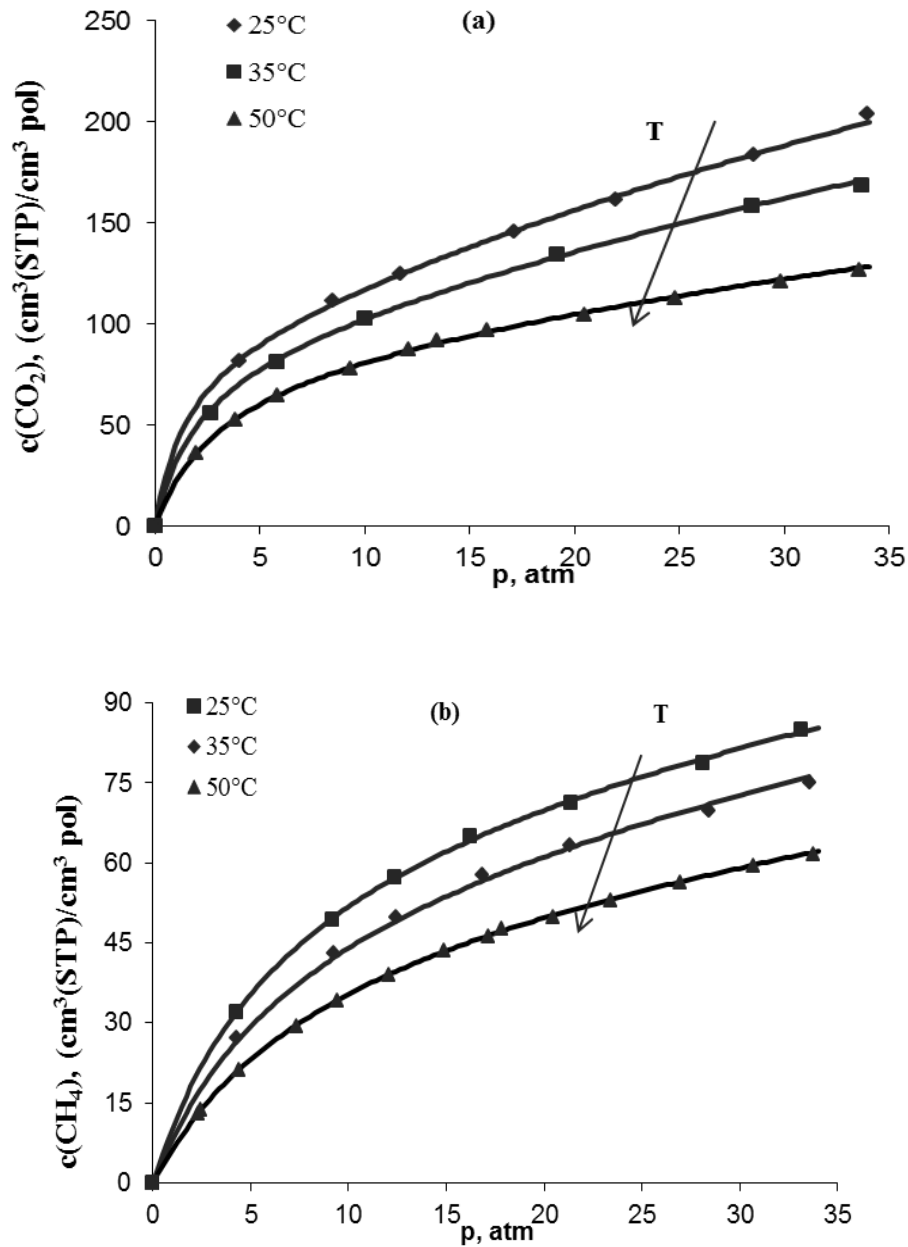


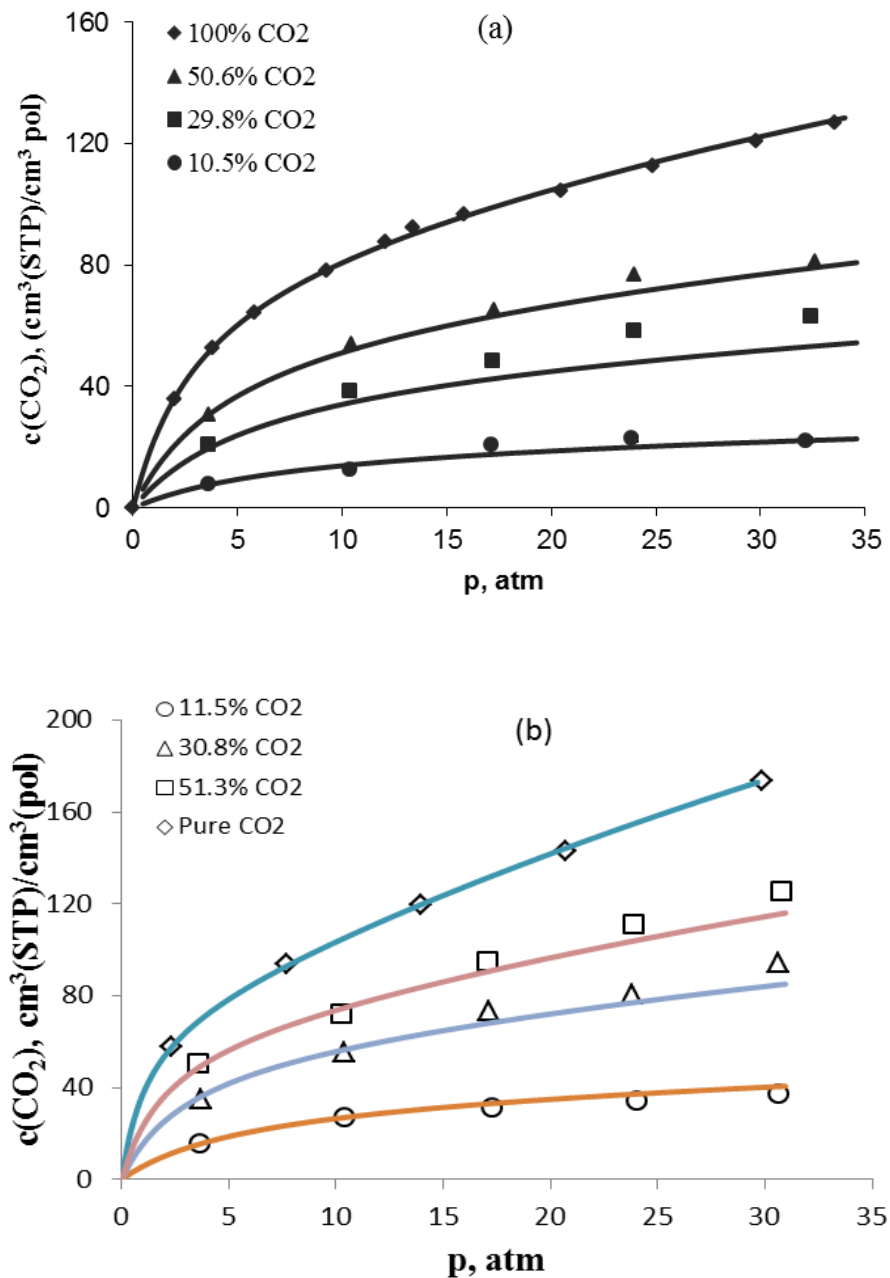
Fig 6.2. Pure gas sorption of PIM-1 at different temperature with dual mode model results; a) CO₂, b) CH₄

Temperature	CO ₂			CH ₄		
	K _D , cm ³ (STP)/cm ³ (pol) atm	C _H , cm ³ (STP)/cm ³ (pol)	b, atm ⁻¹	K _D , cm ³ (STP)/cm ³ (pol) atm	C _H , cm ³ (STP)/cm ³ (pol)	b, atm ⁻¹
25°C	3.97	91.92	0.66	0.68	77.42	0.14
35°C	3.08	88.5	0.49	0.71	66.4	0.13
50°C	1.74	84.87	0.32	0.51	58.29	0.11

Table 6.2. Dual mode parameters for pure CO₂ and pure CH₄ in PIM-1 at different temperature.

6.2.3 Dual mode sorption model for mixed gas sorption

Mixed gas sorption of carbon dioxide and methane was parametrized with dual mode sorption model for all the polymeric membrane studied in this thesis work at different temperatures and pressure range. The results are presented here for PIM-1, TZPIM-1, and Polynonene up to a pressure range of 30 atm. Fig 6.3 and 6.4 represents pure and mixed gas sorption experimental results respectively with dual mode sorption model results. It is clearly visible that dual mode sorption model estimate the experimental results very well in which it can be used in the absence of experimental data.



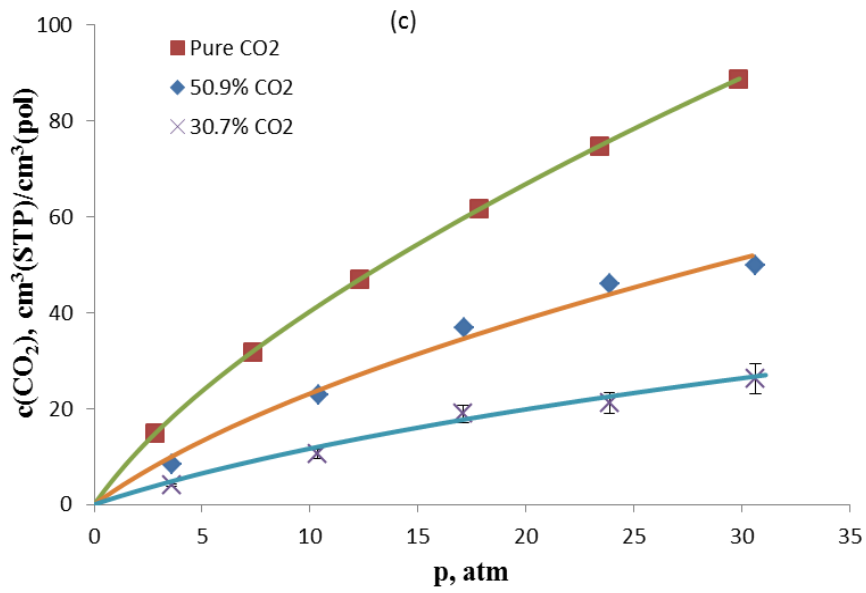
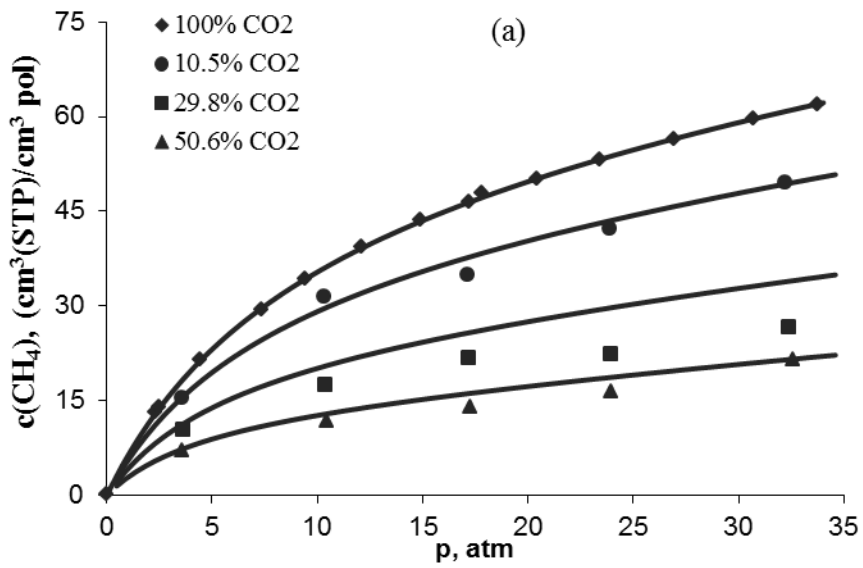


Fig.6.3. Pure and mixed gas sorption of carbon dioxide with dual mode model versus total pressure; a) PIM-1 at 50°C, b). TZPIM-1 at 25°C and c). Polynonene at 35°C



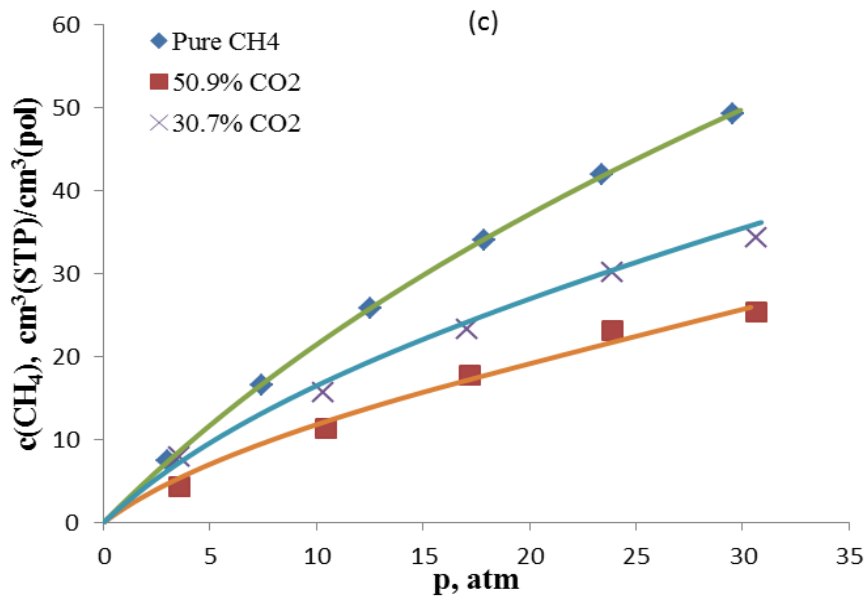
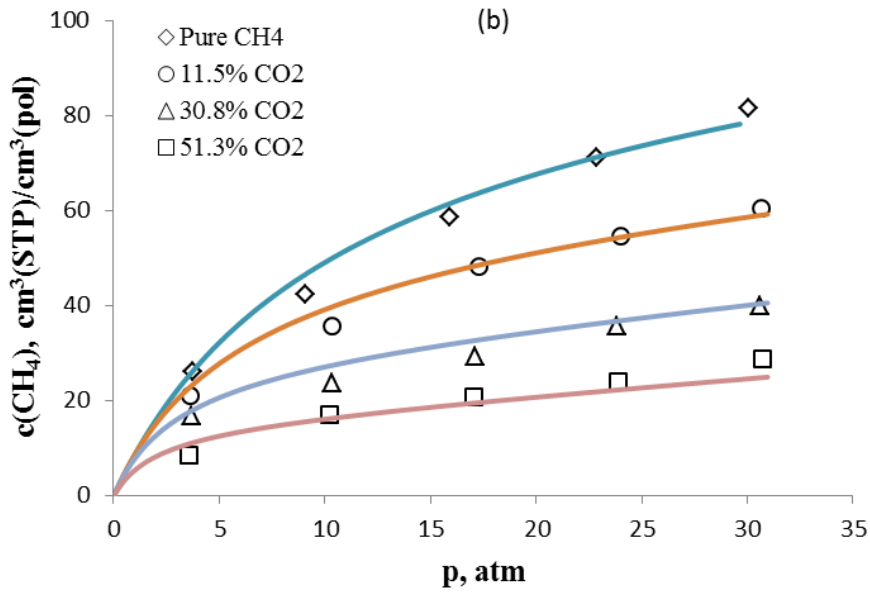


Fig.6.4. Pure and mixed gas sorption of methane with dual mode model versus total pressure; a) PIM-1 at 50°C, b). TZPIM-1 at 25°C and c). Polynonene at 35°C

6.3 Non-Equilibrium Lattice Fluid model

6.3.1 Basic concept

Solubility of gases in rubbery polymer can be modelled using thermodynamic models based on activity coefficient or equation of state (EoS). Since glassy polymers are not at equilibrium such

approach to model the solubility of gases cannot be used. Non-equilibrium Lattice Fluid model is among the most used for such type of polymer. Doghieri et al [217] and Baschetti et al [221] describes in detail about Non-equilibrium Lattice Fluid model for pure penetrants in glassy polymers. The application of NELF for mixed gas penetrant is studied in detail elsewhere [222, 223].

In NELF model the chemical potential of a single penetrant (1) in a glassy polymer (2) has the form:

$$\mu_1 = \mu_1^0 + RT \ln \left(\frac{\phi_1}{\tilde{\rho}} \right) + RT \ln \left(\frac{r_i^0}{v_i^0} \right) \quad (6.4)$$

If we consider sorption of N_p penetrants in a glassy polymer, the chemical potential of i -th penetrant in the solid phase has the form:

$$\mu_i = \mu_i^0 + RT \ln \left(\frac{\phi_i}{\tilde{\rho}} \right) + RT \ln \left(\frac{r_i^0}{v_i^0} \right) \quad (6.5)$$

Where ϕ_i is volume fraction, $\tilde{\rho}$ is dimensionless density, r_i^0 is the number of lattice sites occupied by one mole of species i in the pure component lattice, v_i^0 is characteristic volume. Their description and method of calculation is given elsewhere [217, 221, and 223].

6.3.2 Non-equilibrium lattice fluid model for pure gas sorption

Sorption isotherms of pure carbon dioxide and pure methane in different polymeric membrane are examined using NELF model. The results pure gas solubility of carbon dioxide and methane in PIM-1, TZPIM-1, AO-PIM-1 and polynonene are presented in Fig 6.5. From the Figure it can be seen that Non-equilibrium lattice fluid model represents pure gas sorption experiment data for both carbon dioxide and methane correctly over all the pressure range considered.

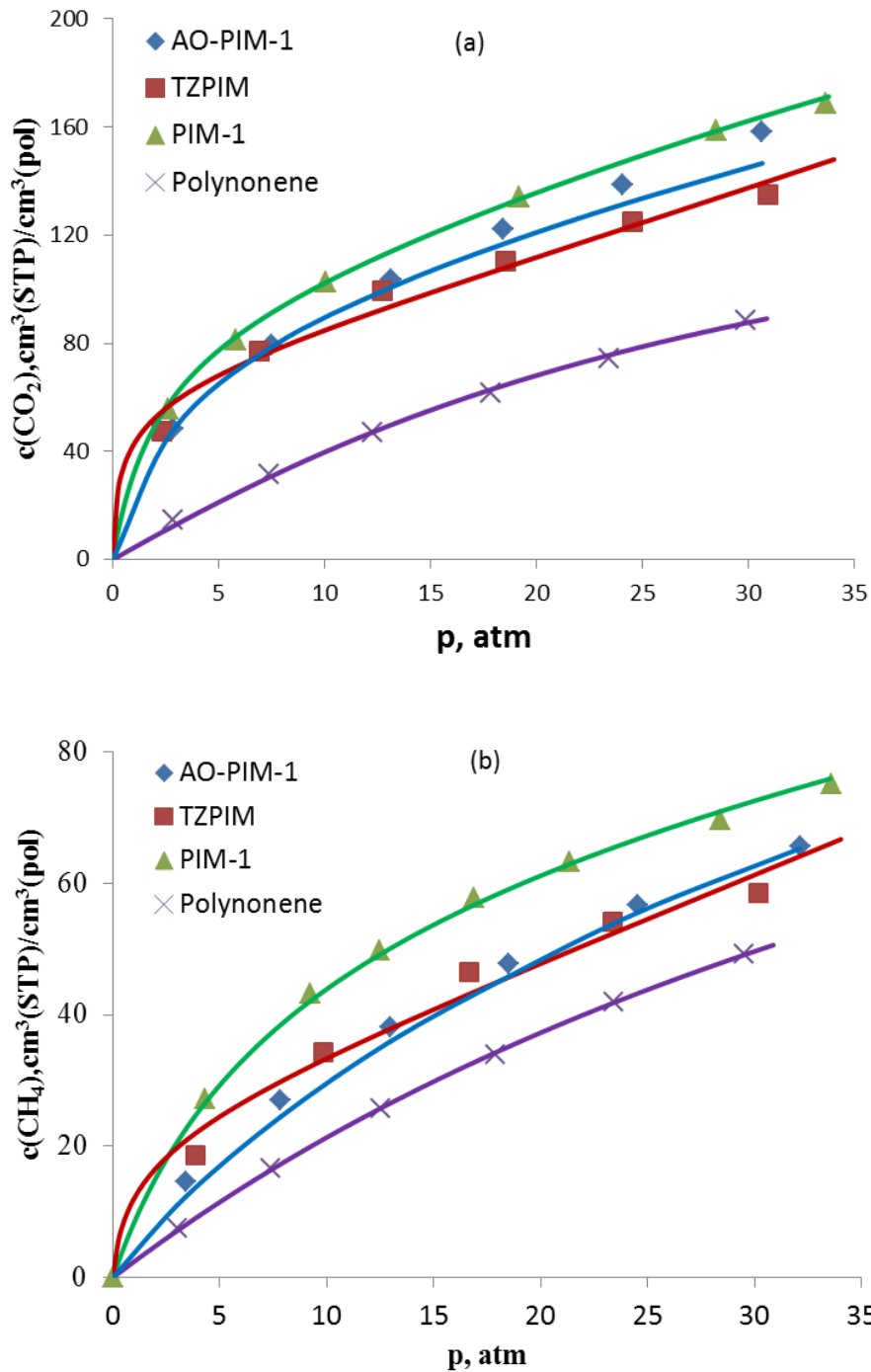


Fig. 6.5. NELF model results of pure gas sorption in different membranes at 35°C; a) CO_2 , b) CH_4 .

The model is also studied for pure gas sorption at different temperature to see its validity under temperature variation. Fig 6.6 plots pure gas experimental results for carbon dioxide and methane in PIM-1 at different temperature. The results indicate that NELF model works very well at different temperature.

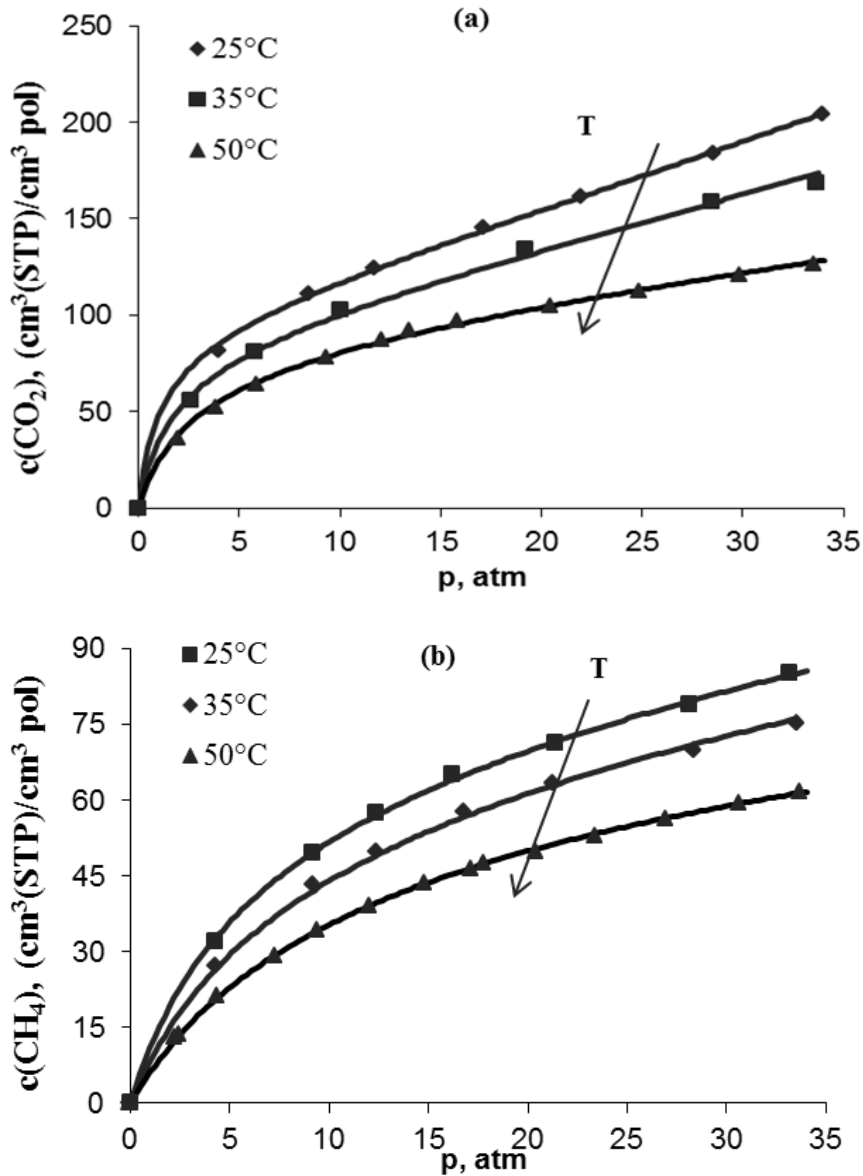


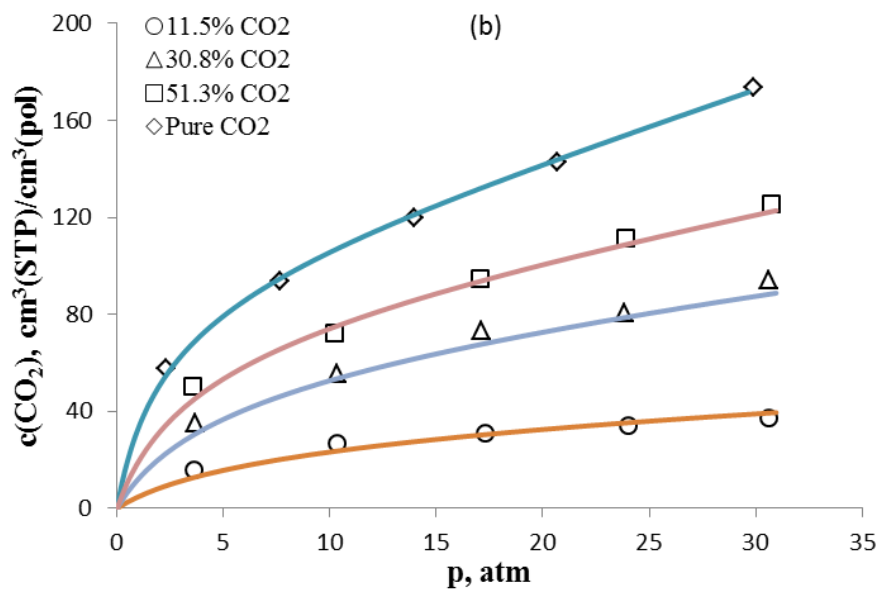
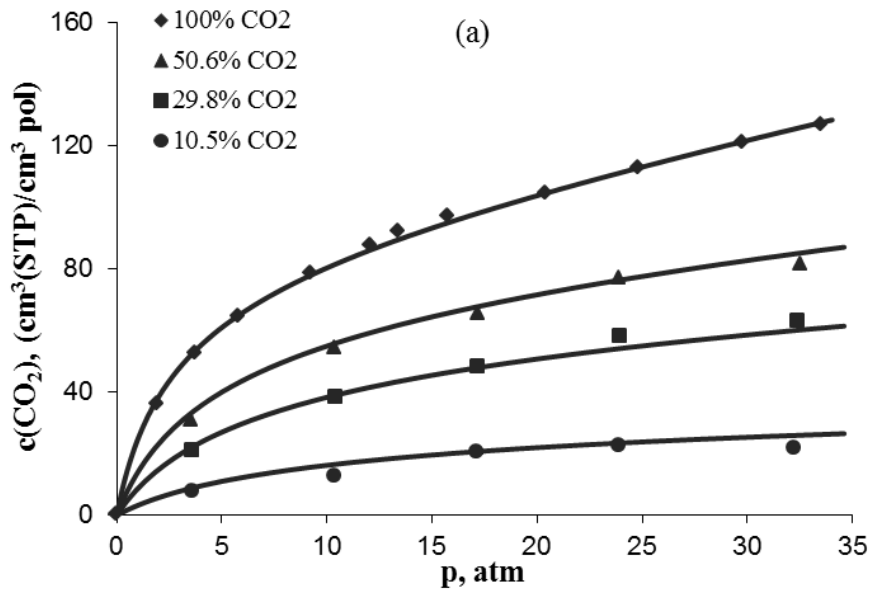
Fig 6.6. Pure gas sorption of PIM-1 at different temperature with NELF model results; a) CO_2 , b) CH_4

6.3.3 Non-equilibrium lattice fluid model for mixed gas sorption

NELF model prediction is performed for PIM-1, TZPIM-1 and polynonene membranes at different temperature and molar concentration of carbon dioxide. Fig 6.7 and 6.8 represents mixed gas sorption results of CO_2 and CH_4 respectively for different membranes.

The results of NELF model represent the experimental data correctly for all the three polymers examined, for all temperature studied and for different molar concentration of CO_2 . NELF model

also predicts the lesser effect of carbon dioxide and methane to each other in polynonene membrane very well in which we can understand that the model could be used as prediction tool for in the absence of experimental results at all temperatures, molar concentration and pressure range.



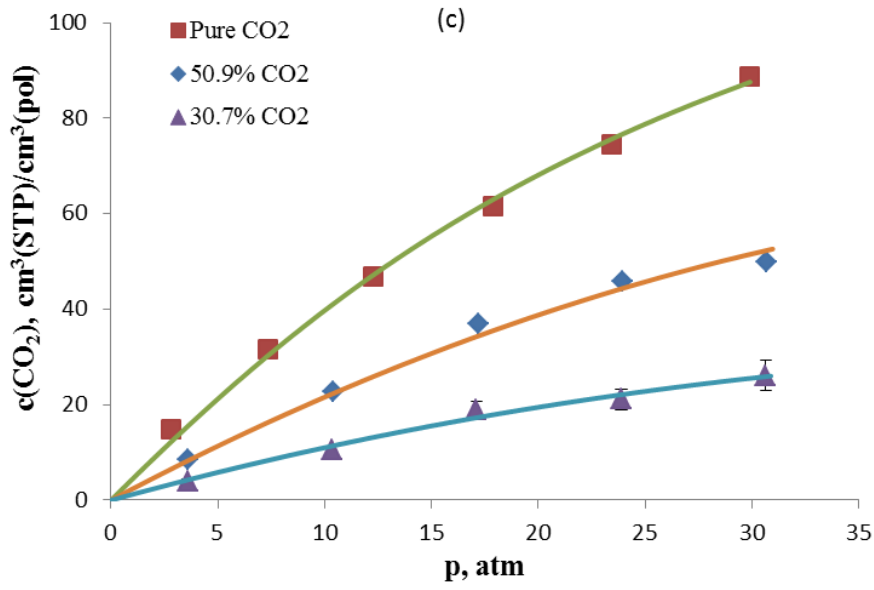
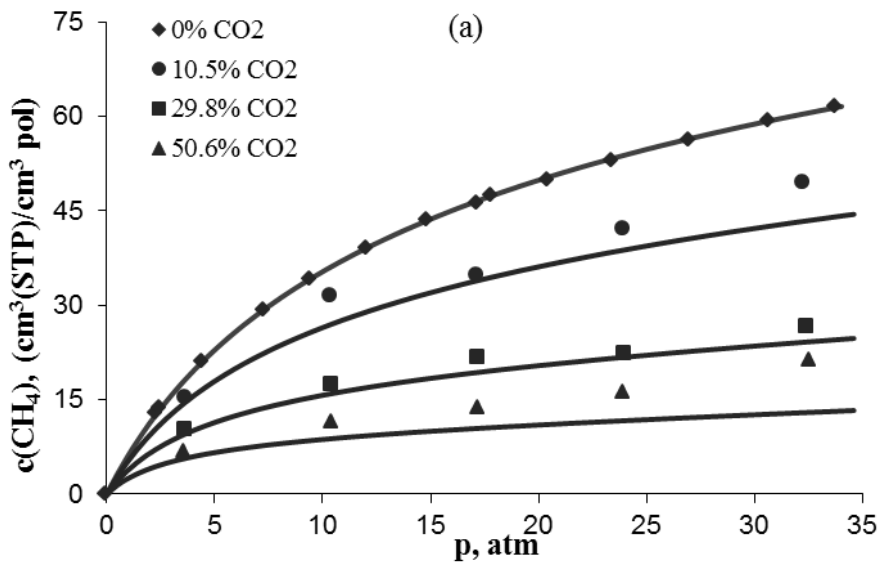


Fig.6.7. Pure and mixed gas sorption of carbon dioxide with NELF model versus total pressure; a) PIM-1 at 50°C, b). TZPIM-1 at 25°C and c). Polynonene at 35°C



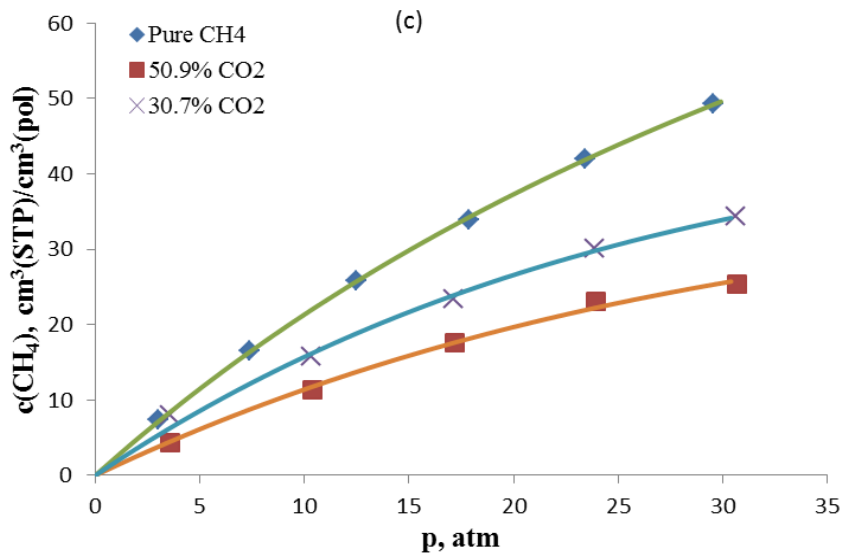
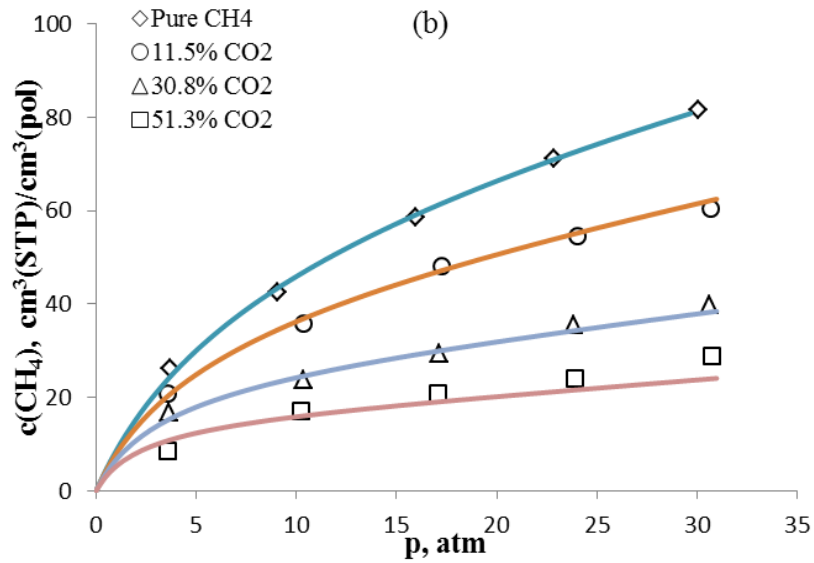


Fig.6.8. Pure and mixed gas sorption of methane with NELF model versus total pressure; a) PIM-1 at 50°C, b). TZPIM-1 at 25°C and c). Polynonene at 35°C

6.4 Conclusion

From the model results and experimental value comparison, we can see that both Dual mode sorption and NELF model fit with the experimental data. The fitting is valid in all molar concentration studied, temperature examined and pressure range for all the polymeric membrane studied in this thesis work. This helps that the model can be used to estimate pure and mixed gas sorption of CO₂ and CH₄ under the absence of experimental results and helps to reduce the time required and effort to make the complex mixed gas sorption experiment.

7 Effect of heat treatment on solubility, diffusivity and permeability of gases in glassy polymers

7.1 Introduction

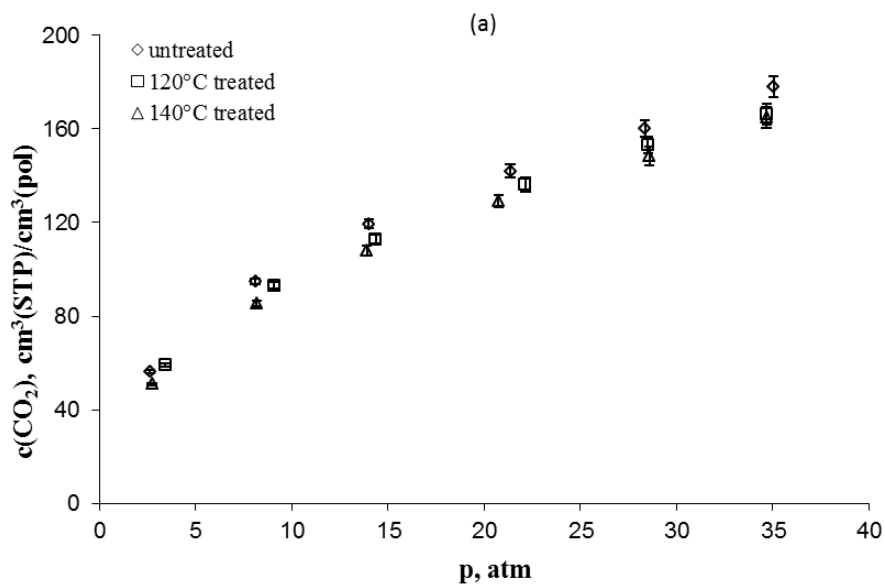
Physical aging, in which glassy polymeric membranes lose excess free volume through time, generally reduces gas permeability and increases selectivity particularly in thin films applied to gas separation system [224].

Heat treatment is applied to polymeric film membrane to fasten physical aging and study its effect on transport properties of gases. PIM-1 and TZPIM-1 membranes are thermally treated at three different temperatures as protocol described in the methodology section. Transport properties are obtained through pure gas sorption experiment of carbon dioxide and methane in the given membranes. This chapter presents the effect of heat treatment on solubility, diffusivity and permeability of pure gases in PIM-1 and TZPIM-1 at different temperature.

7.2 Effect of heat treatment on solubility of pure gases in glassy polymer

Sorption isotherms of carbon dioxide and methane for treated and untreated membrane sample is presented at 35°C for PIM-1 and TZPIM-1 membranes. The treatment temperatures are 120°C, 140°C and 160°C. Fig 7.1 represents sorption isotherms of carbon dioxide and methane in PIM-1 at 35°C and Fig 7.2 represents its solubility coefficient calculated from the ratio of sorbed concentration to fugacity of the given gas.

The result shows that the sorption isotherms of both pure carbon dioxide and pure methane don't vary with heat treatment. There is no variation for solubility coefficients of CO₂ and CH₄ in PIM-1 as can be seen in Fig 7.2.



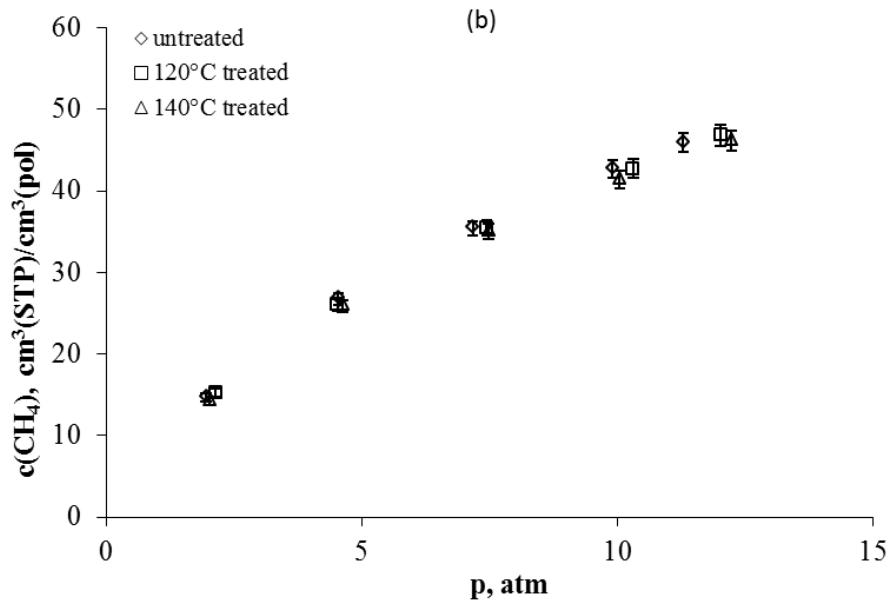
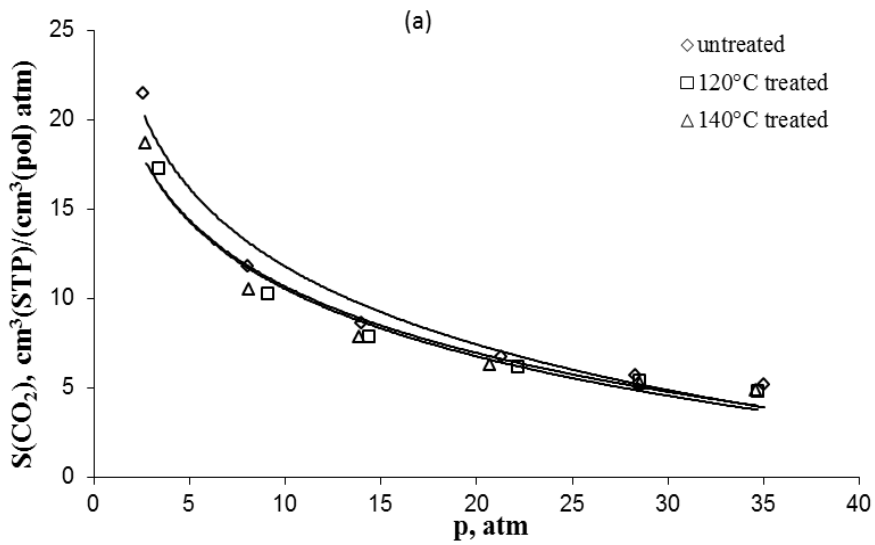


Fig. 7.1. Sorption isotherms of pure gases in thermally untreated and treated PIM-1 at 35°C; a) CO₂, b).CH₄



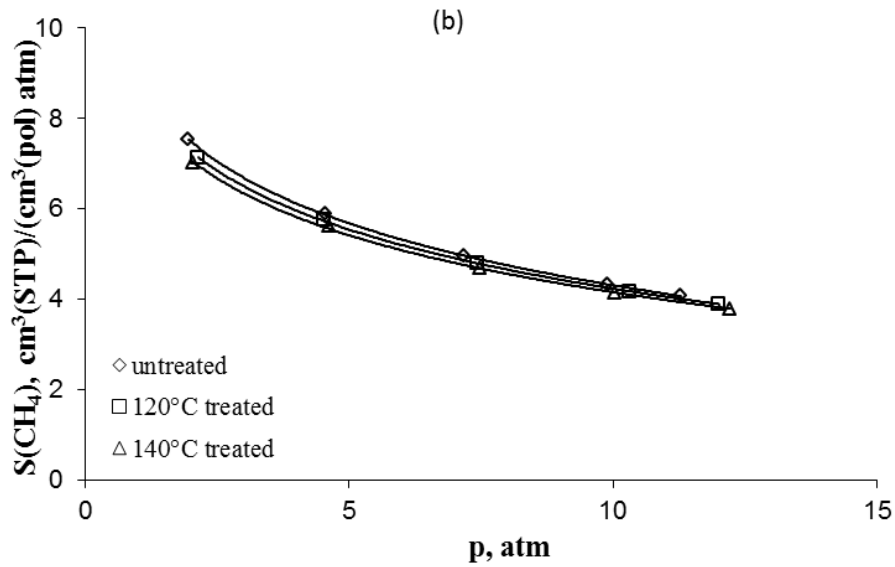
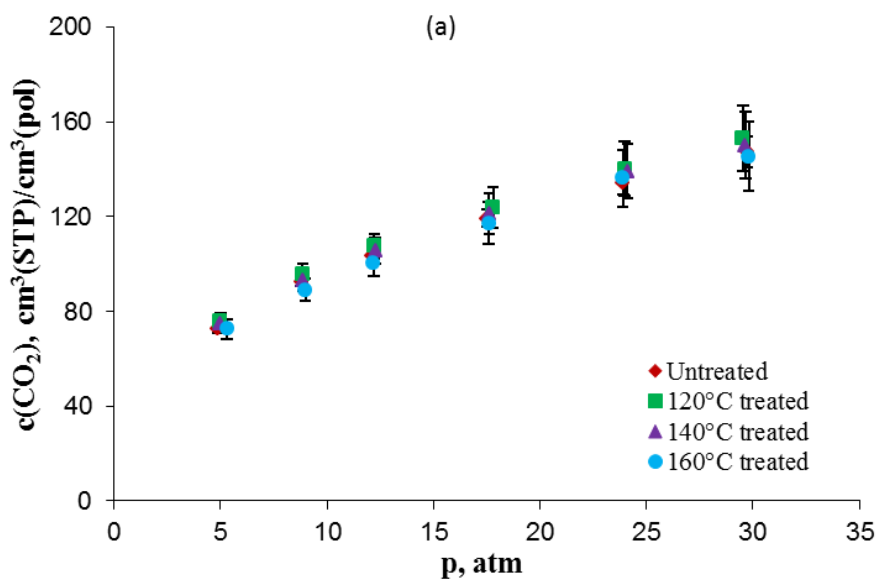


Fig.7.2. Solubility coefficient of pure gases in thermally untreated and treated PIM-1 at 35°C; a) CO₂, b).CH₄

Pure gas sorption of CO₂ and CH₄ in TZPIM-1 are also examined under untreated and treated sample at different temperature up to a pressure range of 35 atm for CO₂ and 15 atm for CH₄. The results obtained for TZPIM-1 are plotted in Fig 7.3 and 7.4.

Sorption isotherms of these gases in TZPIM-1 membrane don't vary due the heat treatment of the sample. Solubility coefficients of carbon dioxide and methane are not affected by the heat treatment the membrane sample as can be seen on the Figure below.



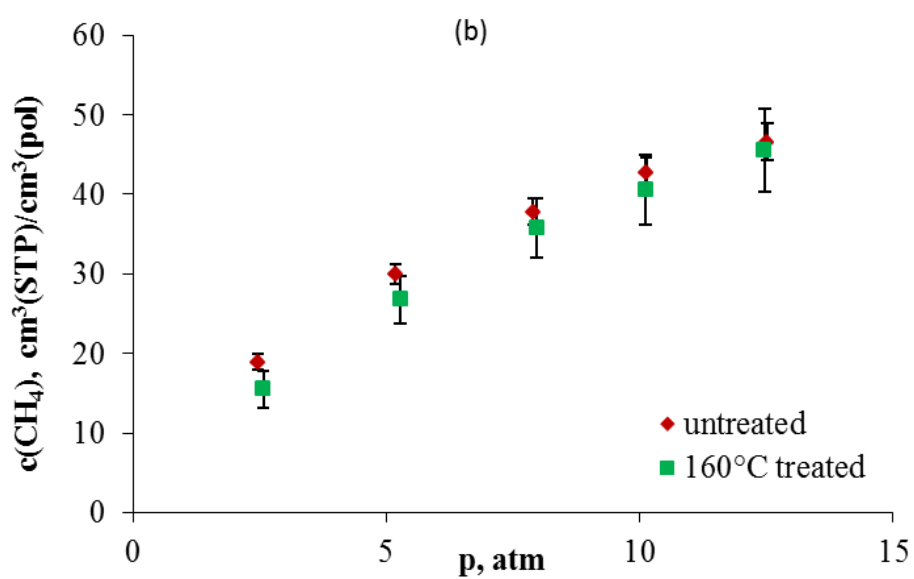
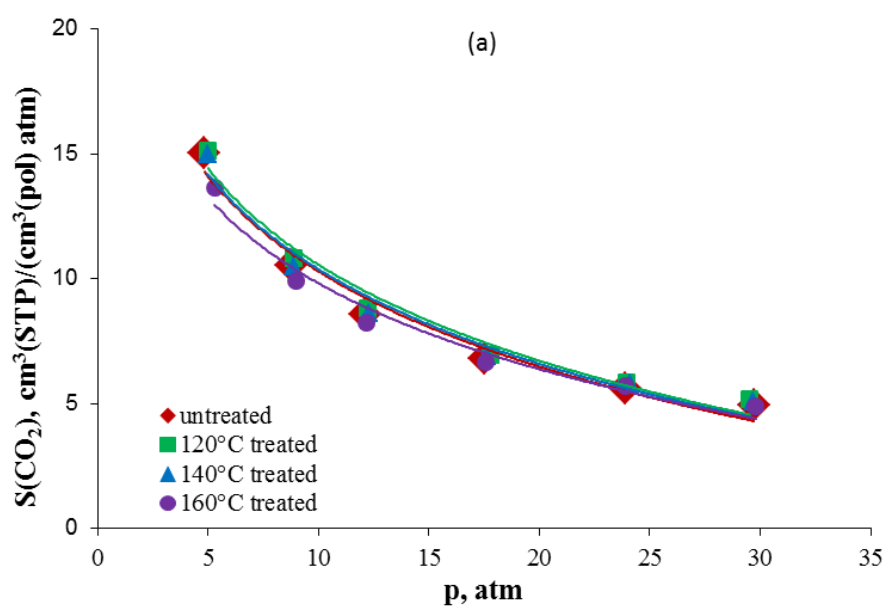


Fig. 7.3. Sorption isotherms of pure gases in thermally untreated and treated TZPIM-1 at 35°C; a) CO₂, b).CH₄



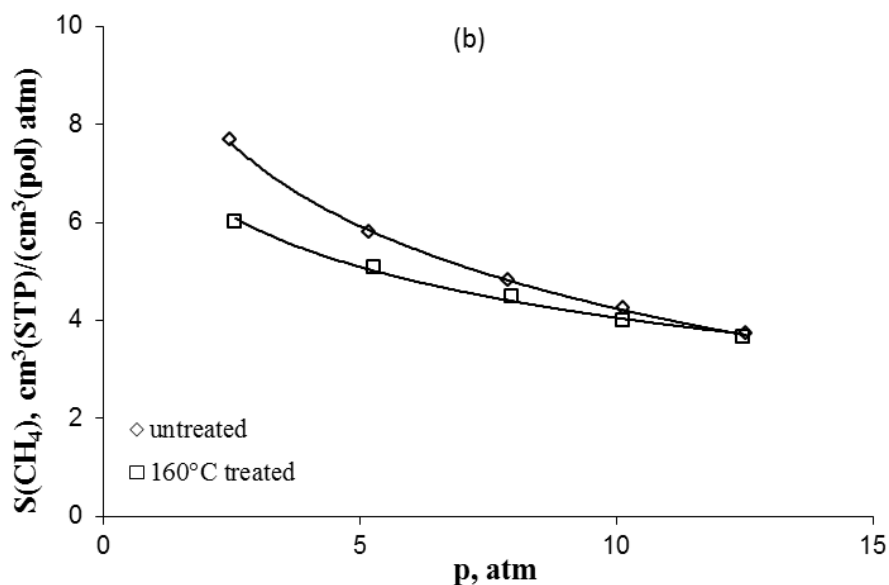


Fig.7.4. Solubility coefficient of pure gases in thermally untreated and treated TZPIM-1 at 35°C; a) CO₂, b).CH₄

7.3 Effect of heat treatment on diffusivity of pure gases in glassy polymer

Diffusivity calculated from sorption kinetics of pure gas sorption experiment of carbon dioxide and methane is compared for heat treated and untreated sample of PIM-1 and TZPIM-1 at different temperatures. The results are plotted in Fig 7.5 and 7.6 for PIM-1 and TZPIM-1 membrane respectively at 35°C up to a pressure range of 35 atm for CO₂ and 15 atm for CH₄. Diffusivity is plotted against the average sorbed concentration of that gas in the polymer.

The result shows that diffusivity coefficient of both carbon dioxide and methane has a decreasing trend with increasing of average sorbed concentration of the gas in the membrane except for methane diffusivity coefficient in TZPIM-1 membrane. The interpolating curves are there to guide eye.

As can be seen from the plot of diffusivity coefficient and average sorbed concentration, diffusivity coefficient of untreated membrane sample is higher than diffusivity coefficient of the gas at all temperatures examined for both PIM-1 and TZPIM-1. Diffusivity selectivity coefficient decreases with increasing of heat treatment temperature as observed from the figure below.

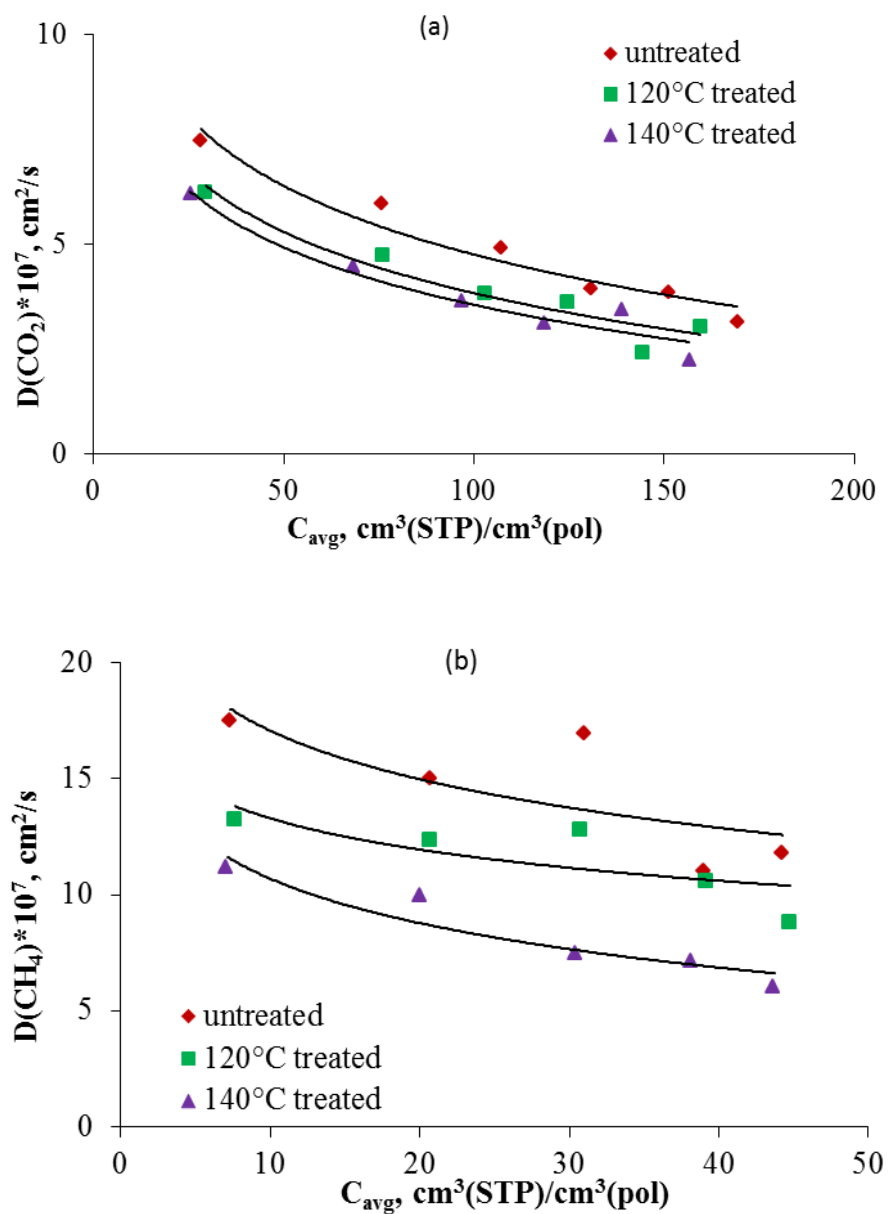


Fig.7.5. Diffusivity coefficient of pure gases in thermally untreated and treated PIM-1 at 35°C; a) CO₂, b).CH₄

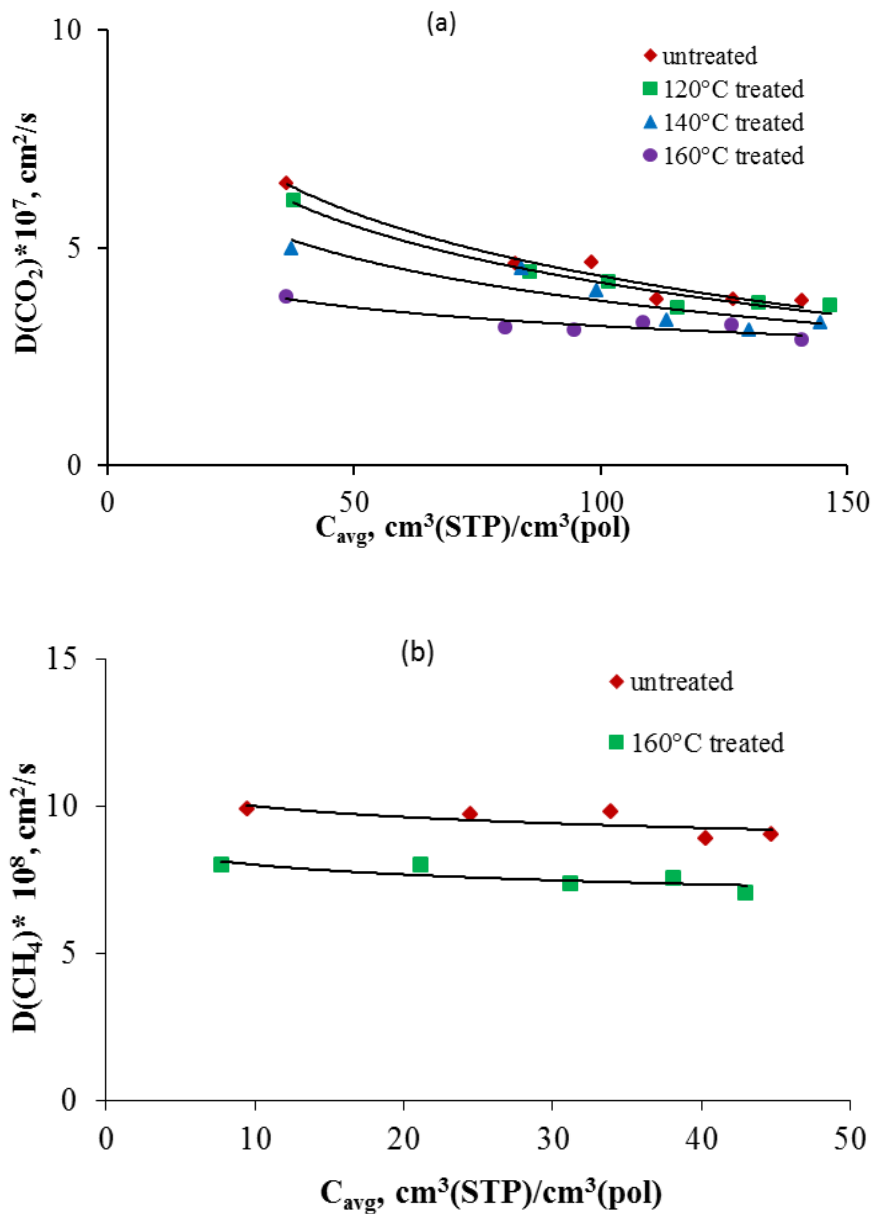


Fig.7.6. Diffusivity coefficient of pure gases in thermally untreated and treated TZPIM-1 at 35°C; a) CO₂, b).CH₄

7.4 Effect of heat treatment on permeability of pure gases in glassy polymer

Permeability of carbon dioxide and methane is calculated from solution-diffusion model using the solubility coefficient and diffusivity coefficient calculated above from pure gas sorption experiment. The samples are untreated and some are treated at three different temperatures as explained before. The results for PIM-1 and TZPIM-1 under different treatment protocol are presented on Fig 7.7 and 7.8 respectively with respect to total pressure.

Fig 7.7 revealed that permeability of both carbon dioxide and methane decreases with increasing of total pressure for all treated and untreated membrane sample. It also shows that the heat treatment on the polymeric membrane sample decreases the permeability of pure gases. As temperature of treatment increases, the permeability of both CO₂ and CH₄ in the PIM-1 membrane decreases. The variation is more seen on permeability of methane than permeability of carbon dioxide.

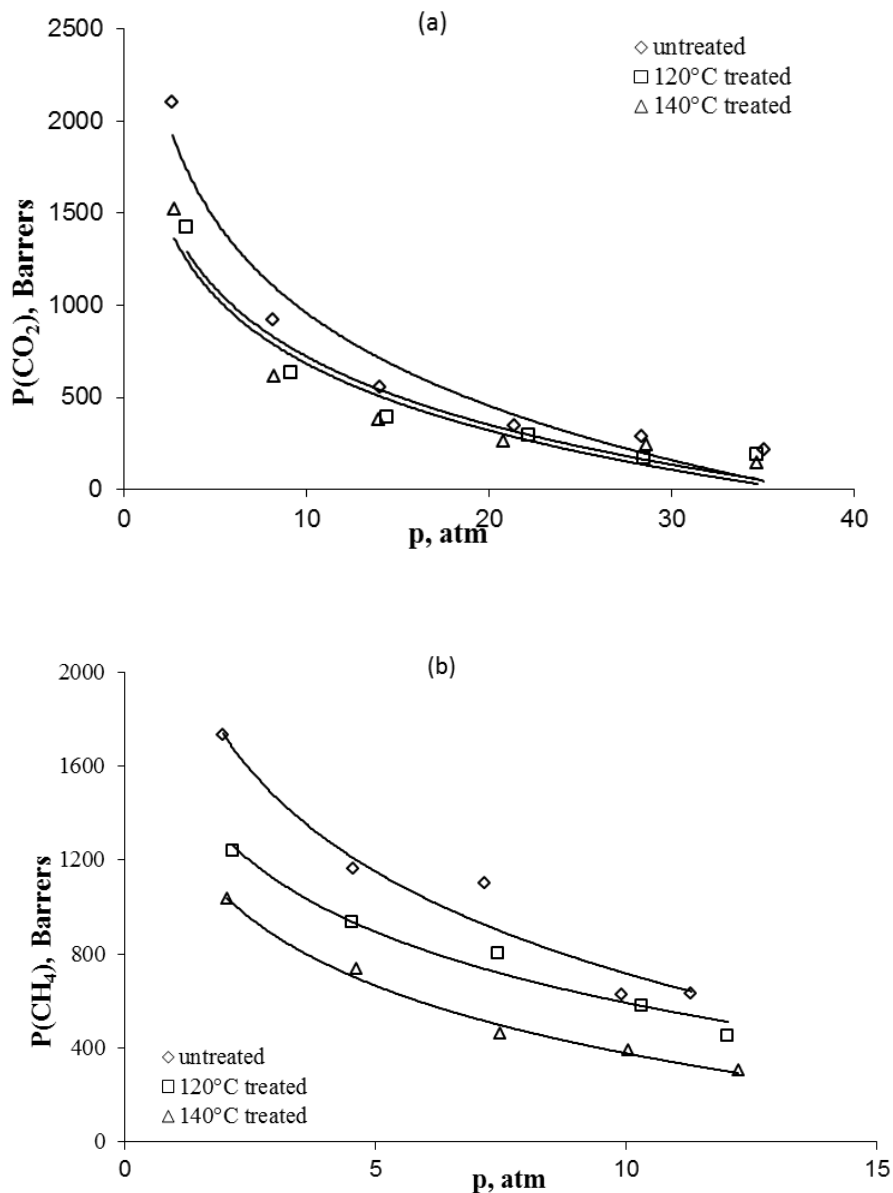


Fig.7.7. Permeability of pure gases in thermally untreated and treated PIM-1 at 35°C; a) CO₂, b).CH₄

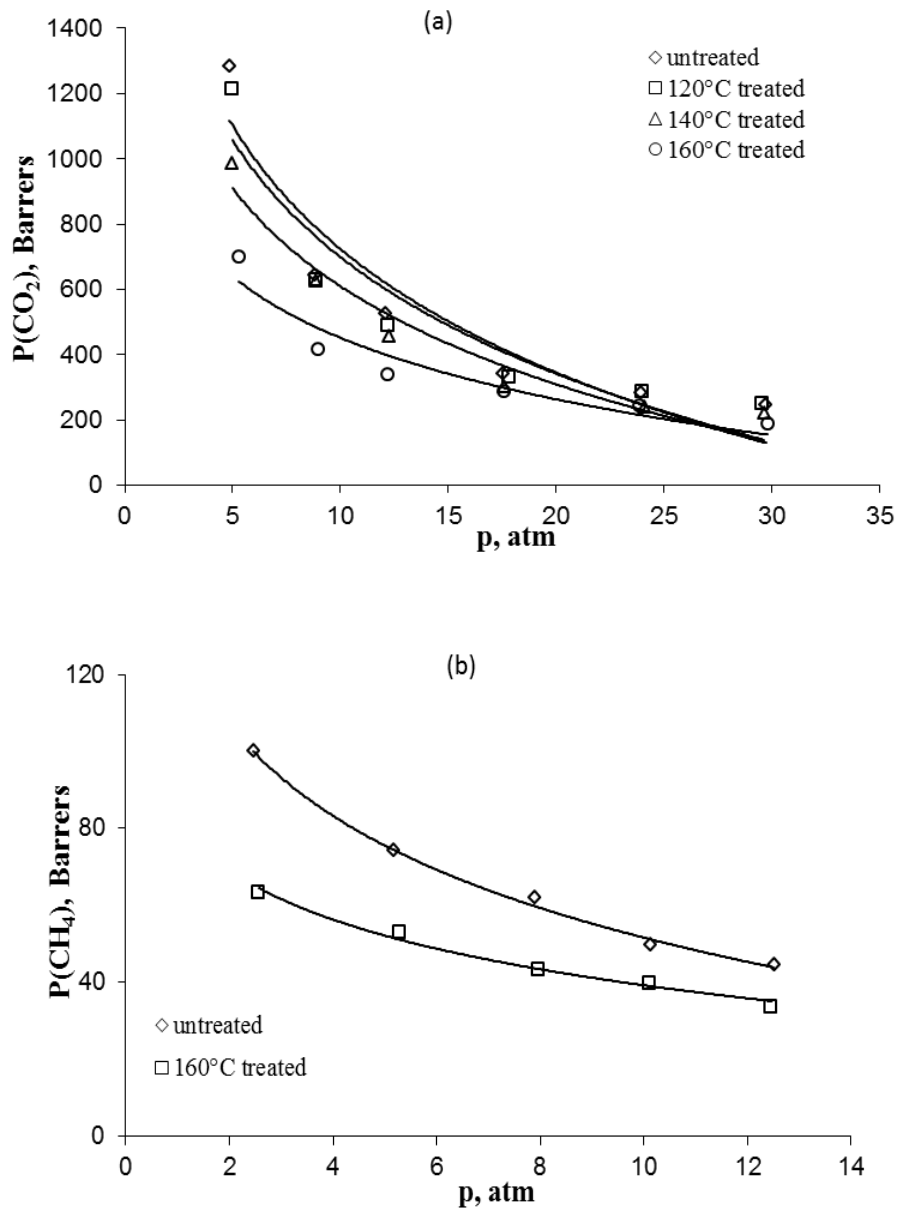


Fig.7.8. Permeability of pure gases in thermally untreated and treated TZPIM-1 at 35°C; a) CO₂, b).CH₄

7.5 Conclusion

Heat treatment of polymeric membranes such as PIM-1 and TZPIM-1 has shown no effect on the sorption isotherms of carbon dioxide and methane and also their solubility coefficient is not affected that much at all temperature studied and pressure range covered under the pure gas sorption experiment.

Diffusivity coefficients show a decreasing trend with respect to average sorbed concentration of the gases in the membrane. Heat treatment decreases the diffusivity coefficient of both carbon dioxide and methane in PIM-1 and TZPIM-1 at all temperature. The variation is more prominent in methane diffusivity coefficient than carbon dioxide. Increasing temperature of heat treatment has a decreasing effect on the diffusivity coefficient in both membranes for both pure gases of CO₂ and CH₄.

Carbon dioxide and methane permeability decreases with respect to total pressure of sorption in the system. Permeability of both gases is affected by heat treatment in which it decreases due to the treatment applied to membrane samples. It has also a decreasing trend with increasing of heat treatment temperature for all temperature the experiment was carried out and pressure range covered for both membranes.

8 Transient and Steady state diffusivity of CO₂ and CH₄ in PIM-1

8.1 Introduction

In this study, the mass transport kinetics of carbon dioxide in PIM-1 is examined, considering both transient sorption and steady-state permeation through the polymeric film. The conventional approach based on the solution-diffusion model, usually suitable to describe mass transport in dense non-porous polymers, is found not appropriate to offer a proper interpretation for the behaviors observed both in transient sorption as well as in continuous permeation.

Transient sorption tests were performed through a pressure decay technique. Differential sorption runs were conducted for each penetrant considered, at 35°C for carbon dioxide. The equilibrium mass uptake was used to estimate solubility while the diffusion coefficient was obtained from the kinetics of the process [225].

Steady state transport was studied through permeation tests performed using the experimental setup already described in the methodology chapter of this thesis work. The upstream pressure was kept at a constant value for each step, while the downstream vessel was initially evacuated and its pressure monitored in time. In the case of lighter penetrants, the downstream pressure was practically always negligible with respect to the pressure of the upstream compartment. Diffusivity coefficient is calculated from time lag method and solubility coefficient is calculated from solution-diffusion model using permeability and diffusivity coefficient calculated from the permeation experiment.

In this chapter the diffusivity results from transient sorption experiment and steady state permeation experiment is presented. Their difference is also presented in the last section of the chapter.

8.2 Transient diffusivity of CO₂ in PIM-1

Diffusivity coefficient calculated from transient sorption experiment using best fitting of mathematical model with experimental kinetics. The equation used for fitting is calculated from Fick's second law using initial and boundary conditions of the system [225]. The model has a form of:

$$\frac{M_t}{M_\infty} = 1 - \sum_{n=1}^{\infty} \frac{2\alpha(1+\alpha)}{1+\alpha+\alpha^2q_n^2} \exp\left(-\frac{Dq_n^2t}{l^2}\right) \quad 8.1$$

Figure below shows the experimental kinetics with fitting of the model as an example.

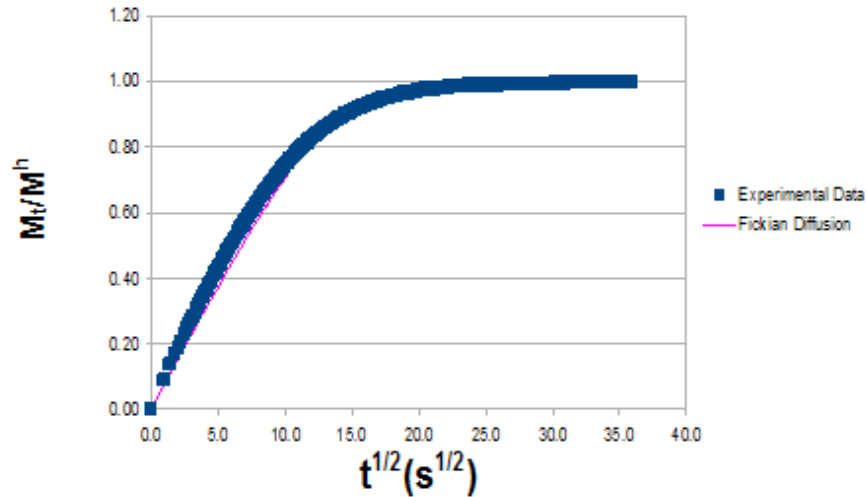


Fig. 8.1 Sorption kinetics of pure gas experiment in polymeric membrane

Transient diffusivity and sorption isotherms calculated from pure gas sorption of carbon dioxide in PIM-1 membrane at different temperatures are presented on Fig 8.2. Transient diffusivity result shows that it decreases with decreasing of experimental temperature as can be seen in Fig 8.2a. It also has a decreasing trend with increasing of sorbed concentration of carbon dioxide in membrane. Sorption isotherms are has a decreasing trend with increasing of temperature as expected. They also have a concave towards the pressure axis the same as the experiment performed before.

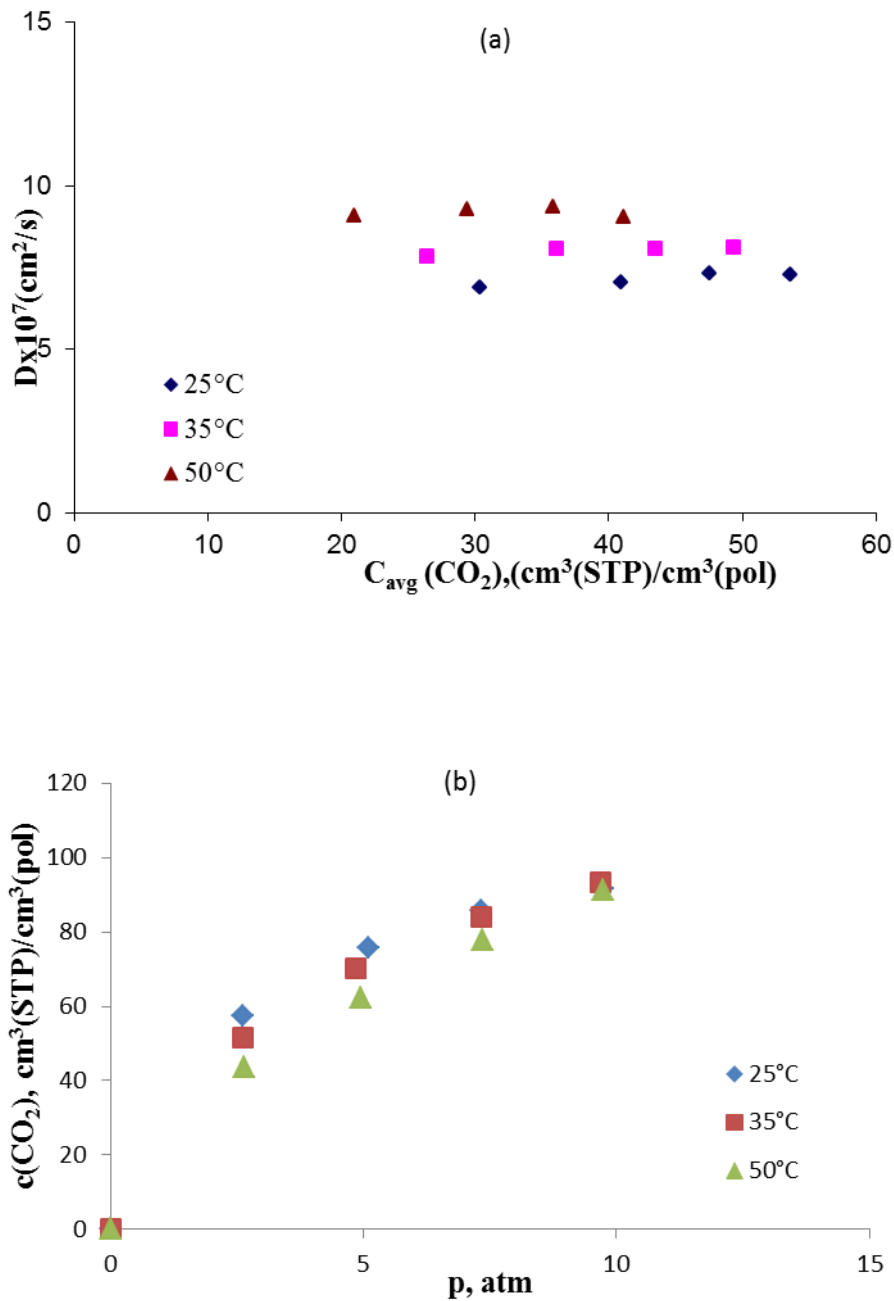


Fig. 8.2 Transient results of a) Diffusivity versus sorbed concentration of CO_2 , b) Sorption isotherm at different temperatures.

8.3 Steady state diffusivity of CO_2 in PIM-1

Steady state diffusivity is calculated from the pure gas permeability experiment using time lag method. Figure 8.3 shows the experimental kinetics of pure gas permeability experiment. The procedure of calculation is explained in detail in methodology chapter of this thesis work. Solubility

coefficient is calculated from solution-diffusion model using permeability and diffusivity coefficient calculated from pure gas permeation experiment.

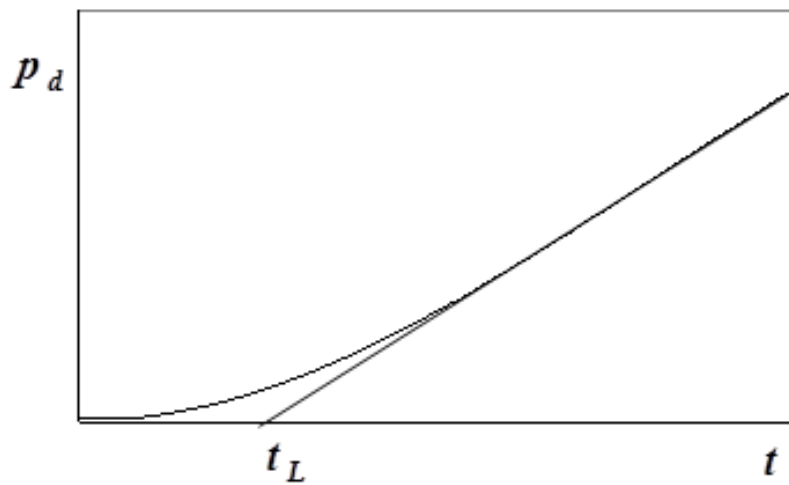
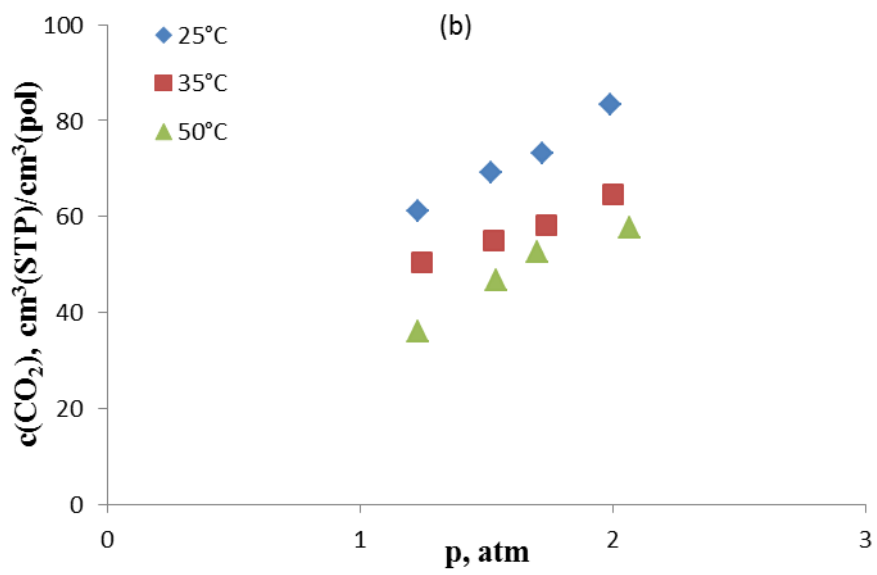
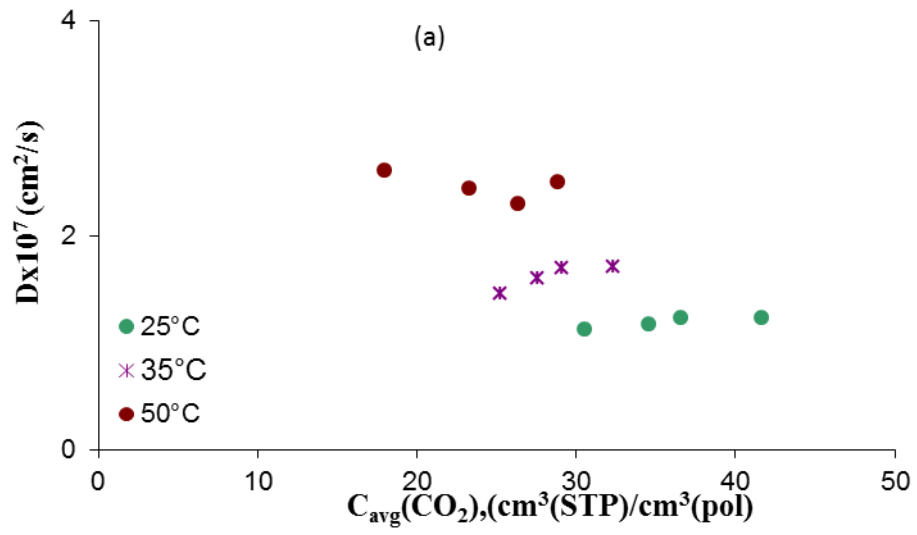


Fig. 8.3 Permeation kinetics of pure gas experiment in polymeric membrane

The steady state diffusivity, sorption isotherms and permeability results at different temperatures are presented on Fig 8.4. The result shows that diffusivity coefficient decreases with decreasing of experimental temperature as the transient diffusivity discussed above. Sorption isotherms calculated from solution-diffusion model is plotted against upstream pressure on Fig 8.4b. The result reveals that the shape is concave towards the pressure axis and it decreases with increasing of experimental temperature. Permeability of carbon dioxide in PIM-1 membrane is plotted against upstream pressure on Fig 8.4c. From the figure it can be revealed that permeability decreases with increasing of pressure and it increases with increasing of experimental temperature.



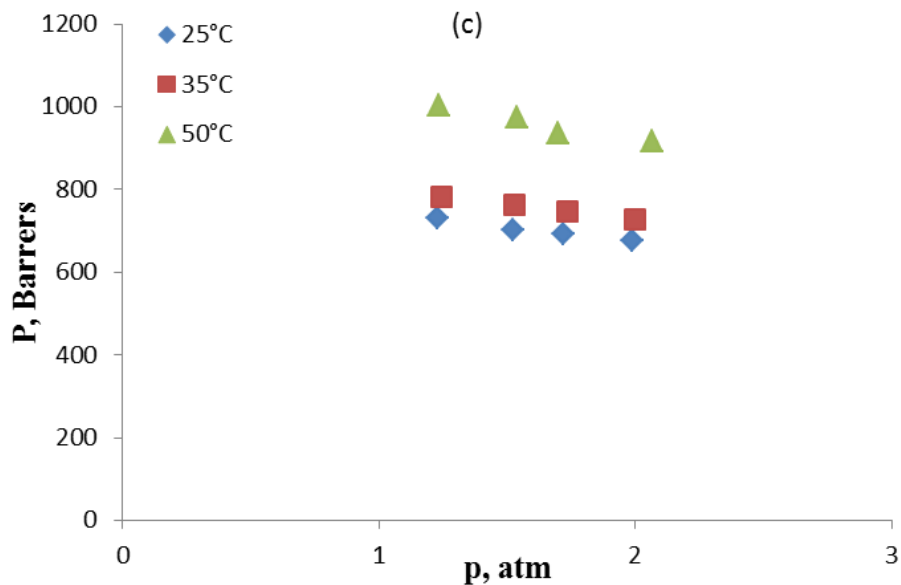


Fig. 8.4 Steady state results of a) Diffusivity versus sorbed concentration of CO₂, b) Sorption isotherm and c) Permeability at different temperatures.

8.4 Comparison of Transient and steady state diffusivity

Transient diffusivity calculated from pure gas sorption experiment of carbon dioxide in PIM-1 membrane is compared with that of steady state diffusivity calculated from pure gas permeation experiment. The result is plotted against average sorbed concentration of carbon dioxide in the membrane as can be seen on Fig 8.5.

From the results it is clearly visible that transient diffusivity is higher than steady state diffusivity of carbon dioxide in PIM-1 for all temperature examined in this thesis work in all the pressure range covered. This explains that sorption experiment over estimates the diffusivity coefficient than pure gas permeation experiment. The study should be further explained with molecular modeling of the polymers.

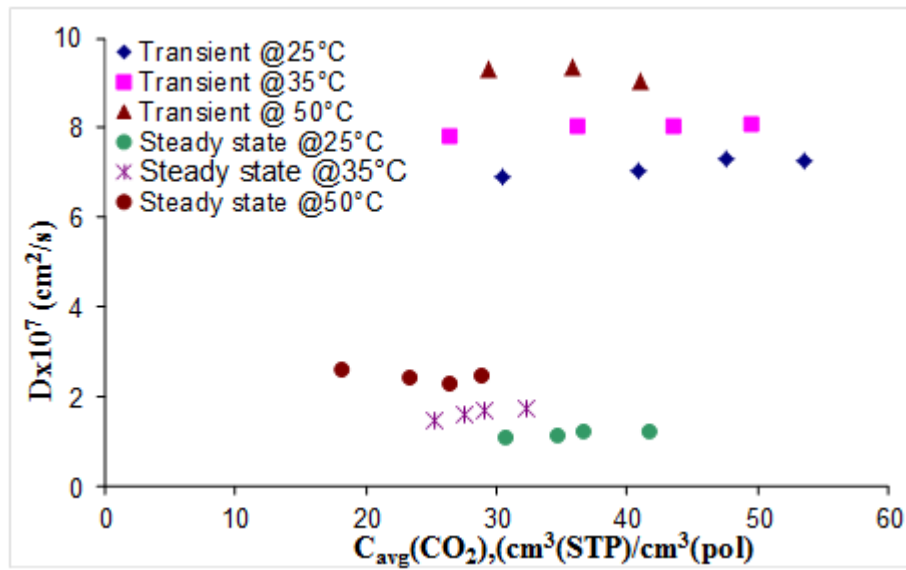


Fig. 8.5 Comparison of Transient and steady state diffusivity at different temperatures

8.5 Conclusion

From the results obtained in pure gas sorption experiment and pure gas permeation experiment of carbon dioxide in PIM-1 membrane at different temperature, it can be seen that transient diffusivity of carbon dioxide is higher than steady state diffusivity in all temperatures examined and pressure range covered in this thesis work. This result has to be further studied and proved using molecular modeling of the membrane in the future.

9 Conclusions and Future perspectives

9.1 Conclusions

Mixed gas sorption of CO₂ and CH₄ is performed for different glassy polymers at different temperature and molar concentration of carbon dioxide up to a pressure range of 35 atm. The results show that the real solubility selectivity is higher than the ideal solubility selectivity this is because the solubility coefficient of methane decreased due to the competition effect of carbon dioxide in the system while solubility coefficient of carbon dioxide remains the same with pure gas solubility coefficient.

Pure gas solubility selectivity of TZPIM-1 is higher than the other membranes studied in this thesis work. The other polymers follow in the order of PIM-1, AO-PIM-1 and Polynonene in decreasing order. Pure gas Solubility selectivity increases with solubility coefficient of CO₂ for higher molar fraction of CO₂ whereas it decreases with solubility coefficient of CO₂ for lower molar fraction of CO₂.

Both pure gas and mixed gas solubility selectivity of polynonene membrane are lower than pure gas and mixed gas solubility selectivity of PIM-based membranes. The methane mixed gas solubility of polynonene membrane is comparable with that of PIM-based membranes while carbon dioxide mixed gas solubility is lower than PIM-based membranes which make the final result of mixed gas solubility selectivity much smaller than the mixed gas solubility selectivity of PIM-based membranes.

There is a slight increase of mixed gas solubility selectivity of polynonene membrane with respect to fugacity of carbon dioxide but pure gas solubility selectivity follows a constant trend with respect to fugacity of carbon dioxide.

From the modeling results and experimental value comparison, we can see that both Dual mode sorption and NELF model fit with the experimental data. The fitting is valid in all molar concentration studied, temperature examined and pressure range for all the polymeric membrane

studied in this thesis work. This helps that the model can be used to estimate pure and mixed gas sorption of CO₂ and CH₄ under the absence of experimental results and helps to reduce the time required and effort to make the complex mixed gas sorption experiment.

Heat treatment of polymeric membranes such as PIM-1 and TZPIM-1 has shown no effect on the sorption isotherms of carbon dioxide and methane and also their solubility coefficient is not affected that much at all temperature studied and pressure range covered under the pure gas sorption experiment.

Diffusivity coefficients show a decreasing trend with respect to average sorbed concentration of the gases in the membrane. Heat treatment decreases the diffusivity coefficient of both carbon dioxide and methane in PIM-1 and TZPIM-1 at all temperature. The variation is more prominent in methane diffusivity coefficient than carbon dioxide. Increasing temperature of heat treatment has a decreasing effect on the diffusivity coefficient in both membranes for both pure gases of CO₂ and CH₄.

Carbon dioxide and methane permeability decreases with respect to total pressure of sorption in the system. Permeability of both gases is affected by heat treatment in which it decreases due to the treatment applied to membrane samples. It has also a decreasing trend with increasing of heat treatment temperature for all temperature the experiment was carried out and pressure range covered for both membranes.

Transient diffusivity of carbon dioxide in PIM-1 calculated from pure gas sorption experiment is higher than that steady state diffusivity calculated from the time lag method of pure gas permeation experiment at different temperature.

9.2 Future perspectives

In this work the binary mixed gas sorption experiment of carbon dioxide and methane is performed. But in reality natural gas has some other impurities like water vapor, hydrogen sulfide etc., which should be considered in the future when mixed gas sorption is going to be studied using polymeric membranes.

Both Dual mode sorption model and NELF model examined for binary mixture should also be extended to tertiary or more mixtures in the future. The NELF model until now is valid and performed for only sorption results of solubility coefficient and sorption isotherms. It has to be extended to diffusivity coefficient and used to predict its value.

It has been seen that heat treatment of polymeric membrane for the protocol described earlier doesn't affect the sorption isotherms of carbon dioxide and methane in PIM-1 and TZPIM-1 at different temperatures. In the future it can be studied in detail by changing the treatment protocol to longer time and higher temperature to see if that affect the sorption isotherm and solubility coefficient.

Transient and steady state diffusivity effect has be further studied using structural modeling of polymeric materials and look in detail why the difference between the two results occurred.

Finally looking for mixed gas permeability experiment will be the best idea to simulate the real life separation of carbon dioxide and methane or more. Modifications of polymeric intrinsic microporosity will be the prominent for the future natural gas purification and carbon dioxide capture.

10 References

1. Mason EA. *Journal of Membr Sci* 1991;60:125-145
2. Boddeker KW. *Journal of Membr Sci* 1995;100:65-68
3. Nollet JA. *Journal of Membr Sci* 1995;100:1-3
4. Koros WJ, Fleming GK. *Journal of Membr Sci* 1993;83(1):1-80
5. S. Sridhar, B. Smitha, T.M. Aminabhavi; Separation of Carbon Dioxide from Natural gas mixtures through polymeric membranes- A Review: *Sep. Purif. Rev.* 2007, 36, 113.
6. A. M. W. Hillock, W. J. Koros; Cross-Linkable polyimide membrane for natural gas purification and Carbon Dioxide plasticization reduction: *Macromolecules* 2007, 40, 583.
7. C. E. Powell, G. G. Qiao; Polymeric CO₂/N₂ gas separation membranes for the capture of carbon dioxide from power plant flue gases: *J. Membr. Sci.* 2006, 279, 1.
8. S. P. Kaldis, G. Skodras, P. Grammelis, G. P. Sakellariopoulos; Application of polymer membrane technology in coal combustion processes; *Chem. Eng. Commun.* 2007, 194, 322.
9. Bernardo, P.; Drioli, E.; Golemme, G, Membrane Gas Separation: A Review/State of the Art; *Ind. Eng. Chem. Res.* 2009, 48, 4638–4663.
10. Baker RW, Future Directions of Membrane Gas Separation Technology; *Industrial and Engineering Chemistry Research* 2002; 41(6):1393-1411.
11. R.W. Baker, K. Lokhandwala, Natural gas processing with membranes: an overview, *Ind. Eng. Chem. Res.* 47 (2008) 2109-2121.
12. Kohl A.L, Nielsen R, Gas purification, 5th Ed, Gulf Publishing; Houston, TX, 1997.
13. Koros WJ, Pinnau I, Membrane formation for gas separation processes, in polymeric gas separation membranes, Paul DR, Yampolski Y, (Eds); CRC press: Boca Raton, FL (1994).
14. Freeman BD, Basis of permeability/selectivity tradeoff relations in polymeric gas separation membranes *Macromolecules*; 32:375(1999).
15. R.W. Rousseau, Handbook of separation process technology, John Wiley & Sons, New York, 1987.
16. V. Stannett, W. Koros, D. Paul, H. Lonsdale, R. Baker, Recent advances in membrane science and technology, in: *Chemistry*, 1979, pp. 69-121.

17. Neil B. McKeown and Peter M. Budd, Polymers of intrinsic microporosity (PIMs): organic materials for membrane separations, heterogeneous catalysis and hydrogen storage; DOI: 10.1039/b600349d.
18. L. M. Robeson, Correlation of separation factor versus permeability for polymeric membranes; *J. Membr. Sci.*, 1991, 62, 165.
19. Du N, Park HB, Robertson GP, Dal-Cin MM, Visser T, Scoles L, et al. Polymer nanosieve membranes for CO₂-capture application; *Nature Mater* 2011;10:372e5.
20. H.A.Patel, C.T.Yavuz, Noninvasive functionalization of polymers of intrinsic microporosity for enhanced CO₂ capture, *Chem.Commun.*48 (2012) 9989–9991.
21. R. Swaidan, B.S. Ghanem, E. Litwiller, I. Pinnau, Pure-and mixed-gas CO₂/CH₄ separation properties of PIM-1 and an amidoxime-functionalized PIM-1. *Journal of Membr Science* 457 (2014) 95–102
22. R. Xu, W. Pang, J. Yu, Q. Huo and J. Chen, *Chemistry of Zeolites and Related Porous Materials: Synthesis and Structure*, John Wiley & Sons (Asia) Pet Ltd., Singapore, 2007.
23. R. T. Yang, *Gas Separation by Adsorption Processes*, Butterworth, Boston, 1987.
24. F. Rouquerol, I. Rouquerol and K. Sing, *Adsorption by Powders and Porous Solids-Principles Methodology and Applications*, Academic Press, London, 1999.
25. J.R Li, R. J Kuppler, H.C Zhou: Selective gas adsorption and separation in metal-organic frameworks, *Chem Society Rev*, DOI: 10.1039/b802426j.
26. R. T. Yang, *Adsorbents: Fundamentals and Applications*, John Wiley & Sons, Hoboken, 2003.
27. J. Seader and M. Henley, *Separation Process Principles*, Wiley, New York, 1998.
28. D. D. Duong, *Adsorption Analysis: Equilibria and Kinetics*, Imperial College Press, London, 1998.
29. D. M. Ruthven, *Principles of Adsorption and Adsorption Processes*, John Wiley& Sons, New York, 1984.
30. A. Dabrowski, *Adv. Colloid Interface Sci.*, 2002, 93, 135–224.
31. S. M. Auerbach, K. A. Carrado and P. K. Dutta, *Handbook of Zeolite Science and Technology*, Marcel Dekker, Inc., New York, 2003.
32. D. W. Beck, *Zeolite Molecular Sieves*, John Wiley & Sons, New York, 1974.
33. B. Sreenivasulu, D.V.Gayatri a, I.Sreedhar, K.V.Raghavan; A journey into the process and engineering aspects of carbon capture technologies, *Renewable and Sustainable Energy Reviews* 41 (2015) 1324–1350.

34. IEA GHG. The capture of carbon dioxide from fossil fuel fired power stations. Cheltenham, UK: IEA GHG; IEA GHG/SR2; 1993.
35. Gupta M, Coyle I, Thambimuthu K. Strawman document for CO₂ capture and storage technology roadmap. Canada: CANMET Energy Technology Centre, Natural Resources; 2003.
36. Axel M, Xiaoshan S. Research and development issues in CO₂ capture. *Energy Convers Manag* 1997; 38:37–42.
37. Aroonwilas A, Tontiwachwuthikul P. Mass transfer coefficients and correlation for CO₂ absorption into 2-amino-2-methyl-1-propanol (AMP) using structured packing. *Ind Eng Chem Res* 1998; 37:569–75.
38. Arashi N, Oda N, Yamada M, Ota H, Umeda S, Tajika M. Evaluation of test results of 1000m³N/h pilot plant for CO₂ absorption using an amine-based solution. *Energy Convers Manag* 1997; 38:S63–8.
39. Setameteekul A, Aroonwilas A, Veawab A. Statistical factorial design analysis for parametric interaction and empirical correlations of CO₂ absorption performance in MEA and blended MEA/MDEA processes. *Sep Purif Technol* 2008; 64:16–25.
40. Marcia S, deMontigny D, Tontiwachwuthikul P. Liquid distribution of MEA in random and structured packing in a square column. *Energy Procedia* 2009; 1:1155–61.
41. Kolev N, Nakov S, Ljutzkanov L, Kolev D. Effective area of a highly efficient random packing. *Chem Eng Process Intensif* 2006; 45:429–36.
42. Yu C-H, Tan C-S. Mixed alkanolamines with low regeneration energy for CO₂ capture in a rotating packed bed. *Energy Procedia* 2013; 37:455–60.
43. Yu C-H, Cheng H-H, Tan C-S. CO₂ capture by alkanolamine solutions containing ethylenetriamine and piperazine in a rotating packed bed. *Int J Greenh Gas Control* 2012; 9:136–47.
44. Y. Kanshaa, A. Kishimotoa, T. Nakagawab, A. Tsutsumia. A novel cryogenic air separation process based on self-heat recuperation, *Separation and Purification Technology* 77 (2011) 389–396.
45. David A. Glasscock, Gary T. Rochelle. Numerical simulation of theories for gas absorption with Chemical reaction, DOI: 10.1002/aic.690350806
46. Zhao, Y.J., Wang, J., Zhang, H., Yan, C., Zhang, Y.J., 2013. Effects of various LED light wavelengths and intensities on microalgae-based simultaneous biogas upgrading and digestate nutrient reduction process. *Bioresour. Technol.* 136, 461–468.

47. Scholz, M., Frank, B., Stockmeier, F., Falß, S., Wessling, M., 2013. Techno-economic analysis of hybrid processes for biogas upgrading. *Ind. Eng. Chem. Res.* 52, 16929–16938.
48. Ryckebosch, E., Drouillon, M., Vervaeren, H., 2011. Techniques for transformation of biogas to biomethane. *Biomass Bioenergy* 35, 1633–1645.
49. Zhang, J., Jia, C., Dong, H., Wang, J., Zhang, X., Zhang, S., 2013. A novel dual amino-functionalized cation-tethered ionic liquid for CO₂ capture. *Ind. Eng. Chem. Res.* 52, 5835–5841.
50. E.Y. Kenig, A. Górak, K. Sundmacher, A. Kienle, A Seidel-Morgenstern (Eds.). *Reactive absorption in Integrated Chemical Processes*, Wiley-VCH Verlag GmbH & Co. KGaA, Weinheim, Germany, 2005.
51. G. Astarita, D.W. Savage, A. Bisio. *Gas Treating with Chemical Solvents*, Wiley, New York, 1983.
52. IEA. *Prospects for CO₂ capture and storage*. Paris, France: OECD/IEA; 2004.
53. Chakravati S, Gupta A, Hunek B. Advanced technology for the capture of carbon dioxide from flue gases. In: *Proceedings of the 1st national conference on carbon sequestration*. Washington, DC; 2001.
54. Park SW, Lee JW, Choi BS, Lee JW. Absorption of carbon dioxide into non aqueous solutions N-methyldiethanolamine. *Kor J Chem Eng* 2006; 23: 806–11.
55. Lee DH, Choi WJ, Moon SJ, Ha SH, Kim IG, Oh KJ. Characteristics of absorption and regeneration of carbon dioxide in aqueous 2-amino-2-methyl-1-propanol/ammonia solutions. *Kor J Chem Eng* 2008; 25:279–84.
56. Lasscock DA, Critchfield JE, Rochelle GT. CO₂ absorption/desorption in mixtures of methyldiethanolamine with monoethanolamine or diethanolamine. *Chem Eng Sci* 1991; 46:2829–45.
57. Versteeg GF, Kuipers JAM, Van Beckum FPH, Van Swaaij WPM. Mass transfer with complex reversible chemical reactions—II. Parallel reversible chemical reactions. *Chem Eng Sci* 1990; 45:183–97.
58. Freeman SA, Dugas R, Wagener DV, Nguyen T, Rochelle GT. Carbon dioxide capture with concentrated, aqueous piperazine. *Energy Procedia* 2009;1: 1489–96.
59. Hammonda GP, Ondo Akwea SS, Williams S. Techno-economic appraisal of fossil-fuelled power generation systems with carbon dioxide capture and storage. *Energy* 2011; 36:975e84.
60. Ramezan M. Carbon dioxide capture from existing coal-fired power plants. Final report. National Energy Technology Laboratory. Available from: <http://www.netl.doe.gov/>

[energy-analyses/pubs/CO2%20Retrofit%20From%20Existing%20Plants%20Revised%20November%202007.pdf](#); 2007 Nov.

61. Edward S, Anand B. A technical, economic, and environmental assessment of amine based CO₂ capture technology for power plant greenhouse gas control, annual technical progress report. Carnegie Mellon University Center for Energy and Environmental Studies [Contract No.: DE-FC26e00NT40935]. Available from: <http://repository.cmu.edu/epp/94/>; 2002 Oct.
62. Working group III of the intergovernmental panel on climate change. IPCC special report on carbon dioxide capture and storage. Cambridge, United Kingdom: Cambridge University Press. Available from: <http://www.ipcc-wg3.de/publications/special-reports/special-report-on-carbon-dioxide-captureand-storage>; 2005.
63. Rezvani S, Huang Y, McIlveen-Wright D, Hewitt N, Mondol J. Comparative assessment of coal fired IGCC systems with CO₂ capture using physical absorption, membrane reactors and chemical looping. *Fuel* 2009; 88:2463-72.
64. Jockenhoevel T, Schneider R, Rode H. Development of an economic post combustion carbon capture process. *Energy Procedia* 2008; 00:1043-50.
65. Yan S, Fang M, Zhang W, Zhong W, Luo Z, Cen K. Comparative analysis of CO₂ separation from flue gas by membrane gas absorption technology and chemical absorption technology in China. *Energy Conversion and Management* 2008; 49:3188-97.
66. A.R. Smith, J. Klosek. A review of air separation technologies and their integration with energy conversion processes, *Fuel Processing Technology* 2001; 70, 115–134
67. R.J. Notz, I. Tönnies, N. McCann, G. Scheffknecht, H. Hasse, CO₂ capture for fossil fuel-fired power plants, *Chem. Eng. Technol.* 34 (2011) 163–172.
68. G.T. Rochelle, Amine scrubbing for CO₂ capture, *Science* 325 (2009) 1652– 1654.
69. Baker RW. *Membrane Technology and Applications*. 2nd ed. New York: John Wiley & Sons, Ltd; 2004.
70. Hale P, Lokhandwala K. *Advances in Membrane Materials Provide New Gas Processing Solutions*. Gas Processors Association. 2004:2-3.
71. Henis JMS, Tripodi MK. Composite hollow fiber membranes for gas separation: the resistance model approach. *J Membr Sci.* 1981; 8:233-46.
72. Luis P, Van Gerven T, Van der Bruggen B. Recent developments in membrane-based technologies for CO₂ capture. *Progr Energy Combust Sci.* 2012; 38:419-48.
73. Pereira Nunes S, Peinemann KV. *Membrane Technology in the Chemical Industry*. Weinheim: Wiley-VCH; 2001.

74. Salavati-Niasari M. Synthesis and characterization of 18- and 20-membered hexaaza macrocycles containing pyridine manganese (II) complex nanoparticles dispersed within nanoreactors of zeolite-Y. *Polyhedron*. 2009; 28:2321-8.
75. Szostak R. *Molecular Sieves: Principles of Synthesis and Identification*. 2nd ed. Berlin: Kluwer Academic Publishers Group; 1998.
76. Koros WJ, Mahajan R. Pushing the limits on possibilities for large scale gas separation: which strategies? *J Membr Sci*. 2000; 175:181-96.
77. Robeson LM. Correlation of separation factor versus permeability for polymeric membranes. *J Membr Sci*. 1991; 62:165-85.
78. Freeman BD. Basis of Permeability/Selectivity Tradeoff Relations in Polymeric Gas Separation Membranes. *Macromolecules*. 1999; 32:375-80.
79. Robeson LM. The upper bound revisited. *J Membr Sci*. 2008; 320:390-400.
80. Rezakazemi M, Amooghin AE, Montazer-Rahmati MM, Ismail AF, Matsuura T, State-of-the-art membrane based CO₂ separation using mixed matrix membranes: An overview on current status and future directions, *Progress in Polymer Science* (2014), <http://dx.doi.org/10.1016/j.progpolymsci.2014.01.003>
81. Al-Marzouqi M. Determining Pore Size Distribution of Gas Separation Membranes from Adsorption Isotherm Data. *Energy Sources, Part A: Recovery, Utilization, and Environmental Effects*. 1999; 21:31 - 8.
82. Mahajan R, Vu DQ, Koros WJ. Mixed Matrix Membrane Materials: An Answer to the Challenges Faced by Membrane Based Gas Separations Today? *J Chin Inst Chem Eng*. 2002; 33:77-86.
83. Rezakazemi M, Razavi S, Mohammadi T, Nazari AG. Simulation and determination of optimum conditions of pervaporative dehydration of isopropanol process using synthesized PVA–APTEOS/TEOS nanocomposite membranes by means of expert systems. *J Membr Sci*. 2011; 379:224-32.
84. Rezakazemi M, Iravaninia M, Shirazian S, Mohammadi T. Transient Computational Fluid Dynamics (CFD) Modeling of Pervaporation Separation of Aromatic/Aliphatic Hydrocarbon Mixtures Using Polymer Composite Membrane. *Polym Eng Sci*. 2013; 53:1494–501.
85. Sanaeepur H, Ebadi Amooghin A, Moghadassi A, Kargari A, Moradi S, Ghanbari D. A novel acrylonitrile–butadiene–styrene/poly (ethylene glycol) membrane: preparation, characterization, and gas permeation study. *Polym Adv Technol*. 2012; 23:1207-18.

86. Magnusson, I., Stenberg, W. V., Batich, C., and Egelberg, J. Connective tissue repair in circumferential periodontal defects in dogs following use of a biodegradable membrane. *J. Clin Periodontol* 1990; 17(4), 243.
87. Gregor, E. C., Tanny, G. B., Shchori, E., and Kenigsberg, Y. Sunbeam Process microporous membranes. A high-performance barrier for protective clothing. *J. Coated Fabrics* 1988; 18, 26.
88. Mueller, M., Oehr, C., Malthaner, H., Goehl, H., Deppisch, R., and Storr, M. A process for production of a regioselective polymeric membrane for purification of biological fluids. *PCT Int. Appl.* 2003; 33 pp.
89. Alves, V. D., Koroknai, B., Belafi-Bako, K., and Coelho, I. M. Using membrane contactors for fruit juice concentration. *Desalination* 2004; 162(1–3), 263.
90. Nagel, R., and Will, T. Microelectronics. Membrane processes for water treatment in the semiconductor industry. *Ultrapure Water* 1999; 16(8), 35.
91. Srivastava, R. C., Sahney, R., Upadhyay, S., and Gupta, R. L. Membrane permeability based cholesterol sensor—A new possibility. *J. Membr. Sci.* 2000; 164(1–2), 45.
92. Smitha, B., Sridhar, S., and Khan, A. A. Solid polymer electrolyte membranes for fuel cell applications—a review. *J. Membr. Sci.* 2005; 259(1–2), 10.
93. Krzysztof, K., Marek, G., and Antoni, M. Membrane processes used for potable water quality improvement. *Desalination* 2002; 145, 315.
94. Stern, S. A. Polymers for gas separations: The next decade. *J. Membr. Sci.* 1994; 94, 1.
95. Pratibha, P., and Chauhan, R. S. Membranes for gas separation. *Prog. Polym. Sci.* 2001; 26, 853.
96. Strathmann, H. Membrane separation processes. *J. Membr. Sci.* 1981; 9, 121.
97. Mulder, M. *Basic Principles of Membrane Technology*. Kluwer Academic, Dordrecht, 2000.
98. Paul, D. R., and Yampolskii, Y. P. *Polymeric Gas Separation Membranes*. CRC Press, London, 1994.
99. Norman N. Li, Anthony G. Fane, W.S. Winston Ho, Takeshi Matsuura. *Advanced membrane technologies and applications*. John Wiley press, New Jersey, 2008.
100. Budd, P. M., Elabas, E. S., Ghanem, B. S., Makhseed, S., McKeown, N. B., Msayib, K. J., Tattershall, C. E., and Wang, D. Solution-processed, organophilic membrane derived from a polymer of intrinsic microporosity. *Adv. Mater.* 2004; 16, 456.
101. Budd, P. M., McKeown, N. B., and Fritsch, D. Free volume and intrinsic microporosity in polymers. *J. Mater. Chem.* 2005; 15, 1977.

102. Budd, P. M., Msayib, K. J., Tattershall, C. E., Ghanem, B. S., Reynolds, K. J., McKeown, N. B., and Fritsch, D. (2005b). Gas separation membranes from polymers of intrinsic microporosity. *J. Membr. Sci.* 2005; 251, 263.
103. McKeown, N. B., Budd, P. M., Msayib, K. J., Ghanem, B. S., Kingston, H. J., Tattershall, C. E., Makhseed, S., Reynolds, K. J., and Fritsch, D. Polymers of intrinsic microporosity (PIMs): Bridging the void between microporous and polymeric materials. *Chem. A Eur. J.* 2005; 11, 26.
104. Park, H. B. et al. Polymers with cavities tuned for fast selective transport of small molecules and ions. *Science.* 2007; 318, 254- 258.
105. S. Zulfiqar, S. Awan, F. Karadas, M. Atilhan, C. T. Yavuz, M. I. Sarwar, Amidoxime porous polymers for CO₂ capture, *RSC Adv.* 3 (2013); 17203–17213.
106. S. Zulfiqar, F. Karadas, J. Park, E. Deniz, G. D. Stucky, Y. Jung, M. Atilhan, C. T. Yavuz. Amidoximes: promising candidates for CO₂ capture, *Energy Environ. Sci.* 4 (2011); 4528–4531.
107. Morisato, A.; Pinnau, I. *J. Membr. Sci.* 1996, 121, 243–250.
108. M. Gringolts, M. Bermeshev, Yu. Yampolskii, L. Starannikova, V. Shantarovich, and E. Finkelshtein. New High Permeable Addition Poly (tricyclononenes) with Si(CH₃)₃ Side Groups. Synthesis, Gas Permeation Parameters, and Free Volume. *Macromolecules* 2010; 43, 7165–7172
109. H. Yang, Z. Xu, M. Fan, R. Gupta, R.B. Slimane, A.E. Bland, I. Wright, Progress in carbon dioxide separation and capture: A review, *Journal of Environmental Sciences*, 2008; 20, 14- 27.
110. CO2CRC, CO2CRC Image Library, in, CO2CRC, 2012.
111. C.A. Scholes, S.E. Kentish, G.W. Stevens, Carbon dioxide separation through polymeric membrane systems for flue gas applications, *Recent Patents on Chemical Engineering*, 2007; 52-66.
112. A.B. Fuertes, T.A. Centeno, Preparation of supported asymmetric carbon molecular sieve membranes, *J. Membr. Sci.*, 1998; 144, 105-111.
113. Jones CW, Koros WJ. Characterization of ultramicroporous carbon membranes with humidified feeds. *Ind Eng Chem Res.* 1995; 34 (1): 158-163
114. H. Takeuchi, A jump motion of small molecules in glassy polymers: A molecular dynamics simulation, *The Journal of Chemical Physics*, 93 (1990) 2062-2067.
115. V.P. Shantarovich, I.B. Kevdina, Y.P. Yampolskii, A.Y. Alentiev, Positron Annihilation Lifetime Study of High and Low Free Volume Glassy Polymers: Effects of

- Free Volume Sizes on the Permeability and Permselectivity, *Macromolecules*, 2000; 33, 7453-7466.
116. I. Pinnau, L.G. Toy, Transport of organic vapors through poly (1-trimethylsilyl-1-propyne), *J. Membr. Sci.*, 1996; 116, 199-209.
 117. A.F. Ismail, W. Lorna, Penetrant-induced plasticization phenomenon in glassy polymers for gas separation membrane, *Separation and Purification Technology*, 27 (2002) 173-194.
 118. W.S.W. Ho, K.K. Sirkar, *Membrane handbook*, Boston: Kluwer Academic Pub. New York, 2001.
 119. S. Kanehashi, K. Nagai, Analysis of dual-mode model parameters for gas sorption in glassy polymers, *J. Membr. Sci.* 2005; 253, 117-138.
 120. C.-L. Lee, H.L. Chapman, M.E. Cifuentes, K.M. Lee, L.D. Merrill, K.L. Ulman, K. Venkataraman, Effects of polymer structure on the gas permeability of silicone membranes, *J. Membr. Sci.* 1988; 38, 55-70.
 121. M.W. Hellums, W.J. Koros, G.R. Husk, D.R. Paul, Fluorinated polycarbonates for gas separation applications, *J. Membr. Sci.* 1989; 46, 93-112.
 122. C.-C. Hu, K.-R. Lee, R.-C. Ruaan, Y.C. Jean, J.-Y. Lai, Gas separation properties in cyclic olefin copolymer membrane studied by positron annihilation, sorption, and gas permeation, *J. Membr. Sci.* 2006; 274, 192-199.
 123. W.M. Lee, Selection of barrier materials from molecular structure, *Polymer Engineering & Science*. 1980; 20, 65-69.
 124. A. Bondi, *Physical properties of molecular crystals, liquids, and glasses*, Wiley, New York, 1968.
 125. J.Y. Park, D.R. Paul. Correlation and prediction of gas permeability in glassy polymer membrane materials via a modified free volume based group contribution method, *J. Membr. Sci.* 1997; 125, 23-39.
 126. A. Shimazu, T. Miyazaki, S. Katayama, Y. Ito. Permeability, permselectivity, and penetrant-induced plasticization in fluorinated polyimides studied by positron lifetime measurements, *J. Polym. Sci., Part B: Polym. Phys.* 2003; 41, 308-318.
 127. W.J. Koros, Model for sorption of mixed gases in glassy polymers, *J. Polym. Sci.: Polym. Phys. Ed.*, 1980; 18, 981-992.
 128. W.J. Koros, R.T. Chern, V. Stannett, H.B. Hopfenberg, A model for permeation of mixed gases and vapors in glassy polymers, *J. Polym. Sci.: Polym. Phys. Ed.*, 1981; 19, 1513-1530.

129. M.B. Hägg, W.J. Koros, J.C. Schmidhauser, Gas sorption and transport properties of bisphenol-I-polycarbonate, *J. Polym. Sci., Part B: Polym. Phys.*, 1994; 32, 1625-1633.
130. H. Fujita, Diffusion in polymer-diluent systems, in: *Fortschritte Der Hochpolymeren-Forschung*, Springer Berlin / Heidelberg, 1961; pp. 1-47.
131. S. Kanehashi, T. Nakagawa, K. Nagai, X. Duthie, S. Kentish, G. Stevens, Effects of carbon dioxide-induced plasticization on the gas transport properties of glassy polyimide membranes, *J. Membr. Sci.*, 2007; 298; 147-155.
132. R. B. Bird, W. E. Stewart, E. N. Lightfoot: *Transport Phenomena*, 2nd edn. (Wiley, New York 2002).
133. K. Ghosal, B. D. Freeman: Gas separation using polymer membranes: An overview, *Polym. Adv. Technol.* 1994; 5, 673–697.
134. R. R. Zolanz, G. K. Fleming: Gas permeation. In: *Membrane Handbook*, ed. by W. S. W. Ho, K. K. Sirkar (Chapman Hall, New York 1992) pp. 17–102.
135. Measurement of Material properties.
136. T. C. Merkel, V. I. Bondar, K. Nagai, B. D. Freeman, I. Pinnau: Gas sorption, diffusion, and permeation in poly (dimethylsiloxane), *J. Polym. Sci., Part B: Polym. Phys.* 2000; 38, 415–434.
137. Lin HQ, Freeman BD. Permeation and diffusion. In: Czichos H, Saito T, Smith L, editors. *Springer handbook for materials measurement methods*. Berlin: Springer; 2011. p. 426-44.
138. Struik LCE. *Physical aging in amorphous polymers and other materials*. Amsterdam, The Netherlands: Elsevier; 1978.
139. Murphy TM, Offord GT, Paul DR. Fundamentals of membrane gas separation. In: Drioli E, Giorno L, editors. *Membrane operations. Innovative separations and transformations*. Weinheim, Germany: Wiley-VCH; 2009. p. 63-82.
140. Rowe BW, Freeman BD, Paul DR. Polymer. Physical aging of ultrathin glassy polymer films tracked by gas permeability. 2009; 50:5565-75.
141. Rowe BW, Freeman BD, Paul DR. Polymer. Influence of previous history on physical aging in thin glassy polymer films as gas separation membranes. 2010; 51:3784-92.
142. Murphy TM, Langhe DS, Ponting M, Baer E, Freeman BD, Paul DR. Physical aging of layered glassy polymer films via gas permeability tracking. *Polymer* 2011; 52:6117-25.

143. Rowe BW, Pas SJ, Hill AJ, Suzuki R, Freeman BD, Paul DR. A variable energy positron annihilation lifetime spectroscopy study of physical aging in thin glassy polymer films. *Polymer* 2009; 50: 6149-56.
144. Cui L, Qiu W, Paul DR, Koros WJ. Physical aging of 6FDA-based polyimide membranes monitored by gas permeability. *Polymer* 2011;52:3374-80.
145. Kim JH, Koros WJ, Paul DR. Physical aging of thin 6FDA-based polyimide membranes containing carboxyl acid groups. Part I. Transport properties. *Polymer* 2006; 47:3094-103.
146. Hutchinson JM. Physical aging of polymers. *Progress in Polymer Science* 1995; 20(4):703-60.
147. McCaig MS, Paul DR. Effect of film thickness on the changes in gas permeability of a glassy polyarylate due to physical aging Part I. Experimental observations. *Polymer* 2000; 41:629-37.
148. Nagai K, Higuchi A, Nakagawa T. Gas permeability and stability of poly(1-trimethylsilyl-1-propyne-co-1-phenyl-1-propyne) membranes. *Journal of Polymer Science, Part B: Polymer Physics* 1995; 33(2):289-98.
149. Langsam M, Robeson LM. Substituted propyne polymers—part II. Effects of aging on the gas permeability properties of poly [1-(trimethylsilyl) propyne] for gas separation membranes. *Polymer Engineering and Science* 1989; 29(1):44-54.
150. Kelman SD, Rowe BW, Bielawski CW, Pas SJ, Hill AJ, Paul DR, et al. Crosslinking poly[1-(trimethylsilyl)-1-propyne] and its effect on physical stability. *Journal of Membrane Science* 2008;320:123-34.
151. Nagai K, Nakagawa T. Effects of aging on the gas permeability and solubility in poly (1-trimethylsilyl-1-propyne) membranes synthesized with various catalysts *Journal of Membrane Science* 1995; 105:261-72.
152. Nagai K, Freeman BD, Hill AJ. *Journal of Polymer Science, Part B: Polymer Physics* 2000; 38:1222-39.
153. Dorkenoo KD, Pfromm PH. Accelerated Physical Aging of Thin Poly [1-(trimethylsilyl)-1-propyne] Films. *Macromolecules* 2000; 33:3747-51.
154. Horn NR, Paul DR. Carbon dioxide plasticization and conditioning effects in thick vs. thin glassy polymer films. *Polymer* 2011; 52:1619-27.
155. Horn NR, Paul DR. Carbon dioxide plasticization of thin glassy polymer films. *Polymer* 2011; 52:5587-94.

156. Huang Y, Paul DR. Experimental methods for tracking physical aging of thin glassy polymer films by gas permeation. *Journal of Membrane Science* 2004; 244:167-78.
157. Huang Y, Paul DR. Physical aging of thin glassy polymer films monitored by gas permeability. *Polymer* 2004; 45:8377-93.
158. Huang Y, Paul DR. Physical Aging of Thin Glassy Polymer Films Monitored by Optical Properties. *Macromolecules* 2006; 39:1554-9.
159. Huang Y, Paul DR. *Industrial & Engineering Chemistry Research* 2007; 46: 2343-7.
160. Huang Y, Paul DR. Effect of molecular weight and temperature on physical aging of thin glassy poly (2,6-dimethyl-1,4-phenylene oxide) films. *Journal of Polymer Science, Part B: Polymer Physics* 2007; 45:1390 -8.
161. Rowe BW, Freeman BD, Paul DR. Effect of Sorbed Water and Temperature on the Optical Properties and Density of Thin Glassy Polymer Films on a Silicon Substrate. *Macromolecules* 2007; 40(8):2806-13.
162. McCaig MS, Paul DR. Effect of UV crosslinking and physical aging on the gas permeability of thin glassy polyarylate films. *Polymer* 1999; 40:7209-25.
163. McCaig MS, Paul DR, Barlow JW. Effect of film thickness on the changes in gas permeability of a glassy polyarylate due to physical aging Part II. Mathematical model. *Polymer* 2000; 41:639-48.
164. Kim JH, Koros WJ, Paul DR. Effects of CO₂ exposure and physical aging on the gas permeability of thin 6FDA-based polyimide membranes Part 1. Without crosslinking. *Journal of Membrane Science* 2006; 282:21-31.
165. Kim JH, Koros WJ, Paul DR. Effects of CO₂ exposure and physical aging on the gas permeability of thin 6FDA-based polyimide membranes Part 2. with crosslinking. *Journal of Membrane Science* 2006; 282:32-43.
166. Barrer, R.M. Nature of the Diffusion Process in Rubber. *Nature*, 1937; 140, 106-107.
167. Rogers, C.E. Permeation of Gases and Vapours in Polymers in *Polymer Permeability*, Comyn, J. (ed.), Elsevier Applied Science, 1985; 11-73
168. Meares, P. The Diffusion of Gases through Polyvinyl Acetate. *J. Am. Chem. Soc.*, 1954; 76, 3415-3422.
169. Meares, P. The Solubilities of Gases in Polyvinyl Acetate. *Trans. Faraday Soc.*, 1958; 54, 40-46.
170. Gee, G. Some Thermodynamic Properties of High Polymers and their Molecular Interpretation. *Quart. Revs.* 1947; 1, 265-298.

171. Crank J. and Park, G.S. (eds.). *Diffusion in Polymers*, Academic Press, 1968; London and New York.
172. Hildebrand, J.H. and Scott, R.L. *The Solubility of Non Electrolytes*, 3rd ed., 1950; Reinhold, New York.
173. Comyn, J. *Polymer Permeability*, Elsevier Applied Science, 1985.
174. Naylor, T.V. Permeation Properties, in *Comprehensive Polymers Science*, 1989; 2, 643-668, Pergamon Press.
175. Van Amerongen, G.J. Influence of Structure of Elastomers on their Permeability to Gases. *J. Polym. Sci.*, 1950; 5, 307- 332.
176. Van Amerongen, G.J. Influence of Structure of Elastomers on their Permeability to Gases. *Rubber Chem. Technol.*, 1951; 24, 109-131.
177. Van Krevelen, D.W. *Properties of Polymers*, 3rd ed., 1990; Elsevier, Amsterdam.
178. Stannett, V. Simple Gases, in *Diffusion in Polymers*, Crank, J. and Park, G.S. (eds.), Academic Press, London and New York, 1968; 41-73.
179. S. Thomas, I. Pinnau, N. Dub, M.D. Guiver, Hydrocarbon/hydrogen mixed-gas permeation properties of PIM-1, an amorphous micro porous spirobisindane polymer, *J. Membr. Sci.* 338 (2009) 1-4.
180. Naiying Du, Ho Bum Park, Gilles P. Robertson, Mauro M. Dal-Cin, Tymen Visser, Ludmila Scoles, Michael D. Guiver. Polymer nanosieve membranes for CO₂-capture applications. doi: 10.1038/nmat2989
181. Peter M. Budd, Kadhum J. Msayib, Carin E. Tattershall, Bader S. Ghanem, Kevin J. Reynolds, Neil B. McKeown, Detlev Fritsch. Gas separation membranes from polymers of intrinsic microporosity. *Journal of Membrane Science*, 2005; 251, 263–269.
182. M. Gringolts, M. Bermeshev, Yu. Yampolskii, L. Starannikova, V. Shantarovich, E. Finkelshtein, New High Permeable Addition Poly(tricyclononenes) with Si(CH₃)₃ Side Groups. *Synthesis, Gas Permeation Parameters, and Free Volume, Macromolecules* 43 (2010) 7165-7172.
183. P.M. Budd, E.S. Elabas, B.S. Ghanem, S. Makhseed, N.B. McKeown, K.J. Msayib, C.E. Tattershall, D. Wang, Solution-processed, organophilic membrane derived from a polymer of intrinsic microporosity, *Adv. Mater.* 16 (2004) 456.
184. Peter M. Budd, Neil B. McKeown, Bader S. Ghanem, Kadhum J. Msayib, Detlev Fritsch, Ludmila Starannikova, Nikolai Belov, Olga Sanfirova, Yuri Yampolskii, Victor Shantarovich. Gas permeation parameters and other physicochemical properties of a polymer of intrinsic microporosity: Polybenzodioxane PIM-1. *Journal of Membrane Science*, 2008; 325, 851–860.

185. S.L. Liu, R. Wang, T.S. Chung, M.L. Chng, Y. Liu, R.H. Vora, Effect of diamine composition on the gas transport properties in 6FDA-durene/3,3'-diaminodiphenyl sulfone copolyimides, *J. Membr. Sci.*, 2002; 202, 165-176.
186. ASTM, Standard Test Methods for Density and Specific Gravity (Relative Density) of Plastics by Displacement, in, ASTM International: West Conshohocken, 1993.
187. S.S. Hosseini, M.M. Teoh, T.S. Chung, Hydrogen separation and purification in membranes of miscible polymer blends with interpenetration networks, *Polymer*, 2008; 49, 1594-1603.
188. E.S. Sanders, W.J. Koros, H.B. Hopfenberg, V. Stannett, Pure and mixed gas sorption of carbon dioxide and ethylene in poly (methyl methacrylate), *J. Membr. Sci.* 1984; 18, 53-74.
189. O. Vopička, M.G. De Angelis, G.C. Sarti, Mixed gas sorption in glassy polymeric membranes: I. CO₂/CH₄ and n-C₄/CH₄ mixtures sorption in poly (1-trimethylsilyl-1-propyne) (PTMSP), *J. Membr. Sci.* 2014; 449, 97-108.
190. Pizzi D, De Angelis MG, Doghieri F, Giacinti Baschetti M, Sarti GC. Moisture sorption and oxygen transport in a nylon-6/ montmorillonite composite. In: Pierucci S, editor. *Chemical Engineering Transactions*, vol. 6. AIDIC; 2005. p. 515–20.
191. M. Minelli, M.G. De Angelis, F. Doghieri, M. Marini, M. Toselli, F. Pilati. Oxygen permeability of novel organic–inorganic coatings: I. Effects of organic–inorganic ratio and molecular weight of the organic component. *European Polymer Journal*. 2008; 44, 2581–2588.
192. Mehler, C.; Risse, W. *Makromol. Chem. Rapid Commun.* 1991, 12, 255–259.
193. Dorkenoo, K. D.; Pfromm, P. H.; Rezac, M. E. *J. Polym. Sci., Part B: Polym. Phys.* 1998, 36, 797–803.
194. Zhao, C.; do Rosario Ribeira, M.; dePinho, M. N.; Subrahmanyam, V. S.; Gil, C. L.; de Lima, A. P. *Polymer* 2001, 42, 2455–2462.
195. Wilks, B. R.; Chung, W. J.; Ludovice, P. J.; Rezac, M. E.; Meakin, P.; Hill, A. J. *J. Polym. Sci., Part B: Polym. Phys.* 2003, 41, 2185–2199.
196. Blank, F.; Janiak, Ch. *Coord. Chem. Rev.* 2009, 253, 827–861.
197. Hennis, A. D.; Polley, J. D.; Long, G. S.; Sen, A.; Yandulov, D.; Lipian, J.; Benedikt, G. M.; Rhodes, L. F.; Huffman, J. *Organometallics* 2001, 20, 2802–2812.
198. Funk, J. K.; Andes, C. E.; Sen, A. *Organometallics* 2004, 23, 1680–1683.
199. Myagmarsuren, G.; Lee, K.-S.; Jeong, O.-Y.; Ihm., S.-K. *Polymer* 2005, 46, 3685–3692.

200. Kaita, Sh.; Matsushita, K.; Tobita, M.; Maruyama, Y.; Wakatsuki, Y. *Macromol. Rapid Commun.* 2006, 27, 1752–1756.
201. Jung, I. G.; Seo, J.; Chung, Y. K.; Shin, D. M.; Chun, S. H.; Son, S. U. *J. Polym. Sci., Part A: Polym. Chem.* 2007, 45, 3042–3052.
202. Masuda, T.; Nagai, K. In *Materials science of membrane for gas and vapor separation*; Yampolskii, Yu., Pinnau, I., Freeman, B. D., Eds.; Wiley: Chichester, U.K., 2006; p231.
203. Hofmann, D.; Entrialgo-Castano, M.; Lerbret, A.; Heuchel, M.; Yampolskii, Yu. *Macromolecules* 2003, 36, 8528–8538.
204. R.M. Barrer, J.A. Barrie, J. Slater, Sorption and diffusion in ethylcellulose. Part III. Comparison between ethyl cellulose and rubber, *J. Polym. Sci.* 27 (1958) 177–197.
205. A.S. Michaels, W.R. Vieth, J.A. Barrie, Solution of gases in polyethylene terephthalate, *J. Appl. Phys.* 34 (1) (1963) 1–12.
206. W.R. Vieth, P.M. Tam, A.S. Michaels, Dual sorption mechanisms in glassy polystyrene, *J. Colloid Interf. Sci.* 22 (1966) 360–370.
207. D.R. Paul, Gas sorption and transport in glassy polymers, *Ber. Bunsenges. Phys. Chem.* 83 (1979) 294–302.
208. Y. Kamiya, K. Mizoguchi, K. Terada, Y. Fujiwara, J.-S. Wang, CO₂ sorption and dilation of poly(methyl methacrylate), *Macromolecules* 31 (1998) 472–478.
209. Y. Tsujita, Gas sorption and permeation of glassy polymers with microvoids, *Prog. Polym. Sci.* 28 (2003) 1377–1401.
210. R. Kirchheim, Partial molar volume of small molecules in glassy polymers, *J. Polym. Sci., Part B: Polym. Phys.* 31 (1993) 1373–1382.
211. H. Hachisuka, H. Takizawa, Y. Tsujita, A. Takizawa, T. Kinoshita, Gas transport properties in polycarbonate films with various unrelaxed volumes, *Polymer* 32 (1991) 2382–2386.
212. A. Morisato, N.R. Miranda, B.D. Freeman, H.B. Hopfenberg, G. Costa, A. Grosso, S. Russo, The influence of chain configuration and, in turn, chain packing on the sorption and transport properties of poly(tert-butyl acetylene), *J. Appl. Polym. Sci.* 49 (1993) 2065–2074.
213. A. Morisato, B.D. Freeman, I. Pinnau, C.G. Casillas, Pure hydrocarbon sorption properties of poly(1-trimethylsilyl-1-propyne) (PTMSP), poly(1-phenyl-1-propyne) (PPP), and PTMSP/PPP blends, *J. Polym. Sci., Part B: Polym. Phys.* 34 (1996) 925–1934.

214. K. Nagai, L.G. Toy, B.D. Freeman, M. Teraguchi, T. Masuda, I. Pinnau, Gas permeability and hydrocarbon solubility of poly[1-phenyl-2-[p-(triisopropylsilyl) phenyl]acetylene], *J. Polym. Sci., Part B: Polym. Phys.* 38 (2000) 1474–1484.
215. S.V. Dixon-Garrett, K. Nagai, B.D. Freeman, Sorption, diffusion, and permeation of ethylbenzene in poly (1-trimethylsilyl- 1-propyne), *J. Polym. Sci., Part B: Polym. Phys.* 38 (2000) 1078–1089.
216. R. Paterson, Y.P. Yampol'skii, Solubility of gases in glassy polymers, *J. Phys. Chem. Ref. Data.* 28 (1999) 1255–1452.
217. Doghieri, F. and Sarti, G. C. Non-equilibrium lattice fluids: a predictive model for the solubility in glassy polymers. *Macromolecules* 29 (1996), 7885.
218. Doghieri, F. and Sarti, G. C. Solubility, diffusivity and mobility of n-pentane and ethanol in poly(1-trimethylsilyl-1-propyne). *J. Polym. Sci. Polym. Phys.* 35 (1997), 2245.
219. Doghieri, F. and Sarti, G. C. Predicting the solubility of gases and vapors in glassy polymers in the low pressure range. *J. Membrane Sci.* (in press).
220. Doghieri, F. and Sarti, G. C. Predictions of the solubility of gases in glassy polymers based on the NELF model. *Chemical Engineering Science*, 53, (1998), 3435-3447
221. M.G. Baschetti, F. Doghieri, G.C. Sarti, Solubility in Glassy Polymers: Correlations through the Nonequilibrium Lattice Fluid Model, *Ind. Eng. Chem. Res.* 40 (2001) 40.
222. M. Minelli, S. Campagnoli, M.G. De Angelis, F. Doghieri, G.C. Sarti, Predictive Model for the Solubility of Fluid Mixtures in Glassy Polymers, *Macromolecules* 44 (2011) 4852–4862.
223. O. Vopička, M. G. De Angelis, N. Du, N. Li, M. D. Guiver, G, C, Sarti; Mixed gas sorption in glassy polymeric membranes: II. CO₂/CH₄ mixtures in a polymer of intrinsic micro porosity (PIM-1), *J. Membr. Sci.* 459 (2014), 264 – 276.
224. Y. Huang, X. Wang, D.R. Paul, Physical aging of thin glassy polymer films: Free volume interpretation, *J. Membr. Sci.* 277 (2006) 219-229.
225. J. Crank, *The Mathematics of Diffusion*, Oxford Press, London, 1956.